Prepared for submission to JHEP version 00v-PS

Semi-Inclusive Deep Inelastic Scattering in Wandzura-Wilczek-type approximation

S. Bastami[a] **H. Avakian**[b] **A. V. Efremov**[c] **A. Kotzinian**[d,e] **B. U. Musch**[f]
B. Parsamyan[e] **A. Prokudin**[g,b] **M. Schlegel**[h] **G. Schnell**[i] **P. Schweitzer**[a,j] **K. Tezgin**[a]

[a] *Department of Physics, University of Connecticut, Storrs, CT 06269, U.S.A.*
[b] *Thomas Jefferson National Accelerator Facility, Newport News, VA 23606, U.S.A.*
[c] *Joint Institute for Nuclear Research, Dubna, 141980 Russia*
[d] *Yerevan Physics Institute, Alikhanyan Brothers St., 375036 Yerevan, Armenia*
[e] *INFN, Sezione di Torino, 10125 Torino, Italy*
[f] *Institut für Theoretische Physik, Universität Regensburg, 93040 Regensburg, Germany*
[g] *Division of Science, Penn State Berks, Reading, PA 19610, USA*
[h] *Department of Physics, New Mexico State University, Las Cruces, NM 88003-001, USA*
[i] *Department of Theoretical Physics, University of the Basque Country UPV/EHU, 48080 Bilbao, Spain, and IKERBASQUE, Basque Foundation for Science, 48013 Bilbao, Spain*
[j] *Institute for Theoretical Physics, Universität Tübingen, D-72076 Tübingen, Germany*

E-mail: saman.bastami@uconn.edu, avakian@jlab.org, efremov@theor.jinr.ru, aram.kotzinian@cern.ch, bmusch@b-mu.de, bakur@cern.ch, prokudin@jlab.org, schlegel@nmsu.edu, gunar.schnell@desy.de, peter.schweitzer@phys.uconn.edu, kemal.tezgin@uconn.edu

Abstract: We present the complete cross-section for pion production in semi-inclusive deep-inelastic scattering up to power-suppressed $\mathcal{O}(1/Q^2)$ terms in the Wandzura–Wilczek-type approximation which consists in a systematic neglect of $\bar{q}gq$–terms with respect to $\bar{q}q$–correlators. We compute all twist-2 and twist-3 structure functions and the corresponding asymmetries, and discuss the applicability of the Wandzura–Wilczek-type approximations on the basis of available data. We make predictions which can be tested by data from Jefferson Lab, COMPASS, HERMES, and the future Electron-Ion Collider. The results of this paper can be readily used for phenomenology and for event generators, and will help to improve our understanding of the TMD theory beyond leading twist.

Keywords: Wandzura–Wilczek approximation, semi-inclusive deep inelastic scattering, transverse momentum dependent distribution functions, spin and azimuthal asymmetries, leading and subleading twist

Contents

1 Introduction

A great deal of what is known about the quark-gluon structure of nucleon is due to studies of parton distribution functions (PDFs) in deep-inelastic reactions. leading–twist PDFs tell us how likely it is to find an unpolarized parton (described by PDF $f_1^a(x)$, $a = q, \bar{q}, g$) or a longitudinally polarized parton (described by PDF $g_1^a(x)$, $a = q, \bar{q}, g$) in a fast-moving unpolarized or longitudinally polarized nucleon, which carries the fraction x of the nucleon momentum. This information depends on the "resolution (renormalization) scale" associated with the hard scale Q of the process. Although the PDFs $f_1^a(x)$ and $g_1^a(x)$ continue being the subject of intense research (small-x, large-x, helicity sea and gluon distributions) they can be considered as rather well-known, and the frontier has been extended in the last years to go beyond the one-dimensional picture offered by those PDFs.

One way to do this consists in a systematic inclusion of transverse parton momenta $k_\perp$ whose effects manifest themselves in terms of transverse momenta of the reaction products in the final state. If these transverse momenta are much smaller than the hard scale Q of the process, the formal description is given in terms of transverse momentum dependent

distribution functions TMDs) and fragmentation functions (FFs) which are defined in terms of quark-quark correlators [1–4], and depend on two independent variables: the fraction x of nucleon momentum carried by parton, and intrinsic transverse momentum $k_\perp$ of the parton. Being a vector in the plane transverse with respect to the light-cone direction singled out by the hard momentum flow in the process, $k_\perp$ allows us to access novel information on the nucleon spin structure through correlations of $k_\perp$ with nucleon and/or parton spin. The latter is a well-defined concept for twist-2 TMDs interpreted in the infinite momentum frame or in lightcone quantization formalism.

One powerful tool to study TMDs are measurements of the semi-inclusive deep-inelastic scattering (SIDIS) process. By exploring various possibilities for electron/muon beam and target polarizations unambiguous information can be accessed on the 8 leading–twist TMDs [2] and, if one assumes factorization, on certain linear combinations of the 16 subleading–twist TMDs [3, 4]. Complementary information can be obtained from the Drell-Yan process [5], and e^+e^- annihilation [6].

In QCD the TMDs are independent functions. Each TMD contains unique information on a different aspect of the nucleon structure. Twist-2 TMDs have partonic interpretations. Twist-3 TMDs give insights on quark-gluon correlations in the nucleon [7–9]. Besides positivity constraints [10] there is little model-independent information on TMDs. An important question with practical applications is: do useful *approximations* for TMDs exist? Experience from collinear PDFs encourages to explore this possibility: the twist-3 $g_T^a(x)$ and $h_L^a(x)$ can be expressed in terms of contributions from twist-2 $g_1^a(x)$ and $h_1^a(x)$, and additional quark-gluon-quark ($\bar{q}gq$) correlations or current quark mass terms [11, 12]. We shall refer to the latter generically as $\bar{q}gq$–terms, keeping in mind one deals in each case with matrix elements of different operators. The $\bar{q}gq$–correlations contain new insights on hadron structure which are worthwhile exploring for their own sake, see [13] on $g_T^a(x)$.

The striking observation is that the $\bar{q}gq$–terms in $g_T^a(x)$ and $h_L^a(x)$ are small: theoretical mechanisms predict this [14–17], and in the case of $g_T^a(x)$ data confirm or are compatible with these predictions [18–20]. This approximation ("neglect of $\bar{q}gq$–terms") is commonly known as Wandzura–Wilczek (WW) approximation [11]. The possibility to apply this type of approximation also to TMDs has been explored in specific cases in [21–27]. In both cases, PDFs and TMDs, one basically assumes that the contributions from $\bar{q}gq$–terms can be neglected with respect to $\bar{q}q$–terms. But the nature of the omitted matrix elements is different, and in the context of TMDs one often prefers to speak about WW-type approximations.

In this work, after introducing the SIDIS process and defining TMDs and FFs (Sec. 2), we shall introduce the WW(-type) approximations, and review what is presently known about them from experiment and theory (Sec. 3). We will show that under the assumption of the validity of these approximations all leading and subleading SIDIS structure functions are described in terms of a basis of 6 TMDs and 2 FFs (Sec. 4), and review how these basis functions describe available data (Sec. 5). We will systematically apply the WW and/or WW-type approximations to SIDIS structure at leading (Sec. 6) and subleading (Sec. 7) twist, and conclude with a critical discussion (Sec. 8).

This is the first study of all SIDIS structure functions up to twist-3 in a unique approach. Our results are of importance for experiments prepared in the near-term at Jefferson Lab

(JLab) with 12 GeV beam energy upgrade and COMPASS or proposed in the long-term (Electron Ion Collider), and provide helpful input for Monte Carlo event generators [28].

Our predictions will either be confirmed within the expected accuracy or not supported by data. This will call for dedicated theoretical studies to explain either why the pertinent $\bar{q}gq$–terms are so small or so sizable. In either case our results will deepen the understanding of $\bar{q}gq$–correlations and help to guide further developments.

2 The SIDIS process in terms of TMDs and FFs

In this section we review the description of the SIDIS process, define structure functions, PDFs, TMDs, FFs and recall how they describe the SIDIS structure functions.

2.1 The SIDIS process

The SIDIS process is sketched in Fig. 1. Here l and P are momenta of incoming lepton and nucleon, and l' and P_h are the momenta of the outgoing electron and produced hadron. The virtual photon momentum $q = l - l'$ selects a z-axis, and l' points in the direction of the x-axis from which azimuthal angles are counted. The relevant kinematic invariants are

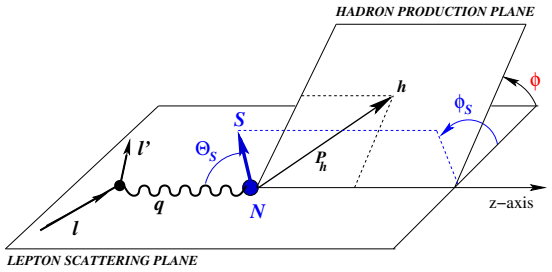

Figure 1. Kinematics of SIDIS process $lN \to l'hX$ in 1-photon exchange approximation.

$$x = \frac{Q^2}{2\,P\cdot q},\quad y = \frac{P\cdot q}{P\cdot l},\quad z = \frac{P\cdot P_h}{P\cdot q},\quad Q^2 = -q^2. \tag{2.1}$$

In addition to x, y, z the cross section is also differential in the azimuthal angle ϕ_h of the produced hadron, the square of its momentum component P_{hT} perpendicular with respect to the virtual photon momentum. In principle the cross section is also differential with respect to the azimuthal angle ψ_l characterizing the overall orientation of the lepton scattering plane in a fixed lab frame. By analyzing the data in the reference frame in Fig. 1 all events are by definition in the "bin" $\psi_l = 0$ (within detector resolution) and the variable ψ_l is practically integrated out leaving us with a 5-dimensional cross section. Below we keep the cross section "differential" in ψ_l for symbolic reasons. It is convenient to define the unpolarized lepton–quark scattering subprocess cross section

$$\frac{d\hat\sigma}{dy} = \frac{4\pi\alpha_{em}^2}{x\,y\,Q^2}\left(1 - y + \frac{1}{2}y^2\right) \tag{2.2}$$

To leading order in $1/Q$ the SIDIS cross-section is given by

$$\begin{aligned}\frac{d^6\sigma_{\rm leading}}{dx\,dy\,dz\,d\psi_l\,d\phi_h\,dP_{hT}^2} = \frac{1}{4\pi}\,\frac{d\hat\sigma}{dy}\,F_{UU}(x,z,P_{hT}^2)\Big\{\,&1 + \cos(2\phi_h)\,p_1\,A_{UU}^{\cos(2\phi_h)}\\ &+S_L\sin(2\phi_h)\,p_1\,A_{UL}^{\sin(2\phi_h)} + \lambda\,S_L\,p_2\,A_{LL}\\ &+\lambda\,S_T\cos(\phi_h-\phi_S)\,p_2\,A_{LT}^{\cos(\phi_h-\phi_S)} + S_T\sin(\phi_h-\phi_S)\,A_{UT}^{\sin(\phi_h-\phi_S)}\\ &+S_T\sin(\phi_h+\phi_S)\,p_1\,A_{UT}^{\sin(\phi_h+\phi_S)} + S_T\sin(3\phi_h-\phi_S)\,p_1\,A_{UT}^{\sin(3\phi_h-\phi_S)}\Big\}\end{aligned} \tag{2.3a}$$

where F_{UU} is the structure function due to transverse polarization of the virtual photon (sometimes denoted as $F_{UU,T}$), and we systematically neglect $1/Q^2$ corrections in kinematic factors and a structure function (sometimes denoted as $F_{UU,L}$) arising from longitudinal

polarization of the virtual photon (and analog for the structure function $\propto S_T \sin(\phi_h - \phi_S)$, see below). The structure functions (and asymmetries) also depend on Q^2 via the scale dependence of TMDs and FFs, which we do not show in formulas throughout this work.

At subleading order in the $1/Q$ expansion one has

$$\begin{aligned}\frac{d^6\sigma_{\text{subleading}}}{dx\,dy\,dz\,d\psi_l\,d\phi_h\,dP_{hT}^2} = \frac{1}{4\pi}\,\frac{d\hat{\sigma}}{dy}\,F_{UU}(x,z,P_{hT}^2)\Big\{&\cos(\phi_h)\,p_3\,A_{UU}^{\cos(\phi_h)}\\ &+\lambda\sin(\phi_h)\,p_4\,A_{LU}^{\sin(\phi_h)} + S_L\sin(\phi_h)\,p_3\,A_{UL}^{\sin(\phi_h)} + S_T\sin(\phi_S)\,p_3\,A_{UT}^{\sin(\phi_S)}\\ &+S_T\sin(2\phi_h-\phi_S)\,p_3\,A_{UT}^{\sin(2\phi_h-\phi_S)} + \lambda\,S_L\cos(\phi_h)\,p_4\,A_{LL}^{\cos(\phi_h)}\\ &+\lambda\,S_T\cos(\phi_S)\,p_4\,A_{LT}^{\cos(\phi_S)} + \lambda\,S_T\cos(2\phi_h-\phi_S)\,p_4\,A_{LT}^{\cos(2\phi_h-\phi_S)}\Big\}\end{aligned} \tag{2.3b}$$

Neglecting $1/Q^2$ corrections, the kinematic prefactors p_i are given by

$$p_1 = \frac{1-y}{1-y+\frac{1}{2}\,y^2}\,,\quad p_2 = \frac{y(1-\frac{1}{2}\,y)}{1-y+\frac{1}{2}\,y^2}\,,\quad p_3 = \frac{(2-y)\sqrt{1-y}}{1-y+\frac{1}{2}\,y^2}\,,\quad p_4 = \frac{y\sqrt{1-y}}{1-y+\frac{1}{2}\,y^2}\,. \tag{2.4}$$

and the asymmetries are defined as

$$A_{XY}^{\text{weight}} \equiv A_{XY}^{\text{weight}}(x,z,P_{hT}) = \frac{F_{XY}^{\text{weight}}(x,z,P_{hT})}{F_{UU}(x,z,P_{hT})}. \tag{2.5}$$

Hereby the first index $X = U(L)$ denotes the unpolarized beam (longitudinally polarized beam with helicity λ). The second index $Y = U(L,T)$ refers to the target which can be unpolarized (or longitudinally, transversely polarized with respect to virtual photon). The superscript "weight" indicates the azimuthal dependence with no index indicating an isotropic angular distribution of the produced hadrons.

In the partonic description the structure functions in (2.3a) are "twist-2." Those in (2.3b) are "twist-3" and contain a factor M/Q in their definitions, see below. In our treatment to $1/Q^2$ accuracy we neglect two structure functions due to longitudinal virtual photon polarization which contribute at order $\mathcal{O}(M^2/Q^2)$ in the partonic description of the process, one being $F_{UU,L}$ and the other contributing to the $\sin(\phi_h - \phi_S)$ angular distribution [4].

Experimental collaborations often define asymmetries in terms of counts $N(\phi_h)$. This means the kinematic prefactors p_i and $1/(x\,y\,Q^2)$ are included in the numerators or denominators of the asymmetries which are averaged over y within experimental kinematics. We will call the corresponding asymmetries $A_{XY,\langle y\rangle}^{\text{weight}}$. For instance, in unpolarized case one has

$$N(x,\ldots,\phi) = \frac{N_0(x,\ldots)}{2\pi}\left(1 + \cos\phi\,A_{UU,\langle y\rangle}^{\cos\phi_h}(x,\ldots) + \cos 2\phi\,A_{UU,\langle y\rangle}^{\cos 2\phi_h}(x,\ldots)\right) \tag{2.6}$$

where N_0 denotes the total (ϕ_h–averaged) number of counts and the dots indicate further kinematic variables in the kinematic bin of interest (which may also be averaged over). It would be preferable if asymmetries were analyzed with known kinematic prefactors divided

out on event-by-event basis. One could then directly compare asymmetries A_{XY}^{weight} measured in different experiments and kinematics, and focus on effects of evolution or power suppression for twist-3. In practice, often the kinematic factors were included. We will define and comment on the explicit expressions as needed.

For completeness we remark that after integrating the cross section over transverse hadron momenta one obtains

$$\frac{d^4\sigma_{\text{leading}}}{dx\,dy\,dz\,d\psi_l} = \frac{1}{2\pi}\,\frac{d\hat{\sigma}}{dy}\,F_{UU}(x,z)\Big\{\,1+\lambda\,S_L\,p_2\,A_{LL}\,\Big\} \tag{2.7a}$$

$$\frac{d^4\sigma_{\text{subleading}}}{dx\,dy\,dz\,d\psi_l} = \frac{1}{2\pi}\,\frac{d\hat{\sigma}}{dy}\,F_{UU}(x,z)\Big\{S_T\sin(\phi_S)\,p_3\,A_{UT}^{\sin(\phi_S)}+\lambda\,S_T\cos(\phi_S)\,p_4\,A_{LT}^{\cos(\phi_S)}\Big\} \tag{2.7b}$$

where (and analog for the other structure functions)

$$F_{UU}(x,z) = \int d^2P_{hT}\;F_{UU}(x,z,P_{hT}) \tag{2.8}$$

and the asymmetries are defined as

$$A_{XY}^{\text{weight}}(x,z) = \frac{F_{XY}^{\text{weight}}(x,z)}{F_{UU}(x,z)}\,. \tag{2.9}$$

The connection of "collinear" SIDIS structure functions in (2.7a, 2.7b) to those known from inclusive DIS is established by integrating over z and summing over hadrons as

$$\sum_h\int dz\;z\;F_{UU}(x,z) \quad\equiv\quad 2\,x\,F_1(x)\,, \tag{2.10a}$$

$$\sum_h\int dz\;z\;F_{LL}(x,z) \quad\equiv\quad 2\,x\,g_1(x)\,, \tag{2.10b}$$

$$\sum_h\int dz\;z\;F_{LT}^{\cos\phi_S}(x,z) \;\equiv\; -\,\gamma\,2\,x\Big(g_1(x)+g_2(x)\Big)\,, \tag{2.10c}$$

$$\sum_h\int dz\;z\;F_{UT}^{\sin\phi_S}(x,z) \;=\; 0\,, \tag{2.10d}$$

where $\gamma = 2M_Nx/Q$ signals the twist-3 character of $F_{LT}^{\cos\phi_S}(x,z)$. As we consequently neglect $1/Q^2$ effects, the twist-4 DIS structure function $F_2(x)$ does not appear in (2.10a). $F_{UT}^{\sin\phi_S}(x,z)$ has no DIS counterpart due to time reversal symmetry of strong interactions.

2.2 TMDs, FFs and structure functions

TMDs are defined in terms of light-front correlators

$$\Phi(x,\boldsymbol{k}_\perp)_{ij} = \int\frac{d\xi^-d^2\boldsymbol{\xi}_\perp}{(2\pi)^3}\,e^{ik\xi}\,\langle N(P,S)|\bar{\psi}_j(0)\,\mathcal{W}_{(0,\infty)}\mathcal{W}_{(\infty,\xi)}\,\psi_i(\xi)|N(P,S)\rangle\Big|_{\substack{\xi^+=0\\ k^+=xP^+}} \tag{2.11}$$

where the Wilson-lines refer to the SIDIS process [29]. For a generic four-vector a^μ we define the light-cone coordinates $a^\mu = (a^+, a^-, a_\perp)$ with $a^\pm = (a^0 \pm a^3)/\sqrt{2}$. The light-cone direction is singled out by the virtual photon momentum and transverse vectors like $\boldsymbol{k}_\perp$ are perpendicular to it. In the virtual-photon–nucleon center-of-mass frame, nucleon and the partons inside it move in the (+)–lightcone direction, while the struck quark and the produced hadron move in (−)–light-cone direction. In the nucleon rest frame the polarization vector is given by $S = (0, \boldsymbol{S}_T, S_L)$ with $\boldsymbol{S}_T^2 + S_L^2 = 1$.

The 8 leading–twist TMDs [2] are projected out from the correlator (2.11) as follows (blue: T-even, red: T-odd; we suppress flavor and renormalization scale dependence)

$$\frac{1}{2}\,\mathrm{Tr}\Big[\gamma^+\,\Phi(x,\boldsymbol{k}_\perp)\Big] = f_1 - \frac{\varepsilon^{jk}k_\perp^j S_T^k}{M_N}\,f_{1T}^\perp\,, \tag{2.12a}$$

$$\frac{1}{2}\,\mathrm{Tr}\Big[\gamma^+\gamma_5\,\Phi(x,\boldsymbol{k}_\perp)\Big] = S_L\,g_1 + \frac{\boldsymbol{k}_\perp\cdot\boldsymbol{S}_T}{M_N}\,g_{1T}^\perp\,, \tag{2.12b}$$

$$\frac{1}{2}\,\mathrm{Tr}\Big[i\sigma^{j+}\gamma_5\,\Phi(x,\boldsymbol{k}_\perp)\Big] = S_T^j\,h_1 + S_L\,\frac{k_\perp^j}{M_N}\,h_{1L}^\perp + \frac{\kappa^{jk}S_T^k}{M_N^2}\,h_{1T}^\perp + \frac{\varepsilon^{jk}k_\perp^k}{M_N}\,h_1^\perp\,, \tag{2.12c}$$

and the 16 subleading twist TMDs [1, 4] are given by

$$\frac{1}{2}\mathrm{Tr}\Big[1\,\Phi(x,\boldsymbol{k}_\perp)\Big] = \frac{M_N}{P^+}\Big[\;e - \frac{\varepsilon^{jk}k_\perp^j S_T^k}{M_N}\,e_T^\perp\Big], \tag{2.12d}$$

$$\frac{1}{2}\mathrm{Tr}\Big[i\gamma_5\Phi(x,\boldsymbol{k}_\perp)\Big] = \frac{M_N}{P^+}\Big[S_L e_L + \frac{\boldsymbol{k}_\perp\cdot\boldsymbol{S}_T}{M_N}\,e_T\Big], \tag{2.12e}$$

$$\frac{1}{2}\mathrm{Tr}\Big[\gamma^j\,\Phi(x,\boldsymbol{k}_\perp)\Big] = \frac{M_N}{P^+}\Big[\frac{k_\perp^j}{M_N}f^\perp + \varepsilon^{jk}S_T^k f_T + S_L\frac{\varepsilon^{jk}k_\perp^k}{M_N}f_L^\perp - \frac{\kappa^{jk}\varepsilon^{kl}S_T^l}{M_N^2}f_T^\perp\Big], \tag{2.12f}$$

$$\frac{1}{2}\mathrm{Tr}\Big[\gamma^j\gamma_5\Phi(x,\boldsymbol{k}_\perp)\Big] = \frac{M_N}{P^+}\Big[S_T^j\,g_T + S_L\,\frac{k_\perp^j}{M_N}g_L^\perp + \frac{\kappa^{jk}S_T^k}{M_N^2}\,g_T^\perp + \frac{\varepsilon^{jk}k_\perp^k}{M_N}\,g^\perp\Big], \tag{2.12g}$$

$$\frac{1}{2}\mathrm{Tr}\Big[i\,\sigma^{jk}\gamma_5\Phi(x,\boldsymbol{k}_\perp)\Big] = \frac{M_N}{P^+}\Big[\frac{S_T^j k_\perp^k - S_T^k k_\perp^j}{M_N}\,h_T^\perp - \varepsilon^{jk}\,h\Big], \tag{2.12h}$$

$$\frac{1}{2}\mathrm{Tr}\Big[i\,\sigma^{+-}\,\gamma_5\,\Phi(x,\boldsymbol{k}_\perp)\Big] = \frac{M_N}{P^+}\Big[S_L\,h_L + \frac{\boldsymbol{k}_\perp\cdot\boldsymbol{S}_T}{M_N}\,h_T\Big]. \tag{2.12i}$$

where $\kappa^{jk} \equiv (k_\perp^j k_\perp^k - \frac{1}{2}\,\boldsymbol{k}_\perp^2\delta^{jk})$. The indices j, k, l refer to the plane transverse with respect to the light-cone, $\epsilon^{ij} \equiv \epsilon^{-+ij}$ and $\epsilon^{0123} = +1$. Dirac-structures not listed in (2.12a–2.12i) are twist-4 [3]. Integrating out transverse momenta in the correlator (2.11) leads to the "usual" PDFs known from collinear kinematics [12, 30], namely at twist-2 level

$$\frac{1}{2}\,\mathrm{Tr}\Big[\gamma^+\,\Phi(x)\Big] = f_1\,, \tag{2.13a}$$

$$\frac{1}{2}\,\mathrm{Tr}\Big[\gamma^+\gamma_5\,\Phi(x)\Big] = S_L\,g_1\,, \tag{2.13b}$$

$$\frac{1}{2}\,\mathrm{Tr}\Big[i\sigma^{j+}\gamma_5\,\Phi(x)\Big] = S_T^j\,h_1\,, \tag{2.13c}$$

and at twist-3 level

$$\frac{1}{2}\,\mathrm{Tr}\Big[1\;\Phi(x)\Big] = \frac{M_N}{P^+}\;e\;, \tag{2.13d}$$

$$\frac{1}{2}\,\mathrm{Tr}\Big[\gamma^j\gamma_5\;\Phi(x)\Big] = \frac{M_N}{P^+}\;S_T^j\,g_T\;, \tag{2.13e}$$

$$\frac{1}{2}\,\mathrm{Tr}\Big[i\,\sigma^{+-}\gamma_5\;\Phi(x)\Big] = \frac{M_N}{P^+}\;S_L\,h_L\;. \tag{2.13f}$$

Other structures drop out either due to explicit $k_\perp$–dependence, or due to the sum rules [4]

$$\int d^2\boldsymbol{k}_\perp\; f_T^a(x,k_\perp^2) = \int d^2\boldsymbol{k}_\perp\; e_L^a(x,k_\perp^2) = \int d^2\boldsymbol{k}_\perp\; h^a(x,k_\perp^2) = 0 \tag{2.14}$$

imposed by time reversal constraints.

The fragmentation functions are similarly defined in terms of the correlator

$$\Delta(z,\boldsymbol{P}_\perp)_{ij} = \sum_X \int \frac{d\xi^+ d^2\boldsymbol{\xi}_\perp}{2z(2\pi)^3}\; e^{ip\xi}\;\langle 0|\mathcal{W}_{(\infty,\xi)}\psi_i(\xi)\,|h,X\rangle\,\langle h,X|\bar\psi_j(0)\mathcal{W}_{(0,\infty)}|0\rangle \Big|_{\substack{\xi^-=0\\ p^-=P_h^-/z\\ \boldsymbol{p}_\perp=-\boldsymbol{P}_\perp/z.}} \tag{2.15}$$

In this work we will consider only unpolarized final state hadrons. If the produced hadron moves fast in the $(-)$ light cone direction, the twist-2 FFs are projected out as

$$\frac{1}{2}\mathrm{Tr}\big[\gamma^-\Delta(z,\boldsymbol{P}_\perp)\big] = D_1\,, \tag{2.16a}$$

$$\frac{1}{2}\mathrm{Tr}\big[i\sigma^{j-}\gamma_5\Delta(z,\boldsymbol{P}_\perp)\big] = \epsilon^{jk}\,\frac{P_\perp^k}{zm_h}H_1^\perp\;, \tag{2.16b}$$

and at twist-3 level

$$\frac{1}{2}\,\mathrm{Tr}\Big[1\;\Delta(z,\boldsymbol{P}_\perp)\Big] = \frac{M_h}{P_h^-}\;E\;, \tag{2.16c}$$

$$\frac{1}{2}\,\mathrm{Tr}\Big[\;\gamma^j\;\Delta(z,\boldsymbol{P}_\perp)\Big] = -\frac{P_\perp^j}{zP_h^-}\;D^\perp\;, \tag{2.16d}$$

$$\frac{1}{2}\,\mathrm{Tr}\Big[\gamma^j\gamma_5\,\Delta(z,\boldsymbol{P}_\perp)\Big] = \varepsilon^{jk}\,\frac{P_\perp^k}{zP_h^-}\,G^\perp\;, \tag{2.16e}$$

$$\frac{1}{2}\,\mathrm{Tr}\Big[i\,\sigma^{jk}\gamma_5\,\Delta(z,\boldsymbol{P}_\perp)\Big] = -\varepsilon^{jk}\,\frac{M_h}{P_h^-}\;H\;. \tag{2.16f}$$

Here besides scale and flavor dependence we also do not indicate the type of hadron h. Integration over transverse hadron momenta leaves us with $D_1(z)$, $E(z)$, $H(z)$ while the other structures drop out due to their $P_\perp$ dependence.

The structure functions in Eqs. (2.3a, 2.3b) are described in Bjorken limit at tree level in terms of convolutions of TMDs and FFs. We define the unit vector $\hat{\boldsymbol{h}} = \boldsymbol{P}_{hT}/P_{hT}$ and use the following convolution integrals (see Appendix B.1 for details)

$$\mathcal{C}\Big[\omega\;f\;D\Big] = x\sum_a e_a^2\int d^2\boldsymbol{k}_\perp d^2\boldsymbol{P}_\perp\;\delta^{(2)}(z\boldsymbol{k}_\perp+\boldsymbol{P}_\perp-\boldsymbol{P}_{hT})\;\omega\;f^a(x,\boldsymbol{k}_\perp^2)\;D^a(z,\boldsymbol{P}_\perp^2)\;, \tag{2.17}$$

where ω is a weight function which in general depends on $\boldsymbol{k}_\perp$ and $\boldsymbol{P}_\perp$. The 8 leading–twist structure functions are

$$F_{UU} = \mathcal{C}\Big[\ \omega^{\{0\}}\, f_1 D_1\ \Big] \tag{2.18a}$$

$$F_{LL} = \mathcal{C}\Big[\ \omega^{\{0\}}\, g_1 D_1\ \Big] \tag{2.18b}$$

$$F_{UT}^{\sin(\phi_h+\phi_S)} = \mathcal{C}\Big[\ \omega_{\rm A}^{\{1\}}\, h_1 H_1^\perp\ \Big] \tag{2.18c}$$

$$F_{UT}^{\sin(\phi_h-\phi_S)} = \mathcal{C}\Big[-\omega_{\rm B}^{\{1\}}\, f_{1T}^\perp D_1\ \Big] \tag{2.18d}$$

$$F_{LT}^{\cos(\phi_h-\phi_S)} = \mathcal{C}\Big[\ \omega_{\rm B}^{\{1\}}\, g_{1T}^\perp D_1\Big] \tag{2.18e}$$

$$F_{UU}^{\cos 2\phi_h} = \mathcal{C}\Big[\ \omega_{\rm AB}^{\{2\}}\, h_1^\perp\, H_1^\perp\ \Big] \tag{2.18f}$$

$$F_{UL}^{\sin 2\phi_h} = \mathcal{C}\Big[\ \omega_{\rm AB}^{\{2\}}\, h_{1L}^\perp H_1^\perp\ \Big] \tag{2.18g}$$

$$F_{UT}^{\sin(3\phi_h-\phi_S)} = \mathcal{C}\Big[\ \omega^{\{3\}}\, h_{1T}^\perp H_1^\perp\ \Big]\,. \tag{2.18h}$$

At subleading–twist we have the structure functions

$$F_{UU}^{\cos\phi_h} = \frac{2M}{Q}\,\mathcal{C}\Big[\ \ \omega_{\rm A}^{\{1\}}\Big(xh\,H_1^\perp + r_h\ f_1\frac{\tilde D^\perp}{z}\Big) - \omega_{\rm B}^{\{1\}}\Big(xf^\perp D_1 + r_h\ h_1^\perp\frac{\tilde H}{z}\Big)\Big] \tag{2.19a}$$

$$F_{LU}^{\sin\phi_h} = \frac{2M}{Q}\,\mathcal{C}\Big[\ \ \omega_{\rm A}^{\{1\}}\Big(x\,e\,H_1^\perp + r_h\ f_1\frac{\tilde G^\perp}{z}\Big) + \omega_{\rm B}^{\{1\}}\Big(xg^\perp D_1 + r_h\ h_1^\perp\frac{\tilde E}{z}\Big)\Big] \tag{2.19b}$$

$$F_{UL}^{\sin\phi_h} = \frac{2M}{Q}\,\mathcal{C}\Big[\ \ \omega_{\rm A}^{\{1\}}\Big(xh_L H_1^\perp + r_h\ g_1\frac{\tilde G^\perp}{z}\Big) + \omega_{\rm B}^{\{1\}}\Big(xf_L^\perp D_1 - r_h\ h_{1L}^\perp\frac{\tilde H}{z}\Big)\Big] \tag{2.19c}$$

$$F_{LL}^{\cos\phi_h} = \frac{2M}{Q}\,\mathcal{C}\Big[-\omega_{\rm A}^{\{1\}}\Big(xe_L H_1^\perp - r_h\ g_1\frac{\tilde D^\perp}{z}\Big) - \omega_{\rm B}^{\{1\}}\Big(xg_L^\perp D_1 + r_h\ h_{1L}^\perp\frac{\tilde E}{z}\Big)\Big] \tag{2.19d}$$

$$\begin{aligned} F_{UT}^{\sin\phi_S} = \frac{2M}{Q}\,\mathcal{C}\Big[\ \ &\omega^{\{0\}}\Big(xf_T D_1\ - r_h\ h_1\frac{\tilde H}{z}\Big) \\ &-\frac{\omega_{\rm B}^{\{2\}}}{2}\Big(xh_T H_1^\perp + r_h\, g_{1T}^\perp\frac{\tilde G^\perp}{z} - xh_T^\perp H_1^\perp + r_h\, f_{1T}^\perp\frac{\tilde D^\perp}{z}\Big)\Big] \end{aligned} \tag{2.19e}$$

$$\begin{aligned} F_{LT}^{\cos\phi_S} = \frac{2M}{Q}\,\mathcal{C}\Big[&-\omega^{\{0\}}\Big(xg_T D_1 + r_h\ h_1\frac{\tilde E}{z}\Big) \\ &+\frac{\omega_{\rm B}^{\{2\}}}{2}\Big(xe_T H_1^\perp - r_h\, g_{1T}^\perp\frac{\tilde D^\perp}{z} + xe_T^\perp H_1^\perp + r_h\, f_{1T}^\perp\frac{\tilde G^\perp}{z}\Big)\Big] \end{aligned} \tag{2.19f}$$

$$\begin{aligned} F_{UT}^{\sin(2\phi_h-\phi_S)} = \frac{2M}{Q}\,\mathcal{C}\Big[\ \ &\frac{\omega_{\rm AB}^{\{2\}}}{2}\Big(xh_T H_1^\perp + r_h\, g_{1T}^\perp\frac{\tilde G^\perp}{z} + xh_T^\perp H_1^\perp - r_h\, f_{1T}^\perp\frac{\tilde D^\perp}{z}\Big) \\ &+\omega_{\rm C}^{\{2\}}\Big(xf_T^\perp D_1 - r_h\ h_{1T}^\perp\frac{\tilde H}{z}\Big)\Big] \end{aligned} \tag{2.19g}$$

$$F_{LT}^{\cos(2\phi_h-\phi_S)} = \frac{2M}{Q}\,\mathcal{C}\Big[-\frac{\omega_{\rm AB}^{\{2\}}}{2}\Big(x e_T H_1^\perp - r_h\, g_{1T}^\perp\,\frac{\tilde D^\perp}{z} - x e_T^\perp H_1^\perp - r_h\, f_{1T}^\perp\,\frac{\tilde G^\perp}{z}\Big) - \omega_{\rm C}^{\{2\}}\Big(x g_T^\perp D_1 + r_h\; h_{1T}^\perp\frac{\tilde E}{z}\Big)\Big] \tag{2.19h}$$

where $r_h = m_h/M_N$ and $F_{XY}^{\rm weight} \equiv F_{XY}^{\rm weight}(x,z,P_{hT})$. The weight functions are defined as

$$\begin{aligned}
\omega^{\{0\}} &= 1\,,\\
\omega_{\rm A}^{\{1\}} &= \frac{\hat{\boldsymbol h}\cdot\boldsymbol P_\perp}{z m_h}\,,\quad \omega_{\rm B}^{\{1\}} = \frac{\hat{\boldsymbol h}\cdot\boldsymbol k_\perp}{M_N}\,,\\
\omega_{\rm A}^{\{2\}} &= \frac{2\,(\hat{\boldsymbol h}\cdot\boldsymbol P_\perp)\,(\hat{\boldsymbol h}\cdot\boldsymbol k_\perp)}{z M_N m_h}\,,\quad \omega_{\rm B}^{\{2\}} = -\frac{\boldsymbol P_\perp\cdot\boldsymbol k_\perp}{z M_N m_h}\,,\quad \omega_{\rm C}^{\{2\}} = \frac{2\,(\hat{\boldsymbol h}\cdot\boldsymbol k_\perp)^2 - \boldsymbol k_\perp^2}{2M_N^2}\,,\\
\omega^{\{3\}} &= \frac{4\,(\hat{\boldsymbol h}\cdot\boldsymbol P_\perp)\,(\hat{\boldsymbol h}\cdot\boldsymbol k_\perp)^2 - 2\,(\hat{\boldsymbol h}\cdot\boldsymbol k_\perp)\,(\boldsymbol k_\perp\cdot\boldsymbol P_\perp) - (\hat{\boldsymbol h}\cdot\boldsymbol P_\perp)\,\boldsymbol k_\perp^2}{2 z M_N^2 m_h}\,,
\end{aligned} \tag{2.20}$$

and $\omega_{\rm AB}^{\{2\}} = \omega_{\rm A}^{\{2\}} + \omega_{\rm B}^{\{2\}}$. In $\omega_i^{\{n\}}$ the index $n = 0, 1, 2, 3$ indicates the (maximal) power $(P_{hT})^n$ with which the corresponding contribution scales, and index i (if any) distinguishes different types of contributions at the given order N. Notice that twist-3 structure functions in Eqs. (2.19a–2.19h) contain an explicit factor M/Q. We also recall that we neglect two structure functions, $F_{UU,L}$ and $F_{UT,L}^{\sin(\phi_h-\phi_S)}$ in the notation of [4], due to longitudinal virtual photon polarization which are of order $\mathcal{O}(M^2/Q^2)$ in the TMD factorization approach.

The structures surviving P_{hT}–integration of the SIDIS cross section in (2.7a, 2.7b) are associated with the trivial weights $\omega^{\{0\}}$ and expressed in terms of collinear PDFs and FFs as follows (here the sum rules (2.14) are used)

$$F_{UU}(x,z) = x\sum_a e_a^2\, f_1^a(x)\, D_1^a(z) \tag{2.21a}$$

$$F_{LL}(x,z) = x\sum_a e_a^2\, g_1^a(x)\, D_1^a(z) \tag{2.21b}$$

$$F_{LT}^{\cos\phi_S}(x,z) = -\frac{2M_N}{Q}\,x\sum_a e_a^2\Big(x\, g_T^q(x)\, D_1^a(z) + r_h\, h_1^a(x)\frac{\tilde E^a(z)}{z}\Big) \tag{2.21c}$$

$$F_{UT}^{\sin\phi_S}(x,z) = -\frac{2\,m_h}{Q}\,x\sum_a e_a^2\, h_1^a(x)\frac{\tilde H^a(z)}{z} \tag{2.21d}$$

Finally, integrating over z, summing over hadrons, and using the sum rules for the T-odd FFs $\sum_h \int dz\; \tilde E^a(z) = 0$ and $\sum_h \int dz\; \tilde H^a(z) = 0$ we recover Eqs. (2.10a–2.10d) and obtain for the DIS structure functions

$$F_1(x) = \frac{1}{2}\sum_a e_a^2\, f_1^a(x) \tag{2.22a}$$

$$g_1(x) = \frac{1}{2}\sum_a e_a^2\, g_1^a(x) \tag{2.22b}$$

$$g_2(x) = \frac{1}{2}\sum_a e_a^2\, g_T^a(x) \;-\; g_1(x) \tag{2.22c}$$

Having established the notation we now define and discuss the approximations.

3 WW and WW-type approximations

In this section we will define the approximations and review what is known about them. The basic idea of the approximations is simple. One uses QCD equations of motion to separate contributions from $\bar{q}q$–terms and $\bar{q}gq$–terms and assumes that the latter can be neglected with respect to the leading $\bar{q}q$–terms with a useful accuracy,

$$\left|\frac{\langle\bar{q}gq\rangle}{\langle\bar{q}q\rangle}\right| \ll 1\,. \tag{3.1}$$

3.1 WW approximation for PDFs

The WW approximation applies in principle to all twist-3 PDFs, Eqs. (2.13d, 2.13e, 2.13f). It was established first for $g_T^a(x)$ [11], and later for $h_L^a(x)$ [12]. The situation of $e^a(x)$ is somewhat special, see below and the review [31].

The origin of the approximations is as follows. The operators defining $g_T^a(x)$ and $h_L^a(x)$ can be decomposed by means of QCD equations of motion in twist-2 parts, and pure twist-3 (interaction dependent) $\bar{q}gq$–terms and current quark mass terms. We denote $\bar{q}gq$–terms and mass-terms collectively and symbolically by functions with a tilde. Such decompositions are possible because $g_T^a(x)$ and $h_L^a(x)$ are "twist-3" not according to the "strict QCD definition" (twist = mass dimension of associated local operator minus its spin). Rather they are classified according to the "working definition" [32] (a function is "twist t" if it contributes to cross sections suppressed by $(M/Q)^{t-2}$ with M a generic hadronic and Q the hard scale). The two definitions coincide for twist-2 quantities, but higher twist observables in general contain "contaminations" by leading twist.

In this way one obtains the decompositions and, if they apply, WW approximations [11, 12] (keep in mind here tilde terms contain pure twist-3 and current quark mass terms)

$$g_T^a(x) = \int_x^1 \frac{dy}{y}\, g_1^a(y) + \tilde{g}_T^a(x) \overset{\text{WW}}{\approx} \int_x^1 \frac{dy}{y}\, g_1^a(y)\,, \tag{3.2a}$$

$$h_L^a(x) = 2x\int_x^1 \frac{dy}{y^2}\, h_1^a(y) + \tilde{h}_L^a(x) \overset{\text{WW}}{\approx} 2x\int_x^1 \frac{dy}{y^2}\, h_1^a(y)\,, \tag{3.2b}$$

$$x\, e^a(x) = x\, \tilde{e}^a(x) \overset{\text{WW}}{\approx} 0 \tag{3.2c}$$

where we included $e^a(x)$ which is a special case in the sense that it receives no twist-2 contribution. A prefactor of x is provided in (3.2c) to cancel a $\delta(x)$–type singularity [31]. After introducing the WW-type approximations for TMDs and FFs, we will come back to (3.2a, 3.2b) and review the theoretical predictions and experimental data supporting them.

3.2 WW-type approximations for TMDs and FFs

Analog to WW approximations for PDFs discussed in Sec. 3.1, also certain TMDs and FFs can be decomposed in twist-2 contributions and tilde-terms. The latter may be assumed, in the spirit of (3.1), to be small. Hereby it is important to keep in mind that one deals with different types of ("unintegrated") $\bar{q}gq$–correlations, and we prefer to refer to them as WW-type approximations.

In the T-even case one obtains the following approximations, where the terms on the left-hand-side are twist-3, those on the right-hand-side (if any) are twist-2,

$$xe^q(x,k_\perp^2) \overset{\text{WW-type}}{\approx} 0, \tag{3.3a}$$

$$xf^{\perp q}(x,k_\perp^2) \overset{\text{WW-type}}{\approx} f_1^q(x,k_\perp^2), \tag{3.3b}$$

$$xg_L^{\perp q}(x,k_\perp^2) \overset{\text{WW-type}}{\approx} g_1^q(x,k_\perp^2), \tag{3.3c}$$

$$xg_T^{\perp q}(x,k_\perp^2) \overset{\text{WW-type}}{\approx} g_{1T}^{\perp q}(x,k_\perp^2), \tag{3.3d}$$

$$xg_T^q(x,k_\perp^2) \overset{\text{WW-type}}{\approx} g_{1T}^{\perp(1)q}(x,k_\perp^2), \tag{3.3e}$$

$$xh_L^q(x,k_\perp^2) \overset{\text{WW-type}}{\approx} -2\,h_{1L}^{\perp(1)q}(x,k_\perp^2), \tag{3.3f}$$

$$xh_T^q(x,k_\perp^2) \overset{\text{WW-type}}{\approx} -h_1^q(x,k_\perp^2) - h_{1T}^{\perp(1)}(x,k_\perp^2), \tag{3.3g}$$

$$xh_T^{\perp q}(x,k_\perp^2) \overset{\text{WW-type}}{\approx} h_1^q(x,k_\perp^2) - h_{1T}^{\perp(1)}(x,k_\perp^2). \tag{3.3h}$$

In the T-odd case one obtains the approximations

$$xe_L^q(x,k_\perp^2) \overset{\text{WW-type}}{\approx} 0, \tag{3.4a}$$

$$xe_T^q(x,k_\perp^2) \overset{\text{WW-type}}{\approx} 0, \tag{3.4b}$$

$$xe_T^{\perp q}(x,k_\perp^2) \overset{\text{WW-type}}{\approx} 0, \tag{3.4c}$$

$$xg^{\perp q}(x,k_\perp^2) \overset{\text{WW-type}}{\approx} 0, \tag{3.4d}$$

$$xf_L^{\perp q}(x,k_\perp^2) \overset{\text{WW-type}}{\approx} 0, \tag{3.4e}$$

$$xf_T^{\perp q}(x,k_\perp^2) \overset{\text{WW-type}}{\approx} f_{1T}^{\perp q}(x,k_\perp^2), \tag{3.4f}$$

$$xf_T^q(x,k_\perp^2) \overset{\text{WW-type}}{\approx} -f_{1T}^{\perp(1)q}(x,k_\perp^2), \tag{3.4g}$$

$$xh^q(x,k_\perp^2) \overset{\text{WW-type}}{\approx} -2\,h_1^{\perp(1)}(x,k_\perp^2), \tag{3.4h}$$

where the superscript "(1)" denotes transverse moments of TMDs defined generically as

$$f^{(1)}(x,k_\perp^2) = \frac{k_\perp^2}{2M^2}\,f(x,k_\perp^2)\,, \quad f^{(1)}(x) = \int d^2\boldsymbol{k}_\perp f^{(1)}(x,k_\perp^2)\,. \tag{3.5}$$

Two very useful WW-type approximations follow from combining the WW approximations (3.2a, 3.2b) with the WW-type approximations (3.3e, 3.3f). This yields [1, 24, 27]

$$g_{1T}^{\perp(1)a}(x) \overset{\text{WW-type}}{\approx} x\int_x^1 \frac{dy}{y}\,g_1^a(y)\,, \tag{3.6a}$$

$$h_{1L}^{\perp(1)a}(x) \overset{\text{WW-type}}{\approx} -x^2\int_x^1 \frac{dy}{y^2}\,h_1^a(y)\,. \tag{3.6b}$$

Aspects and phenomenological applications of some of the above WW-type approximations were discussed in [1, 21–27].

WW-relations for FFs are actually not needed: in Eqs. (2.18, 2.19) either twist-2 FFs D_1^q, $H_1^{\perp q}$ enter or tilde FFs, as a consequence of how the azimuthal angles are defined [4]. For completeness we quote the WW-type approximations for FFs [4]

$$E(z, P_\perp^2) \overset{\text{WW-type}}{\approx} 0\,, \tag{3.7a}$$

$$G^\perp(z, P_\perp^2) \overset{\text{WW-type}}{\approx} 0\,, \tag{3.7b}$$

$$D^\perp(z, P_\perp^2) \overset{\text{WW-type}}{\approx} z\, D_1(z, P_\perp^2)\,, \tag{3.7c}$$

$$H(z, P_\perp^2) \overset{\text{WW-type}}{\approx} -\frac{P_\perp^2}{z M_h^2}\, H_1^\perp(z, P_\perp^2)\,. \tag{3.7d}$$

Having introduced the WW- and WW-type approximations, we will review in the following what is currently known from theory and experiment about our approximations.

3.3 Predictions from instanton vacuum model

Insights on the relative size of hadronic matrix elements, such as Eq. (3.1), require a non-perturbative approach. It is by no means obvious which small parameter in the strong interaction regime would allow one to explain such results .

A powerful non-perturbative approach is provided by the instanton model of the QCD vacuum [33–35]. This semi-classical approach assumes that properties of the QCD vacuum are dominated by instantons and anti-instantons, topological non-perturbative gluon field configurations, which form a strongly interacting medium. The approach provides a natural mechanism for dynamical chiral symmetry breaking, the dominant feature of strong interactions in the nonperturbative regime. It was shown with variational and numerical methods that the strongly interacting instanton medium is dilute. The ratio of average instanton size $\rho_{\rm av}$ and average instanton separation $R_{\rm av}$ is a non-trivial small parameter, numerically $\rho_{\rm av}/R_{\rm av} \sim 1/3$ [33–35], which can be explored.

Applying the instanton vacuum model to studies of $g_T^a(x)$ and $h_L^a(x)$ it was predicted that matrix elements of the $\bar{q}gq$ operators defining $\tilde{g}_T^a(x)$ [14] and $\tilde{h}_L^a(x)$ [15] are strongly suppressed by powers of the small parameter $\rho_{\rm av}/R_{\rm av}$ with respect to contributions from the respective twist-2 parts which are of the order $(\rho_{\rm av}/R_{\rm av})^0$. Numerically it was found

$$\left|\frac{\langle\bar{q}gq\rangle}{\langle\bar{q}q\rangle}\right| \sim \left(\frac{\rho}{R}\right)^4 \log\left(\frac{\rho}{R}\right) \sim 10^{-2} \tag{3.8}$$

in these 2 cases. This result strongly supports the generic approximation in Eq. (3.1) with the instanton packing fraction providing the non-trivial small parameter justifying the neglect of tilde-terms. The instanton calculus has not yet been applied to $\tilde{e}^a(x)$.

Noteworthy, the instanton vacuum predictions for $\tilde{g}_T^a(x)$ [14] were made before the advent of the first precise data on $g_2(x)$ which we discuss in the next section.

3.4 Tests of WW approximation in DIS experiments

The presently available phenomenological information on $g_T^a(x)$ is due to measurements of the structure function $g_2(x)$, Eq. (2.22c), in DIS off various transversely polarized targets. In the WW-approximation (3.2a) one can write $g_2(x)$ as a total derivative expressed in terms of the experimentally well known twist-2 structure function $g_1(x)$ as follows

$$g_2(x) \overset{\text{WW}}{\approx} g_2(x)_{\text{WW}} \equiv \frac{d}{dx}\left[x\int_x^1 \frac{dy}{y}\, g_1(y)\right]. \tag{3.9}$$

Data support (3.9) to a good accuracy [18–20], although especially at smaller x more stringent tests are not yet possible. Overall it has been estimated that the WW approximation for $g_2(x)$ and $g_T^a(x)$ works with an accuracy of about 40 % or better [36].

We present calculations of $g_2(x)_{WW}$ in Fig. 2. How well does the WW approximation describe data if we allow for a theoretical "uncertainty band" of about 40 % as deduced in Ref. [36]? To investigate this question, we split this uncertainty in two parts, $\varepsilon_1 = \pm 20\,\%$ and $\varepsilon_2(x) = \pm 20\,\%(1-x)^\epsilon$ with a small $\epsilon > 0$, and estimate the impact of this uncertainty as

$$g_2(x)_{\text{WW}} = (1 \pm \varepsilon_1)\frac{d}{dx}\left[x\int_x^1 \frac{dy}{y}\left(\frac{1}{2}\sum_a e_a^2\, g_1^a(y(1\pm\varepsilon_2))\right)\right]. \tag{3.10}$$

The effect of ε_1 is to change the magnitude of $g_2(x)_{\text{WW}}$, ε_2 varies the position of its zero. The x–dependence of ε_2 preserves $\lim_{x\to 1} g_2(x) = 0$; we use $\epsilon = 0.05$ which yields $\varepsilon_2 \approx 20\,\%$ up to the highest measured x–bin. The good agreement of $g_2(x)_{\text{WW}}$ with data is encouraging, and in line with theory predictions [14]. Our estimate with the splitted uncertainties $\varepsilon_{1,2}$ may overestimate in certain x–bins the 40 %–"uncertainty band" estimated in [36]. This however helps us to display a conservative estimate of possible uncertainties. We conclude that the WW–approximation works reasonably well possibly except for very small x at HERMES, see Fig. 2.

Presently $h_L^a(x)$ is unknown. With phenomenological information on $h_1^a(x)$ [37–39], the WW approximation (3.2b) for $h_L^a(x)$ could be tested experimentally in Drell-Yan [40].

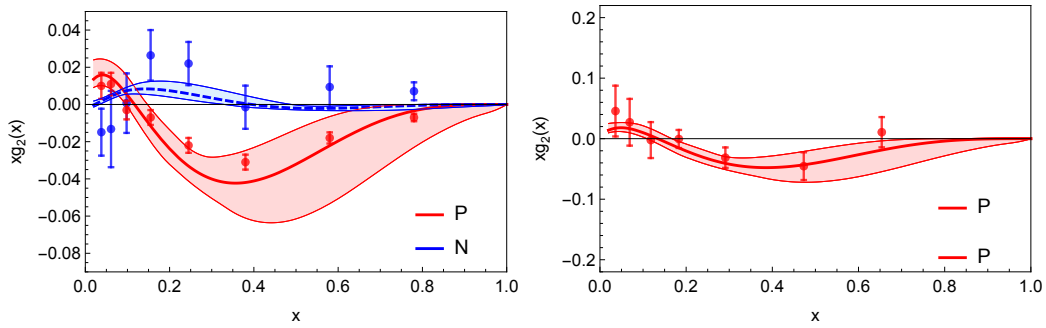

Figure 2. The structure function $xg_2(x)$ in WW-approximation at $Q^2 = 7.1\,\text{GeV}^2$, Eq. (3.9), for proton (P) and neutron (N) targets. Left panel: data from E144 and E155 experiments at $\langle Q^2\rangle = 7.1\,\text{GeV}^2$ [18, 19]. Right panel: HERMES data at $\langle Q^2\rangle = 2.4\,\text{GeV}^2$ [20]. The estimate of the theoretical uncertainty is described in the text.

3.5 Tests in lattice QCD

The lowest Mellin moments of the PDF $g_T^q(x)$ were studied in lattice QCD in the quenched approximation [16] and with $N_f = 2$ flavors of light dynamical quarks [17]. The obtained results were compatible with a small $\tilde{g}_T^q(x)$. We are not aware of lattice QCD studies related to the PDF $h_L^a(x)$, and turn now our attention to TMD studies in lattice QCD.

After first exploratory investigations of TMDs on the lattice [41, 42], recent years have witnessed considerable progress and improvements with regard to rigor, realism and methodology [43–46]. However, numerical results from recent calculations are only available for a subset of observables, and the quantities calculated are not in a form that lends itself to straighforward tests of the WW-type relations as presented in this paper. Details about recent works and future perspectives are discussed at the end of this section.

For the time being, we content ourselves with rather crude comparisons based on the data published in Refs. [41, 42]. These early works explored all nucleon and quark polarizations, but they used a gauge link that does not incorporate the final or initial state interactions present in SIDIS or Drell-Yan experiments. In other words, the transverse momentum dependent quantities computed in [41, 42] are not precisely the TMDs measurable in experiment. More caveats will be discussed along the way.

Let us now translate the approximations (3.6a, 3.6b) into expressions for which we have a chance to compare them with available lattice data. For that we multiply the Eqs. (3.6a, 3.6b) by x^N with $N = 0,\ 1,\ 2,\ \ldots$ and integrate over $x \in [-1, 1]$ which yields

$$\int_{-1}^{1} dx\ x^N g_{1T}^{\perp(1)q}(x) \overset{\text{WW-type}}{\approx} \frac{1}{N+2} \int_{-1}^{1} dx\ x^{N+1} g_1^q(x)\ , \tag{3.11}$$

$$\int_{-1}^{1} dx\ x^N h_{1L}^{\perp(1)q}(x) \overset{\text{WW-type}}{\approx} -\frac{1}{N+3} \int_{-1}^{1} dx\ x^{N+1}\, h_1^q(x)\ . \tag{3.12}$$

with the understanding that negative x refer to antiquark distributions $g_1^{\bar{q}}(x) = +\, g_1^q(-x)$, $h_1^{\bar{q}}(x) = -\, h_1^q(-x)$, $g_{1T}^{\perp(1)\bar{q}}(x) = -g_{1T}^{\perp(1)q}(-x)$, $h_{1L}^{\perp(1)\bar{q}}(x) = +\, h_{1L}^{\perp(1)q}(-x)$ depending on C–parity of the involved operators [1]. The right hand sides of Eqs. (3.11, 3.12) are x–moments of parton distributions, and those can be obtained from lattice QCD using well-established methods based on operator product expansion. The left hand sides are moments of TMDs in x and $\boldsymbol{k}_\perp$. We have to keep in mind that TMDs diverge for large $\boldsymbol{k}_\perp$. Therefore, without regularizing these divergences in a scheme suitable for the comparison of left and right hand side, a test of the above relations is meaningless, even before we get to address the issues of lattice calculations. Let us not give up at this point and take a look at the lattice observables of Ref. [42]. Here, the TMDs are obtained from amplitudes $\tilde{A}_i(l^2, \ldots)$ in Fourier space, where $\boldsymbol{k}_\perp$ is encoded in the Fourier conjugate variable $\boldsymbol{\ell}_\perp$, which is the transverse displacement of quark operators in the correlator evaluated on the lattice. In Fourier-space, the aforementioned divergent behavior for large $\boldsymbol{k}_\perp$ translates into strong lattice scale and scheme dependences at short distances $\boldsymbol{\ell}_\perp$ between the quark operators. The $\boldsymbol{k}_\perp$ integrals needed for the left hand sides of Eqs. (3.11, 3.12) correspond to the amplitudes at $\boldsymbol{\ell}_\perp = 0$, where scheme and scale-dependence is greatest. In Ref. [42] Gaussian fits have been performed to the amplitudes *excluding* data at short quark separations $\boldsymbol{\ell}_\perp$. The Gaussians

describe the long range data quite well and bridge the gap at short distances $\boldsymbol{\ell}_\perp$. Taking the Gaussian fit at $\boldsymbol{\ell}_\perp = 0$, we get a value which is (presumably) largely lattice scheme and scale independent. We have thus swept the problem of divergences under the rug. The Gaussian fit acts as a crude regularization of the divergences that appear in TMDs at large $\boldsymbol{k}_\perp$ and manifest themselves as short range artefacts on the lattice. Casting this line of thought into mathematics, we get

$$\int_{-1}^{1} dx\; g_{1T}^{\perp(1)q}(x) = \int_{-1}^{1} dx \int d^2\boldsymbol{k}_\perp \tfrac{k_\perp^2}{2M^2} g_{1T}^{\perp q}(x,k_\perp) = -2\tilde{A}_{7,q}(\ell=0) \overset{\text{Gaussian}}{=} -c_{7,q} \quad (3.13)$$

$$\int_{-1}^{1} dx\; h_{1L}^{\perp(1)q}(x) = \int_{-1}^{1} dx \int d^2\boldsymbol{k}_\perp \tfrac{k_\perp^2}{2M^2} h_{1T}^{\perp q}(x,k_\perp) = -2\tilde{A}_{10,q}(\ell=0) \overset{\text{Gaussian}}{=} -c_{10,q} \quad (3.14)$$

where the amplitudes $\tilde{A}$ and constants c are those of Ref. [42]. We have thus expressed the left hand side of Eqs. (3.11, 3.12) in terms of amplitudes $c_{7,q}$ and $c_{10,q}$ of the Gaussian fits on the lattice. Before quoting numbers, a few more comments are in order. The overall multiplicative renormalization in Ref. [42] was fixed by setting the Gaussian integral $c_{2,u-d}$ of the unpolarized TMD f_1 in the isovector channel (u-d) to the nucleon quark content, namely, to 1. One then assumes that the normalization of the lattice results for the unpolarized TMD f_1 also fixes the normalization for polarized quantities correctly. This assumption holds if renormalization is mutliplicative and flavor-independent for the non-local lattice operators. This is not true for all lattice actions [43] but presumably it is true if the lattice action preserves chiral symmetry, as it does in the present case. The Gaussian fits along with the normalization prescription serve as a crude form of renormalization, and this is needed to attempt a comparison of left and right hand sides of equations Eqs. (3.11, 3.12).

There is yet another issue to be discussed. The gauge link that goes into the evaluation of the quark-quark correlator introduces a power divergence that has to be subtracted. Ref. [42] employs a subtraction scheme on the lattice but establishes no connection with a subtraction scheme designed for experimental TMDs and the corresponding gauge link geometry. The gauge link renormalization mainly influences the width of the Gaussian fits; the amplitudes are only slightly affected, so it may not play a big role for our discussion. Altogether, the significance of our numerical "tests" of WW-relations should be taken with a grain of salt.

For the test of Eq. (3.11), we use the numbers $\int dx\; g_{1T}^{\perp(1)u}(x) \overset{\text{Gaussian}}{=} -c_{7,u} = 0.1041(85)$ and $\int dx\; g_{1T}^{\perp(1)d}(x) \overset{\text{Gaussian}}{=} -c_{7,d} = -0.0232(42)$ from [42]. Lattice data for $\int dx\, x^N g_1^q(x)$ [47, 48] and $\int dx\, x^N h_1^q(x)$ [49] are available for $N = 0,\ 1,\ 2,\ 3$. These values have been computed using (quasi-) local operators which have been renormalized to the $\overline{MS}$ scheme at the scale $\mu^2 = 4\,\text{GeV}^2$. According to [48] (data set 4: with $a\,m_{u,d} = 0.020$ with $m_\pi \approx 500\,\text{MeV}$) one has $\int dx\; x\, g_1^{u-d}(x) = 0.257(10)$ and $\int dx\; x\, g_1^{u+d}(x) = 0.159(14)$. Decomposing the

results from [48] into individual flavors, and inserting them into Eq. (3.11) we obtain

$$\begin{aligned}
\underbrace{\int dx\; g_{1T}^{\perp(1)u}(x)}_{=0.1041(85)\text{ Ref. [42]}} &\overset{!}{\approx} \underbrace{\frac{1}{2}\int dx\; x\, g_1^u(x)}_{=0.104(9)\text{ Ref. [48]}} \quad , \\
\underbrace{\int dx\; g_{1T}^{\perp(1)d}(x)}_{=-0.0232(42)\text{ Ref. [42]}} &\overset{!}{\approx} \underbrace{\frac{1}{2}\int dx\; x\, g_1^d(x)}_{=-0.025(9)\text{ Ref. [48]}} \quad ,
\end{aligned} \tag{3.15}$$

which confirms the approximation (3.11) for $N = 0$ within the statistical uncertainties of the lattice calculations. In order to test (3.12) we use $\int dx\; h_{1L}^{\perp(1)u}(x) \overset{\text{Gaussian}}{=} -c_{10,u} = -0.0881(72)$ and $\int dx\; h_{1L}^{\perp(1)d}(x) \overset{\text{Gaussian}}{=} -c_{10,d} = 0.0137(34)$ from [42] and the lattice data $\int dx\; x\, h_1^u(x) = 0.28(1)$ and $\int dx\; x\, h_1^d(x) = -0.054(4)$ from QCDSF [49].[1] Inserting these numbers into (3.12) for the case $N = 0$ we obtain

$$\begin{aligned}
\underbrace{\int dx\; h_{1L}^{\perp(1)u}(x)}_{=-0.0881(72)\text{ Ref. [42]}} &\overset{!}{\approx} \underbrace{-\frac{1}{3}\int dx\; x\, h_1^u(x)}_{=-0.093(3)\text{ Ref. [48]}} \quad , \\
\underbrace{\int dx\; h_{1L}^{\perp(1)d}(x)}_{=0.0137(34)\text{ Ref. [42]}} &\overset{!}{\approx} \underbrace{-\frac{1}{3}\int dx\; x\, h_1^d(x)}_{=0.018(1)\text{ Ref. [48]}} \quad .
\end{aligned} \tag{3.16}$$

which again confirms the WW-type approximation within the statistical uncertainties of the lattice calculations.

Several more comments are in order concerning the, at first glance, remarkably good confirmation of the WW-type approximations by lattice data in Eqs. (3.15, 3.16).

First, the relations refer to lattice parameters corresponding to pion masses of 500 MeV. We do not need to worry about that too much. The lattice results do provide a valid test of the approximations in a "hadronic world" with somewhat heavier pions and nucleons. All that matters in our context is that the relative size of $\bar{q}gq$–matrix elements is small with respect to $\bar{q}q$–matrix elements.

Second, we have to revisit carefully which approximations the above lattice calculations actually test. As mentioned above, in the lattice study [41, 42] a specific choice for the path of the gauge link was chosen, which is actually different from the paths required in SIDIS or Drell-Yan. With the path choice of [41, 42] there are effectively only (T-even) A_i amplitudes, the B_i amplitudes are absent. Therefore the test (3.15) of the WW-type approximation (3.11) actually constitutes a test of the WW-approximation (3.2a) and confirms earlier lattice work [16, 17], cf. Refs. [25, 26] and Sec. 3.6. Similarly, the test (3.16) of the WW-type approximation (3.12) actually constitutes a test of the WW-approximation (3.2b). The latter however has not been reported previously in literature, and is a new result.

Third, to be precise: Eqs. (3.15, 3.16) test the first Mellin moments of the WW approximations (3.2a, 3.2b), which corresponds to the Burkardt-Cottingham sum rule for $g_T^a(x)$

[1] These numbers are read off from a figure in [49], and were computed on a different lattice. We interpolate them to a common value of the pion mass $m_\pi \approx 500\,\text{MeV}$, and estimate the uncertainty conservatively in order to take systematic effects into account due to the use of a different lattice.

and an analog sum rule for $h_L^a(x)$, see [32] and references there in. In view of the long debate on the validity of those sum rules [31, 50, 51], this is in an interesting result in itself.

It is important to stress that in view of the pioneering and exploratory status of the TMD lattice calculations [41, 42], this is already a remarkable and very interesting result. Thus, apart from the instanton calculus [15] also lattice data provide support for the validity of the WW approximation (3.2b). At the same time, however, we also have to admit that we do not really reach our goal of testing the WW-type approximations on the lattice. We have to wait for better lattice data. Meanwhile we may try to gain insights into the quality of WW-type approximations from models.

3.6 Tests in models

Effective approaches and models such as bag [12, 52–54], spectator [55], chiral quark-soliton [56], or light-cone constituent [57, 58] models support the approximations (3.2a, 3.2b) for PDFs within an accuracy of $(10-30)\,\%$ at low hadronic scale below 1 GeV.

Turning to TMDs, we recall that in models without gluon degrees of freedom certain relations among TMDs hold, the so-called quark model Lorentz-invariance relations (qLIRs). Initially thought to be exact [1, 27] qLIRs were shown in models with gluons [59, 60] and in QCD [61] to be invalid. They originate from decomposing the (completely unintegrated) quark correlator in terms of Lorentz-invariant amplitudes, and TMDs are certain integrals over those amplitudes. When gluons are absent, the correlator consists of 12 amplitudes [1, 27], i.e. fewer amplitudes than TMDs which implies relations: the qLIRs. In QCD the correct Lorentz decomposition requires the consideration of gauge links which introduces further amplitudes. As a result one has as many amplitudes as TMDs and no relations exist [61]. However, qLIRs "hold" in QCD in the WW-type approximation [25]. In models without gluon degrees of freedom they are exact [25, 26, 54, 55].

The bag, spectator and light-cone constituent quark models support the approximations (3.6a, 3.6b) within an accuracy of $(10-30)\,\%$ [54, 55, 57, 58]. The spectator and bag model support WW-type approximations within $(10-30)\,\%$ [54]. As they are defined in terms of quark bilinear expressions (2.11) it is possible to evaluate twist-3 functions in quark models [12]. The tilde-terms arise due to the different model interactions, and it is important to discuss critically how realistically they describe the $\bar{q}gq$–terms of QCD [62, 63].

In the covariant parton model with intrinsic 3D-symmetric parton orbital motion [64] quarks are free, $\bar{q}gq$ correlations absent, and all WW and WW-type relations exact [65, 66]. The phenomenological success of this approach [64] may hint at a general smallness of $\bar{q}gq$ terms, although many of the predictions from this model have yet to be tested [65].

Noteworthy is the result from the chiral quark soliton model where the WW-type approximation (3.3b) happens to be exact: $x f^{\perp q}(x, k_\perp^2) = f_1^q(x, k_\perp^2)$ for quarks and antiquarks [62]. The degrees of freedom in this model are quarks, antiquarks and Goldstone bosons which are strongly coupled (the coupling constant is ~ 4) and has to be solved using nonperturbative techniques (expansion in $1/N_c$ where N_c is the number of colors) with the nucleon described as a chiral soliton. In general the model predicts non-zero tilde-terms, for instance $\tilde{e}^a(x) \neq 0$ [67–69]. However, despite strong interactions in this effective theory, the

tilde term $\tilde{f}^{\perp q}(x, k_\perp^2)$ vanishes exactly in this model [62] and the WW-type approximation (3.3b) becomes exact at the low initial scale of this model of $\mu_0 \sim 0.6\,\text{GeV}$.

Let us finally discuss quark-target models, where gluon degrees of freedom are included and WW(-type) approximations badly violated [59, 60, 70, 71]. This is natural in this class of models for two reasons. First, quark-mass terms are of $\mathcal{O}(m_q/M_N)$ and negligible in the nucleon case, but of $\mathcal{O}(100\,\%)$ in a quark target where m_q plays also the role of M_N. Second, even if one refrains from mass terms the approximations are spoiled by gluon radiation, see for instance [72] in the context of (3.2a). This means that perturbative QCD does not support the WW-approximations: they certainly are not preserved by evolution. However, scaling violations *per se* do not need to be large. What is crucial in this context are dynamical reasons for the smallness of the *matrix elements* of $\bar{q}gq$–operators. This requires the consideration of chiral symmetry breaking effects reflected in the hadronic spectrum, as considered in the instanton vacuum model [14, 15] but out of scope in quark-target models.

We are not aware of systematic tests of WW-type approximations for FFs. One information worth mentioning in this context is that in spectator models [55] tilde-contributions to FFs are proportional to the offshellness of partons [62, 63]. This natural feature may indicate that in the region dominated by effects of small $P_\perp$ tilde-terms might be small. On the other hand, quarks have sizable constituent masses of the order of few hundred MeV in spectator models and the mass-terms are not small. The applicability of WW-type approximations to FFs remains the least tested point in our approach.

3.7 Basis functions for the WW-type approximations

The leading–twist 6 TMDs $f_1^a,\ f_{1T}^{\perp a},\ g_1^a,\ h_1^a,\ h_1^{\perp a},\ h_{1T}^{\perp a}$ and 2 FFs $D_1^a,\ H_1^{\perp a}$ provide a basis. Below we shall see that, under the assumption of the validity of WW-type approximations, it is possible to express all SIDIS structure in terms of the basis functions. Notice that SIDIS alone is of course not sufficient to determine the basis functions uniquely: the 8 basis functions appear in 6 SIDIS structure functions. It is crucial to take advantage of other processes: Drell-Yan for PDFs and TMDs and hadron production in e^+e^- annihilation for FFs. Other processes play also important roles.

These basis functions allow us to describe in WW-type approximation all other TMDs, and experiments will decide how well the approximations work. In some cases, however, we know in advance that the WW-type approximations have limitations, see next section.

3.8 Limitation of WW-type approximation for certain T-odd TMDs

The WW-type approximations have limitations in the description of those twist-3 T-odd TMDs which appear in the decomposition of the correlator (2.11) with no prefactor of $k_\perp$. There are three cases: $f_T^a(x, k_\perp)$, $h^a(x, k_\perp)$, $e_L^a(x, k_\perp)$. Such TMDs in principle survive integration of the correlator over $k_\perp$ and would have PDF counterparts if there were not the sum rules in Eq. (2.14). These sum rules arise because hypothetical PDF versions of T-odd TMDs vanish: they have a simple straight gauge link along the lightcone, and such objects vanish due to parity and time-reversal symmetry of strong interactions. This argument does not apply to other T-odd TMDs because they drop out from the $k_\perp$–integrated correlator due to explicit factors of e.g. $k_\perp^j$ in the case of the Sivers function.

Let us first discuss the case of $f_T^a(x,k_\perp)$. Taking the WW-type approximation (3.4g) literally means $x\int d^2k_\perp\, f_T^a(x,k_\perp) \stackrel{!?}{=} -f_{1T}^{\perp(1)a}(x) \neq 0$ at variance with the sum rule (2.14). We have $xf_T^a(x,k_\perp) = x\tilde{f}_T^a(x,k_\perp) - f_{1T}^{\perp(1)a}(x,k_\perp)$ from QCD equations of motion [4] which yields (3.4g). The point is that in this case it is essential to keep the tilde-function. The situation for the chirally and T-odd twist-3 TMD $h^a(x,k_\perp)$ is analog. The third function in (2.14) causes no issues since $e_L^a(x,k_\perp) = \tilde{e}_L^a(x,k_\perp) \approx 0$ in WW-type approximation.

Does this mean WW-type approximations fail for $f_T^a(x,k_\perp)$ and $h^a(x,k_\perp)$? Not necessarily. One has to keep in mind the formal character of the sum rules (2.14) which include integration in the large-$k_\perp$ region where the TMD description does not apply. Thus, issues with the sum rules (2.14) do not need to exclude the possibility that the WW-type approximations for $f_T^a(x,k_\perp)$ and $h^a(x,k_\perp)$ in (3.4g, 3.4h) may work at small $k_\perp$ where we use them in our TMD approach. This would mean the UV region is essential to realize the sum rules (2.14). Alternatively, one could also envision the sum rules (2.14) to be sensitive to the IR region through gluonic or fermionic pole contributions manifest in tilde-terms.

Presently too little is known in the theory of subleading twist TMDs. Below in Sec. 7.6 and 7.8 we will present a pragmatic solution how to deal with the TMDs $f_T^a(x,k_\perp)$ and $h^a(x,k_\perp)$ phenomenologically. For now let us keep in mind that one has to keep a vigilant eye on all WW-type approximations, and especially on those for $f_T^a(x,k_\perp)$ and $h^a(x,k_\perp)$.

4 SIDIS in WW-type approximation and Gaussian model

In this section we consequently apply the WW- and WW-type approximation to SIDIS, and describe our procedure to evaluate the structure functions in this approximation and the Gaussian Ansatz which we use to model the $k_\perp$ dependence of TMDs.

4.1 Leading structure functions amenable to WW-type approximations

The WW- and WW-type approximations are useful for the following two leading–twist structure functions

$$F_{LT}^{\cos(\phi_h-\phi_S)} \stackrel{\text{WW}}{=} \mathcal{C}\left[\omega_{\text{B}}^{\{1\}}\, g_{1T}^\perp D_1\right]\Big|_{\substack{g_{1T}^{\perp a}\to g_1^a \\ \text{Eq. (3.6a)}}} \tag{4.1a}$$

$$F_{UL}^{\sin 2\phi_h} \stackrel{\text{WW}}{=} \mathcal{C}\left[\omega_{\text{AB}}^{\{2\}}\, h_{1L}^\perp H_1^\perp\right]\Big|_{\substack{h_{1L}^{\perp a}\to h_1^a \\ \text{Eq. (3.6b)}}} \tag{4.1b}$$

4.2 Subleading structure functions in WW-type approximations

In the case of the subleading twist structure functions the WW-type approximations in Eqs. (3.3a–3.4h) lead to considerable simplifications. We obtain the approximations

$$F_{LU}^{\sin\phi_h} \overset{\text{WW}}{=} 0\,, \tag{4.2a}$$

$$F_{LT}^{\cos\phi_S} \overset{\text{WW}}{=} \frac{2M}{Q}\,\mathcal{C}\Big[-\omega^{\{0\}}\,x\,g_T D_1\Big]\Big|_{\substack{g_T^a \to g_1^a \\ \text{Eq. (3.2a)},}} \tag{4.2b}$$

$$F_{LL}^{\cos\phi_h} \overset{\text{WW}}{=} \frac{2M}{Q}\,\mathcal{C}\Big[-\omega_{\text{B}}^{\{1\}}\,x g_L^\perp D_1\Big]\Big|_{\substack{g_L^{\perp a} \to g_1^a \\ \text{Eq. (3.3c)},}} \tag{4.2c}$$

$$F_{LT}^{\cos(2\phi_h-\phi_S)} \overset{\text{WW}}{=} \frac{2M}{Q}\,\mathcal{C}\Big[-\omega_{\text{C}}^{\{2\}}\,x g_T^\perp D_1\Big]\Big|_{\substack{g_T^{\perp a} \to g_1^a \\ \text{Eqs. (3.3d, 3.6a)},}} \tag{4.2d}$$

$$F_{UL}^{\sin\phi_h} \overset{\text{WW}}{=} \frac{2M}{Q}\,\mathcal{C}\Big[\;\omega_{\text{A}}^{\{1\}}\,x\,h_L H_1^\perp\Big]\Big|_{\substack{h_L^a \to h_{1L}^{\perp a} \\ \text{with Eq. (3.3f)},}} \tag{4.2e}$$

$$F_{UU}^{\cos\phi_h} \overset{\text{WW}}{=} \frac{2M}{Q}\,\mathcal{C}\Big[\;\omega_{\text{A}}^{\{1\}}\,x\,h\,H_1^\perp - \omega_{\text{B}}^{\{1\}}\,x\,f^\perp D_1\Big]\Big|_{\substack{f^{\perp a} \to f_1^a,\; h^a \to h_1^{\perp a} \\ \text{with Eqs. (3.3b, 3.4h)},}} \tag{4.2f}$$

$$F_{UT}^{\sin\phi_S} \overset{\text{WW}}{=} \frac{2M}{Q}\,\mathcal{C}\Big[\;\omega^{\{0\}}\,x\,f_T D_1 - \frac{\omega_{\text{B}}^{\{2\}}}{2}\,(x h_T - x h_T^\perp)\,H_1^\perp\Big]\Big|_{\substack{f_T^a \to f_{1T}^{\perp a}, \\ h_T^a - h_T^{\perp a} \to h_1^a \\ \text{(3.4g, 3.3g, 3.3h)},}} \tag{4.2g}$$

$$F_{UT}^{\sin(2\phi_h-\phi_S)} \overset{\text{WW}}{=} \frac{2M}{Q}\,\mathcal{C}\Big[\,\omega_{\text{C}}^{\{2\}}\,x\,f_T^\perp D_1 + \frac{\omega_{\text{AB}}^{\{2\}}}{2} x(h_T + h_T^\perp) H_1^\perp\Big]\Big|_{\substack{f_T^{\perp a} \to f_{1T}^{\perp a}, \\ (h_T^a + h_T^{\perp a}) \to h_{1T}^{\perp a} \\ \text{with (3.4f, 3.3g, 3.3h)}.}} \tag{4.2h}$$

4.3 Gaussian Ansatz for TMDs

In this work we will use the so-called Gaussian Ansatz for the TMDs and FFs. This Ansatz, which for a generic TMD or FF is given by

$$f(x,k_\perp^2) = f(x)\,\frac{e^{-k_\perp^2/\langle k_\perp^2\rangle}}{\pi\langle k_\perp^2\rangle}\,, \quad D(z,P_\perp^2) = D(z)\,\frac{e^{-P_\perp^2/\langle P_\perp^2\rangle}}{\pi\langle P_\perp^2\rangle}\,, \tag{4.3}$$

is popular not only because it considerably simplifies the calculations. In fact, all convolution integrals of the type (2.17) can be solved analytically with this Ansatz. Far more important is the fact that it works phenomenologically with a good accuracy in many practical applications [73–78]. Of course this Ansatz is only a rough approximation. For instance, it is not consistent with general matching expectations when $k_\perp$ becomes large [79].

Nevertheless, if one limits oneself to work in a regime where the transverse momenta (of hadrons produced in SIDIS, dileptons produced in the Drell-Yan process, etc) are small compared to the hard scale in the process, then the Ansatz works quantitatively very well. The most recent and detailed tests were reported in [76], where the Gaussian Ansatz was shown to describe the most recent SIDIS data: no deviations were observed within the error bars of the data provided one takes into account the broadening of the Gaussian widths with increasing energy [76] according with expectations from QCD [80]. The Gaussian Ansatz is approximately compatible with the $k_\perp$–shapes obtained from evolution [80] or fits to high-energy Tevatron data on weak-boson production [81]. Effective models at low [54, 57, 58] and high [66] renormalization scales support this Ansatz as a good approximation.

4.4 Evaluation of structure functions in WW-type & Gaussian approximation

The Gaussian Ansatz is compatible with many WW-type type approximations but not all. The trivial approximations (3.3a) and (3.4a–3.4e) of course cause no issue. The Gaussian Ansatz can also be applied to the nontrivial approximations in Eqs. (3.3b–3.3d) and (3.4f), provided the corresponding Gaussian widths are defined to be equal to each other: for example, in the WW-type approximation (3.3b), $xf^{\perp q}(x,k_\perp^2) \approx f_1^q(x,k_\perp^2)$, one may assume Gaussian $k_\perp$–dependence for $f^{\perp q}(x,k_\perp^2)$ and for $f_1^q(x,k_\perp^2)$ as long as the Gaussian widths of these two TMDs are assumed to be equal.

In the case of the approximations (3.3e–3.3h) the situation is different because here twist-3 TMDs are related to transverse moments of twist-2 TMDs. In such cases the Gaussian Ansatz is not compatible with the WW-type approximations: for instance, the approximation (3.3e) relates $xg_T^q(x,k_\perp^2) \approx \frac{k_\perp^2}{2M_N^2}\, g_{1T}^q(x,k_\perp^2)$, i.e. if $g_{1T}^q(x,k_\perp^2)$ was exactly Gaussian then $g_T^q(x,k_\perp^2)$ certainly could not be Gaussian. If one wanted to take the Gaussian Ansatz and WW-type approximations literally, one clearly would deal with an incompatibility. However, we of course must keep in mind that both are approximations.

Some comments are in order to understand how the usage of the Gaussian Ansatz and the WW-type approximations can be reconciled. First, let us remark that the individual TMDs, say $g_T^q(x,k_\perp^2)$ and $g_{1T}^q(x,k_\perp^2)$ in our example, may each by itself be assumed to be approximately Gaussian in $k_\perp$ which is supported by quark model calculations [54]. Second, we actually do not need the unintegrated WW-type approximations. For phenomenological applications we can use the WW-type approximations in "integrated form."

Let us stress that if one took an unintegrated WW-type approximation of the type $xg_T^q(x,k_\perp^2) \approx \frac{k_\perp^2}{2M_N^2}\, g_{1T}^q(x,k_\perp^2)$ literally and assumed both TMDs to be exactly Gaussian, one would find "incompatibilities:" perhaps most strikingly in the limit $k_\perp \to 0$ where the left-hand side is finite while the right-hand side vanishes. However, such incompatibilities are washed out and not apparent after the convolution integrals defining the structure functions are solved. Notice that the failure of the WW-type approximations (3.3e–3.3h) in the limit $k_\perp \to 0$ is not specific to the Gaussian model, but a general feature caused by neglecting tilde-terms. This indicates a practical scheme how to use responsibly the WW-type approximations in Eqs. (3.3e–3.3h).

Our procedure is as follows. In a first step we assume that all TMDs and FFs are (approximately) Gaussian, and solve the convolution integrals. In the second step we use the integrated WW-type approximations to simplify the results for the structure functions.

Notice that in some cases (when T-even TMDs are involved) one could choose a different order of the steps: first apply WW-type approximations and then solve convolution integrals with Gaussian Ansatz. In general this would yield different (and bulkier) analytical expressions, but we convinced ourselves that the differences are numerically within the accuracy expected for this approach. However, for the structure functions discussed in Secs. 7.6 and 7.8 such an "alternative scheme" would give results at variance with the sum rules in for the twist-3 T-odd TMDs in Eq. (2.14), as discussed in Sec. 3.8. The scheme presented here will allow us to implement those sum rules in a convenient and consistent way. We will follow up on this in more detail in Secs. 7.6 and 7.8.

To summarize, our procedure is to solve first the convolution integrals in Gauss Ansatz, and use then WW-type approximations. When implementing this procedure we will see that the results for the structure functions can be conveniently expressed in terms of the basis TMDs or their adequate transverse moments.

4.5 Phenomenological information on basis functions

We have seen that the following 6 TMDs and 2 FFs provide a basis (Sec. 3) and allow us to express all SIDIS structure functions (Sec. 4) in WW-type approximation:

$$\text{basis:} \quad f_1^a,\ f_{1T}^{\perp a},\ g_1^a,\ h_1^a,\ h_1^{\perp a},\ h_{1T}^{\perp a};\ D_1^a,\ H_1^{\perp a}\,. \tag{4.4}$$

Phenomenological information is available for all basis functions at least to some extent. In Fig. 3 we present plots of the basis functions, and refer to App. A for details. The four functions f_1^a, g_1^a, h_1^a, D_1^a are related to twist-2 collinear functions. All collinear functions are calculated at $Q^2 = 2.4$ GeV^2. Collinear $f_1^a(x)$ are from Ref. [82], $g_1^a(x)$ are from

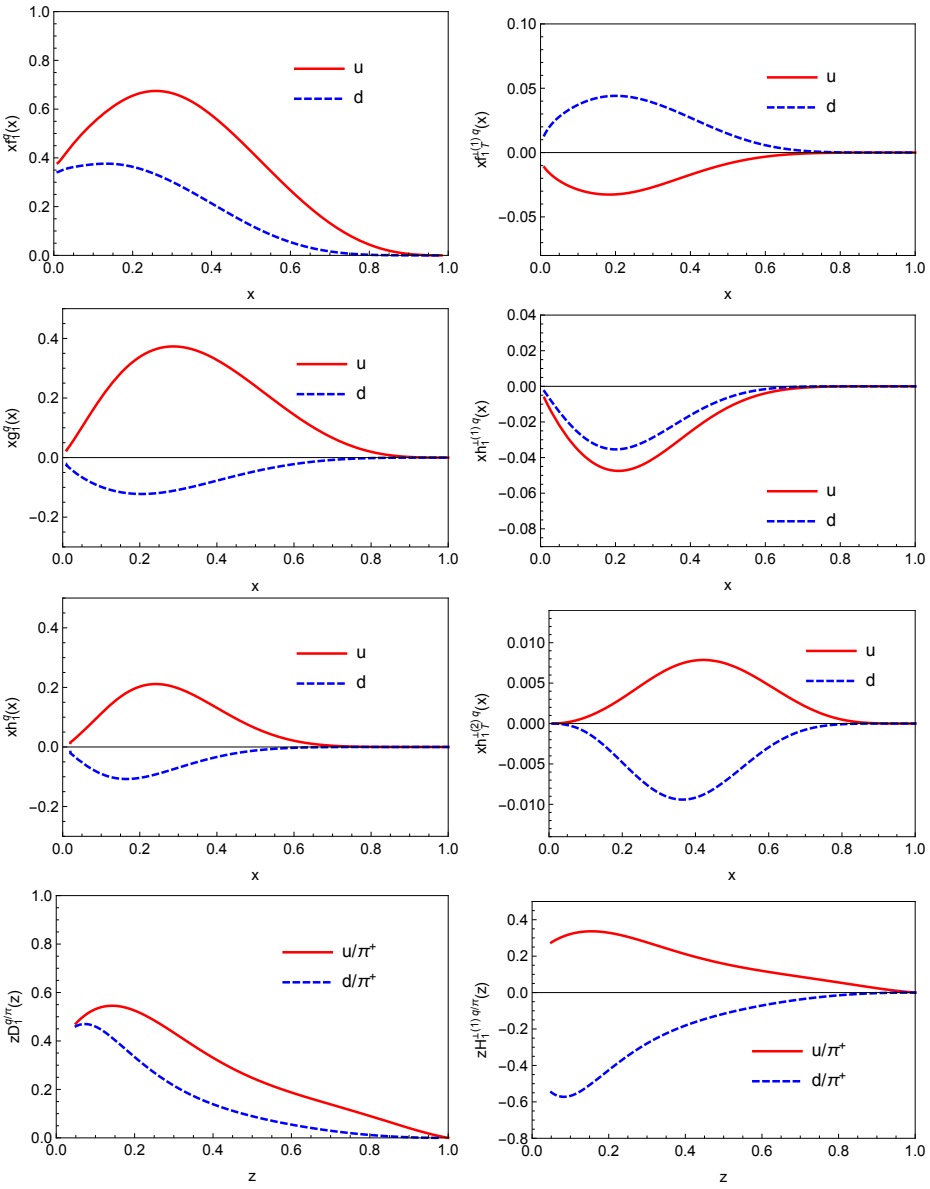

Figure 3. The basis functions f_1^a, g_1^a, h_1^a, $f_{1T}^{\perp a}$, $h_1^{\perp a}$, $h_{1T}^{\perp a}$; D_1^a, $H_1^{\perp a}$. For details see App. A.

Ref. [83], and D_1^a are from Ref. [84]. The other four TMDs have no collinear counterparts. For $f_{1T}^{\perp a}$, $h_1^{\perp a}$, $H_1^{\perp a}$ it is convenient to consider their (1)-moments, and for $h_{1T}^{\perp a}$ the (2)-moment. This has two important advantages. First, this step simplifies the Gaussian model expressions, and the Gaussian width parameters are largely absorbed in the definitions of the transverse moments which helps to minimize the model-dependence. Second, the $k_\perp$–moments of these TMDs have in principle simple definitions in QCD (whereas e.g. the function $f_{1T}^{\perp q}(x)$ can be computed in models but is very cumbersome to define in QCD). Thus the parametrizations for the basis functions read

$$f_1^a(x,k_\perp^2) = f_1^a(x)\,\frac{1}{\pi\langle k_\perp^2\rangle_{f_1}}\,e^{-k_\perp^2/\langle k_\perp^2\rangle_{f_1}}\,, \tag{4.5a}$$

$$D_1^a(z,P_\perp^2) = D_1^a(z)\,\frac{1}{\pi\langle P_\perp^2\rangle_{D_1}}\,e^{-P_\perp^2/\langle P_\perp^2\rangle_{D_1}}\,, \tag{4.5b}$$

$$g_1^a(x,k_\perp^2) = g_1^a(x)\,\frac{1}{\pi\langle k_\perp^2\rangle_{g_1}}\,e^{-k_\perp^2/\langle k_\perp^2\rangle_{g_1}}\,, \tag{4.5c}$$

$$h_1^q(x,k_\perp^2) = h_1^q(x)\,\frac{1}{\pi\langle k_\perp^2\rangle_{h_1}}\,e^{-k_\perp^2/\langle k_\perp^2\rangle_{h_1}}\,, \tag{4.5d}$$

$$H_1^\perp(z,P_\perp^2) = H_1^{\perp(1)}(z)\,\frac{2z^2m_h^2}{\pi\langle P_\perp^2\rangle_{H_1^\perp}^2}\,e^{-P_\perp^2/\langle P_\perp^2\rangle_{H_1^\perp}}\,, \tag{4.5e}$$

$$f_{1T}^{\perp q}(x,k_\perp^2) = f_{1T}^{\perp(1)q}(x)\,\frac{2M^2}{\pi\langle k_\perp^2\rangle_{f_{1T}^\perp}^2}\,e^{-k_\perp^2/\langle k_\perp^2\rangle_{f_{1T}^\perp}}\,, \tag{4.5f}$$

$$h_1^{\perp q}(x,k_\perp^2) = h_1^{\perp(1)q}(x)\,\frac{2M^2}{\pi\langle k_\perp^2\rangle_{h_1^\perp}^2}\,e^{-k_\perp^2/\langle k_\perp^2\rangle_{h_1^\perp}}\,, \tag{4.5g}$$

$$h_{1T}^{\perp q}(x,k_\perp^2) = h_{1T}^{\perp(2)q}(x)\,\frac{2M^4}{\pi\langle k_\perp^2\rangle_{h_{1T}^\perp}^3}\,e^{-k_\perp^2/\langle k_\perp^2\rangle_{h_{1T}^\perp}}\,. \tag{4.5h}$$

The parametrizations of the basis functions and the Gaussian model parameters are described in detail in App. A.

5 Leading twist asymmetries and basis functions

In this section we review how the basis functions describe available SIDIS data. This is of importance to asses the reliability of the predictions presented in the next sections.

5.1 Leading twist F_{UU} and Gaussian Ansatz

As explained in Sec. 4.3 the Gaussian Ansatz is chosen not only because it considerably simplifies the calculations, but more importantly because it works phenomenologically with a good accuracy in many processes including SIDIS [73–78].

The Gaussian Ansatz for the unpolarized TMD and FF is given by Eqs. (4.5a, 4.5b). The parameters $\langle k_\perp^2\rangle_{f_1}$ and $\langle P_\perp^2\rangle_{D_1}$ can be assumed to be flavor- and x– or z–dependent, as present data do not allow us to constrain too many parameters, see App. A.1 for a review. This assumption can be relaxed, e.g. theoretical studies in chiral effective field theories predict a strong flavor-dependence in the $k_\perp$–behavior of sea and valence quark TMDs [85].

The structure function F_{UU} needed for our analysis reads

$$F_{UU}(x,z,P_{hT}) = x\sum_q e_q^2\, f_1^q(x)\, D_1^q(z)\, \mathcal{G}(P_{hT})\,, \tag{5.1a}$$

$$F_{UU}(x,z) = x\sum_q e_q^2\, f_1^q(x)\, D_1^q(z)\,, \tag{5.1b}$$

where we introduce the notation $\mathcal{G}(P_{hT})$, which is defined as

$$\mathcal{G}(P_{hT}) = \frac{\exp(-P_{hT}^2/\lambda)}{\pi\,\lambda}\,, \quad \lambda = z^2\,\langle k_\perp^2\rangle_{f_1} + \langle P_\perp^2\rangle_{D_1}\,, \tag{5.2}$$

with the understanding that the convenient abbreviation λ is expressed in terms of the Gaussian widths of the *preceeding* TMD and FF. Notice that $\mathcal{G}(P_{hT}) \equiv \mathcal{G}(x,z,P_{hT})$ and that in general $\mathcal{G}(P_{hT})$ appears under the flavor sum due to a possible flavor-dependence of the involved Gaussian widths. The normalization $\int d^2P_{hT}\,\mathcal{G}(P_{hT}) = 1$ correctly connects the structure function $F_{UU}(x,z,P_{hT})$ in (5.1a) with its P_{hT}–integrated counterpart (5.1b). In our effective description this is step is trivial. In QCD the connection of TMDs to PDFs is subtle [89]. Figure 4 illustrates how the Gaussian Ansatz describes selected SIDIS data: the left panel shows CLAS data [86] on π^+ production from proton with a 5.75 GeV beam which exhibit Gaussian P_{hT}–dependence over 2 orders of magnitude, see [76] for details. The middle panel in Fig. 4 displays the HERMES multiplicity [87]

$$M_n^h(x,z,P_{hT}) \equiv 2\pi P_{hT}\frac{F_{UU}(x,z,P_{hT})}{x\sum_q e_q^2\, f_1^q(x)} \tag{5.3}$$

at $\langle Q^2\rangle = 2.87\,\mathrm{GeV}^2$, $\langle x\rangle = 0.15$, $\langle z\rangle = 0.22$ for π^+ production on the proton target. The right panel of Fig. 4 shows the COMPASS multiplicity [88]

$$n^h(x,z,P_{hT}) \equiv \pi\frac{F_{UU}(x,z,P_{hT})}{x\sum_q e_q^2\, f_1^q(x)} \tag{5.4}$$

at $\langle Q^2\rangle = 20\,\mathrm{GeV}^2$, $\langle x\rangle = 0.15$, $\langle z\rangle = 0.2$ for h^+ production on the deuterium target.

To streamline the presentation we refer to the comprehensive Appendix on the used parametrizations (App. A), and for technical details on the Gaussian Ansatz (App. B).

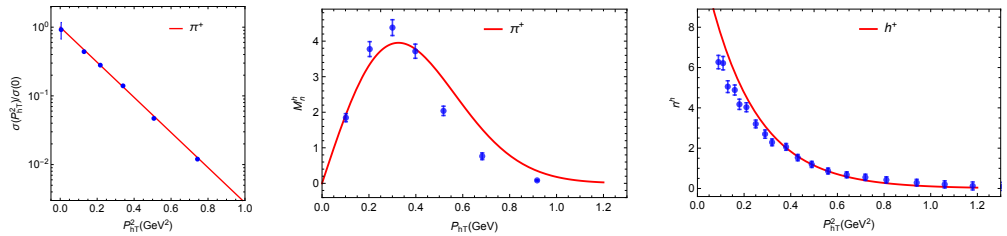

Figure 4. Examples of the description of transverse momenta of hadrons in unpolarized SIDIS. Left panel: $F_{UU}(P_{hT}^2)$ for π^+ production normalized with respect to its value at zero transverse momentum at $\langle Q^2\rangle = 2.37\,\mathrm{GeV}^2$, $\langle x\rangle = 0.24$, $\langle z\rangle = 0.30$ at JLab with 5.75 GeV beam [86], cf. [76]. Middle panel: HERMES multiplicity (5.3) at $\langle Q^2\rangle = 2.87\,\mathrm{GeV}^2$, $\langle x\rangle = 0.15$, $\langle z\rangle = 0.22$ from [87]. Right panel: COMPASS multiplicity (5.4) at $\langle Q^2\rangle = 20\,\mathrm{GeV}^2$, $\langle x\rangle = 0.15$, $\langle z\rangle = 0.2$ from [88].

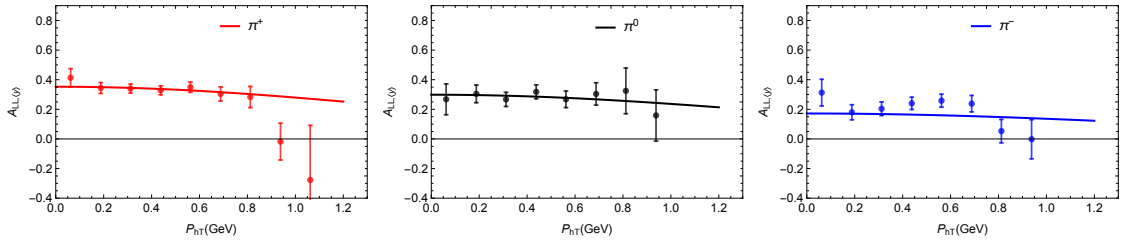

Figure 5. $A_{LL,\langle y\rangle}$ asymmetry compared to JLab data [90] for π^+, π^0, π^-. The solid lines are our computations for the mean values of kinematical variable $\langle x\rangle = 0.25$, $\langle z\rangle = 0.5$, $\langle Q^2\rangle = 1.67$ GeV^2.

5.2 Leading twist A_{LL} and first test of Gaussian Ansatz in polarized scattering

The Gaussian Ansatz is useful in unpolarized case [73–78], but nothing is known about its applicability to spin assymetries. The JLab data [90] on $A_{LL}(P_{hT})$ put us in the position to conduct a first "test" for polarized partons. We assume Gaussian form for $g_1^a(x, k_\perp^2)$, Eq. (4.5c), and use lattice QCD results [41] to estimate the width $\langle k_\perp^2\rangle_{g_1}$, see App. A.2. With $\lambda = z^2\langle k_\perp^2\rangle_{g_1} + \langle P_\perp^2\rangle_{D_1}$ implicit in $\mathcal{G}(P_{hT})$, the structure function F_{LL} reads

$$F_{LL}(x, z, P_{hT}) = x \sum_q e_q^2\, g_1^q(x)\, D_1^q(z)\, \mathcal{G}(P_{hT})\,, \tag{5.5a}$$

$$F_{LL}(x, z) = x \sum_q e_q^2\, g_1^q(x)\, D_1^q(z)\,. \tag{5.5b}$$

The first experimental results on the P_{hT}–dependence of $A_{LL} = F_{LL}/F_{UU}$ were presented by Jefferson Lab (JLab) [90]. The definition of the asymmetry in [90] was

$$A_{LL,\langle y\rangle}(x, z, P_{hT}) = \langle p_2\, A_{LL}(x, z, P_{hT})\rangle = \frac{\langle y(2-y)\, F_{LL}(x, z, P_{hT})\rangle}{\langle (1+(1-y)^2)\, F_{UU}(x, z, P_{hT})\rangle} \tag{5.6}$$

where $p_2 = y(2-y)/(1+(1-y)^2)$ and averaging (separately in numerator and denominator) over the kinematics of [90] is implied. We use the lattice data [41] to constrain the Gaussian width $\langle k_\perp^2\rangle_{g_1}$ as described in App. A.2. All other ingredients in (5.6) are known and tested through other observables in Sec. 5.1. Therefore the comparison of our results to JLab data [90] shown in Fig. 5 provides several important tests.[2] First, the JLab data [90] are compatible with the Gaussian Ansatz within error bars. Second, the lattice results in the way we use them in App. A.2 give an appropriate description of the data.

Encouraged by these findings we will use lattice predictions from Ref. [41] below also for the Gaussian widths of $g_{1T}^{\perp(1)a}$ and $h_{1L}^{\perp(1)a}$. Of course, at this point one could argue that the WW- and WW-type approximations (3.6a, 3.6b) also dictate that $g_{1T}^\perp$ and $h_{1L}^\perp$ have the same Gaussian widths as g_1 and h_1. In fact, the lattice results for the respective widths are numerically similar, which can be interpreted as yet another argument in favor of the usefulness of the approximations. The practical predictions depend only weakly on the choice of parameters.

[2] Another important test was already presented in [90]: the P_{hT}–integrated ("collinear") asymmetry (5.5b) is compatible with data from other experiments and with theoretical results obtained from parametrizations of $f_1^a(x)$, $g_1^a(x)$, $D_1^a(z)$. This shows that even at the moderate beam energies of the pre-12GeV era one was indeed probing DIS at JLab, at least to a very good approximation [90].

5.3 Leading twist $A_{UT}^{\sin(\phi_h-\phi_S)}$ Sivers asymmetry

The $F_{UT}^{\sin(\phi_h-\phi_S)}$ structure function is related to the Sivers function [91], which describes the distribution of unpolarized quarks inside a transversely polarized proton, has so far received the widest attention, from both phenomenological and experimental points of view.

The Sivers function $f_{1T}^{\perp}$ is related to initial and final state interactions of the struck quark and the rest of the nucleon and could not exist without the contribution of the orbital angular momentum of partons to the spin of the nucleon. As such it encodes the correlation between the partonic intrinsic motion and the transverse spin of the nucleon, and it generates a dipole deformation in momentum space. Over the years, the Sivers function has been extracted from SIDIS data by several groups, with consistent results [74, 92–98].

The structure function $F_{UT}^{\sin(\phi_h-\phi_S)}$ reads

$$F_{UT}^{\sin(\phi_h-\phi_S)}(x,z,P_{hT}) \;=\; -x\sum_q e_q^2\, f_{1T}^{\perp(1)q}(x)\, D_1^q(z)\, b_{\rm B}^{(1)}\left(\frac{zP_{hT}}{\lambda}\right)\mathcal{G}(P_{hT})\,, \tag{5.7a}$$

$$F_{UT}^{\sin(\phi_h-\phi_S)}(x,z,\langle P_{hT}\rangle) \;=\; -x\sum_q e_q^2\, f_{1T}^{\perp(1)q}(x)\, D_1^q(z)\, c_{\rm B}^{(1)}\left(\frac{z}{\lambda^{1/2}}\right), \tag{5.7b}$$

where $\lambda = z^2\langle k_\perp^2\rangle_{f_{1T}^\perp} + \langle P_\perp^2\rangle_{D_1}$ and $b_{\rm B}^{(1)} = 2M_N$ and $c_{\rm B}^{(1)} = \sqrt{\pi}\,M_N$, see App. B.5 for details.

Notice that integrating structure functions over P_{hT} is different from integrating the cross section over P_{hT} where azimuthal hadron modulations drop out. Only if the relevant weight is $\omega^{\{0\}}$ we obtain "collinear structure functions:" $F_{UU}(x,z)$, $F_{LL}(x,z)$ in Secs. 5.1, 5.2 and below in Secs. 7.2, 7.6. In all other cases, despite integration over P_{hT}, we end up always with true convoluted TMDs (here within Gaussian model). We stress this important point by displaying the dependence of the structure functions on the mean hadron momenta, for instance $F_{UT}^{\sin(\phi_h-\phi_S)}(x,z,\langle P_{hT}\rangle) = \int d^2P_{hT} F_{UT}^{\sin(\phi_h-\phi_S)}(x,z,P_{hT})$ in (5.7b).

The asymmetries $A_{UT}^{\sin(\phi_h-\phi_S)} = F_{UT}^{\sin(\phi_h-\phi_S)}/F_{UU}$ are plotted in Fig. 6 in comparison to HERMES data on charged pion production from a proton target [99]. The x– and P_{hT}–dependencies of the asymmetry are displayed. The latter shows that the Gaussian model works well also in this case. COMPASS data are described equally well by the fit [100].

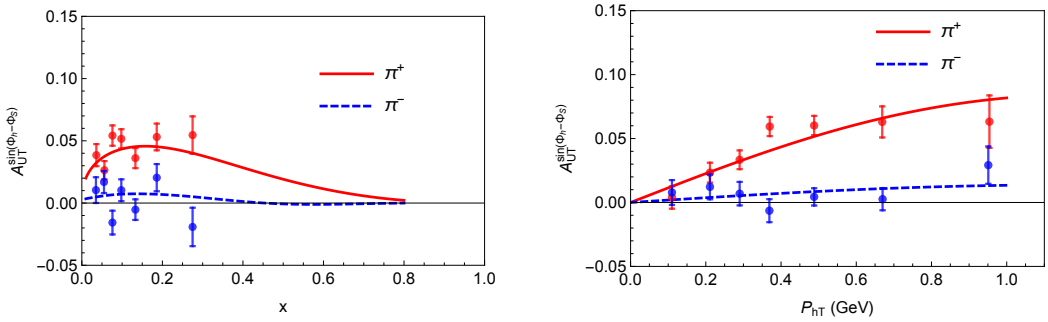

Figure 6. The Sivers asymmetry $A_{UT}^{\sin(\phi_h-\phi_S)}$ as a function of x (left panel) and P_{hT} (right panel). The data are from the HERMES experiment and refer to the mean values $\langle x\rangle = 0.1$, $\langle z\rangle = 0.34$, $\langle Q^2\rangle = 2.4$ GeV^2 [99]. The theoretical curves are based on the fit results of Ref. [100].

5.4 Leading twist $A_{UT}^{\sin(\phi_h+\phi_S)}$ Collins asymmetry

The $F_{UT}^{\sin(\phi_h+\phi_S)}$ modulation of the SIDIS cross section is due to the convolution of the transversity distribution h_1 and the Collins FF $H_1^\perp$. Transversity can in principle be accessed also as a PDF in Drell-Yan. It describes the distribution of transversely polarized quarks in a transversely polarized nucleon, and is the only source of information on the tensor charge of the nucleon. The Collins FF $H_1^\perp$ decodes the fundamental correlation between the transverse spin of a fragmenting quark and the transverse momentum of the final produced hadron [101].

There are many extractions of h_1 and $H_1^\perp$ from a combined fit of SIDIS and e^+e^- data, for instance those of Refs. [102–104]. In this work we will use the extractions of h_1 and $H_1^\perp$ from Ref. [102].

The structure function $F_{UT}^{\sin(\phi_h+\phi_S)}$ reads

$$F_{UT}^{\sin(\phi_h+\phi_S)}(x,z,P_{hT}) = x\sum_q e_q^2\, h_1^q(x)\, H_1^{\perp(1)q}(z)\, b_{\rm A}^{(1)}\left(\frac{zP_{hT}}{\lambda}\right)\mathcal{G}(P_{hT})\,, \tag{5.8a}$$

$$F_{UT}^{\sin(\phi_h+\phi_S)}(x,z,\langle P_{hT}\rangle) = x\sum_q e_q^2\, h_1^q(x)\, H_1^{\perp(1)q}(z)\, c_{\rm A}^{(1)}\left(\frac{z}{\lambda^{1/2}}\right), \tag{5.8b}$$

where $\lambda = z^2\langle k_\perp^2\rangle_{h_1} + \langle P_\perp^2\rangle_{H_1^\perp}$ and $b_{\rm A}^{(1)} = 2m_h$ and $c_{\rm A}^{(1)} = \sqrt{\pi}\, m_h$, see App. B.5 for details.

The asymmetries $A_{UT}^{\sin(\phi_h+\phi_S)} = F_{UT}^{\sin(\phi_h+\phi_S)}/F_{UU}$ are plotted in Fig. 7 in comparison to HERMES data on charged pion production from a proton target [105]. Also in Fig. 7 we show the x– and P_{hT}–dependencies of this azimuthal spin asymmetry. The right panel of Fig. 7 on the P_{hT}–dependence shows that the data are compatible with the Gaussian Ansatz. Let us remark that the COMPASS data are described equally well by the fit of Ref. [102].

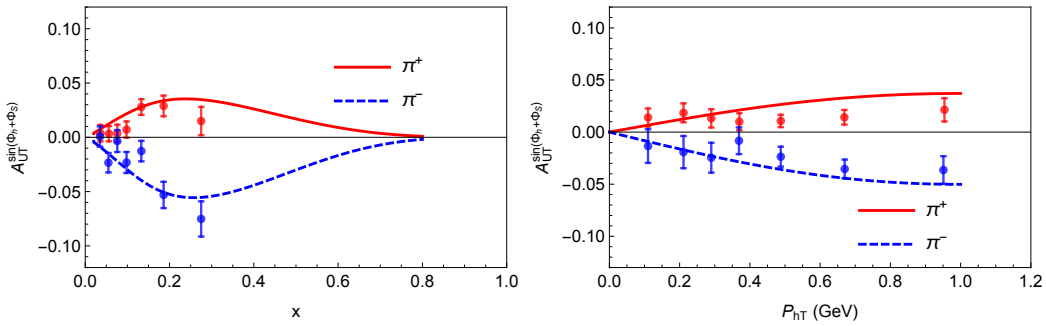

Figure 7. The Collins asymmetry $A_{UT}^{\sin(\phi_h+\phi_S)}$ as a function of x (left panel) and P_{hT} (right panel). The data are from the HERMES experiment and refer to the mean values $\langle x\rangle = 0.1$, $\langle z\rangle = 0.34$, $\langle Q^2\rangle = 2.4$ GeV^2 [105]. The theoretical curves are based on the fit results of Ref. [102].

5.5 Leading twist $A_{UU}^{\cos(2\phi_h)}$ Boer-Mulders asymmetry

The structure function $F_{UU}^{\cos(2\phi_h)}$ reads

$$F_{UU}^{\cos(2\phi_h)}(x,z,P_{hT}) = x\sum_q e_q^2\, h_1^{\perp(1)q}(x)\, H_1^{\perp(1)q}(z)\, b_{\rm AB}^{(2)} \left(\frac{zP_{hT}}{\lambda}\right)^2 \mathcal{G}(P_{hT})\,, \tag{5.9a}$$

$$F_{UU}^{\cos 2\phi_h}(x,z,\langle P_{hT}\rangle) = x\sum_q e_q^2\, h_1^{\perp(1)q}(x)\, H_1^{\perp(1)q}(z)\, c_{\rm AB}^{(2)} \left(\frac{z}{\lambda^{1/2}}\right)^2, \tag{5.9b}$$

where $\lambda = z^2\langle k_\perp^2\rangle_{h_1^\perp} + \langle P_\perp^2\rangle_{H_1^\perp}$ and $b_{\rm AB}^{(2)} = 4M_N m_h$ and $c_{\rm AB}^{(2)} = 4M_N m_h$, see App. B.5.

Asymmetries $A_{UU}^{\cos(2\phi_h)} = F_{UU}^{\cos(2\phi_h)}/F_{UU}$ for HERMES are plotted in Fig. 8 where we only considered the Boer-Mulders contribution to $A_{UU}^{\cos(2\phi_h)}$ which does not describe the data accurately. In fact, it is suspected that this observable receives a significant contribution from the Cahn effect [108], a term of higher twist character of the type $\langle P_{hT}^2\rangle/Q^2$ which is not negligible in fixed target experiments [76]. This contribution was estimated and corrected for in the phenomenological works [106, 109, 110] which was of importance to obtain a picture of the Boer-Mulders function undistorted from Cahn effect. The point is that this substantial twist-4 contamination can be estimated phenomenologically, even though there is no rigorous theoretical basis for the description of such power-suppressed terms. In this work we consistently neglect power-suppressed contributions of order $1/Q^2$, and do so also in Fig. 8. Nevertheless we of course use the parametrizations of [106, 109, 110] offering the best currently available parametrizations for $h_1^\perp$ which were corrected for Cahn effect as good as it is possible at the current state of art. It is unknown whether other asymmetries could be similarly effected by such type of power-corrections. This is an important point to be kept in mind as the lesson from Fig. 8 shows.

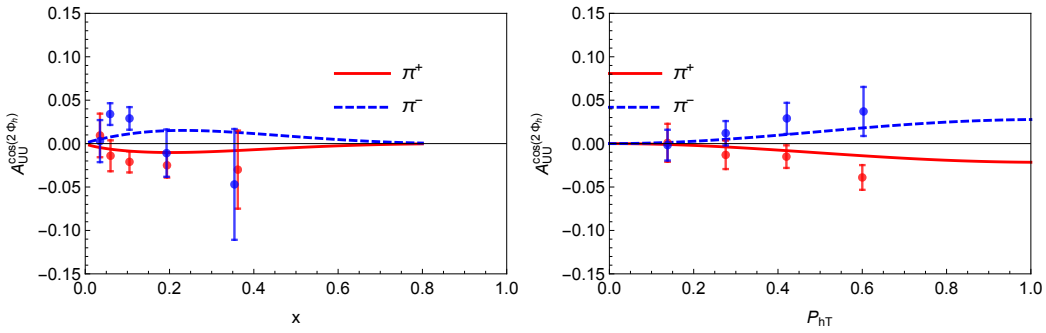

Figure 8. Comparison of calculation of $A_{UU}^{\cos(2\phi_h)}$ using fit results of Ref. [106] as a function of x (left panel), and as a function of P_{hT} (right panel) at $\langle x\rangle = 0.15$, $\langle z\rangle = 0.34$, $\langle Q^2\rangle = 2.4$ GeV^2 and HERMES data [107].

5.6 Leading twist $A_{UT}^{\sin(3\phi_h-\phi_S)}$ asymmetry

The structure function $F_{UT}^{\sin(3\phi_h-\phi_S)}$ reads

$$F_{UT}^{\sin(3\phi_h-\phi_S)}(x,z,P_{hT}) = x\sum_q e_q^2\, h_{1T}^{\perp(2)q}(x)\, H_1^{\perp(1)q}(z)\, b^{(3)} \left(\frac{zP_{hT}}{\lambda}\right)^3 \mathcal{G}(P_{hT})\,, \quad (5.10a)$$

$$F_{UT}^{\sin(3\phi_h-\phi_S)}(x,z,\langle P_{hT}\rangle) = x\sum_q e_q^2\, h_{1T}^{\perp(2)q}(x)\, H_1^{\perp(1)q}(z)\, c^{(3)} \left(\frac{z}{\lambda^{1/2}}\right)^3, \quad (5.10b)$$

where $\lambda = z^2\langle k_\perp^2\rangle_{h_{1T}^\perp} + \langle P_\perp^2\rangle_{H_1^\perp}$ and $b^{(3)} = 2M_N^2 m_h$ and $c^{(3)} = 3/2\sqrt{\pi}\, M_N^2 m_h$, see App. B.5.

The preliminary COMPASS data [111] for $A_{UT}^{\sin(3\phi_h-\phi_S)} = F_{UT}^{\sin(3\phi_h-\phi_S)}/F_{UU}$ are plotted in Fig. 9. Clearly, the pretzelosity TMD is the least known of the basis TMDs. Nevertheless it is of fundamental importance, as it provides one of the basis functions in our approach. It is so difficult to access it experimentally, because its contribution to the SIDIS cross section is proportional to P_{hT}^3, the TMD approach requires us to necessarily operate at $P_{hT} \ll Q$, and so far only moderate values of Q could be achieved in the fixed target experiments. A notable exception is COMPASS where the largest x–bins (where Q^2 is largest) bear the best hints on this TMD, see Fig. 9. Future high luminosity data from JLab 12 are expected to significantly improve our knowledge of this TMD.

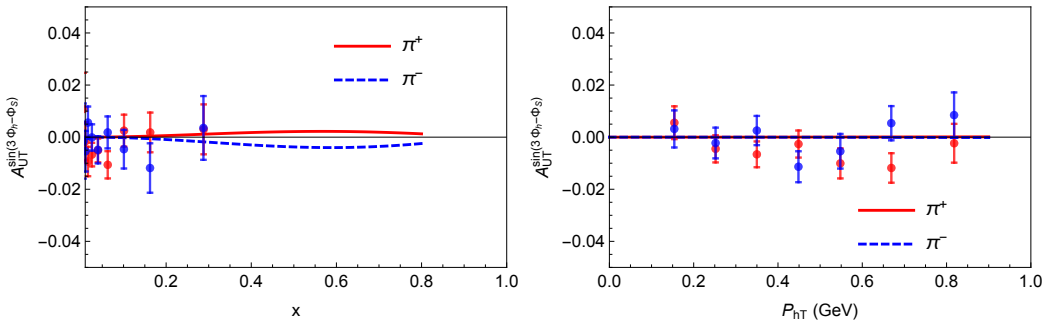

Figure 9. $A_{UT}^{\sin(3\phi_h-\phi_S)}$ as a function of x (left panel) and P_{hT} (right panel) at $\langle x\rangle = 0.05$, $\langle z\rangle = 0.36$, $\langle Q^2\rangle = 3.6$ GeV^2 on the basis of fits from [112] vs preliminary COMPASS data [111].

6 Leading twist asymmetries in WW-type approximation

Two out of the 8 leading–twist structure functions can be described in WW-type approximation thanks to Eqs. (3.6a, 3.6b) which relate $g_{1T}^{\perp(1)q}(x)$ and $h_{1L}^{\perp(1)q}(x)$ to the basis functions $g_1^q(x)$ and $h_1^q(x)$, see Fig. 10. In this section we discuss the associated asymmetries.

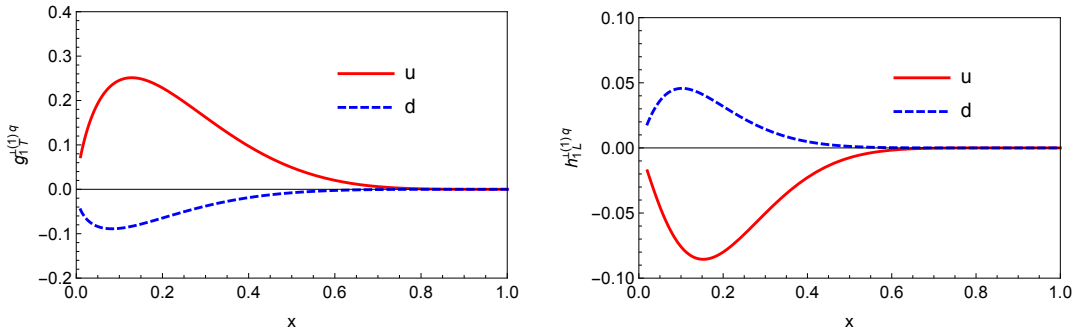

Figure 10. $g_{1T}^{\perp(1)q}(x)$ (left panel) and $h_{1L}^{\perp(1)q}(x)$ distributions (right panel) for u– and d–flavor as predicted by the WW-ype approximations in Eqs. (3.6a, 3.6b).

6.1 Leading twist $A_{LT}^{\cos(\phi_h-\phi_S)}$

We assume for $g_{1T}^{\perp}$ the Gaussian Ansatz as shown in Eq. (B.9a) of App. B.3, see also [23], and evaluate $g_{1T}^{\perp(1)q}(x)$ using Eq. (3.6a) which yields the result shown in Fig. 10. For our numerical estimates we use $\langle k_\perp^2\rangle_{g_{1T}^\perp} = \langle k_\perp^2\rangle_{g_1}$ which is supported by lattice results [41].

In the Gaussian Ansatz the structure function $F_{LT}^{\cos(\phi_h-\phi_S)}$ has the form

$$F_{LT}^{\cos(\phi_h-\phi_S)}(x,z,P_{hT}) = x\sum_q e_q^2\, g_{1T}^{\perp(1)q}(x)\, D_1^q(z)\, b_{\rm B}^{(1)}\left(\frac{zP_{hT}}{\lambda}\right)\mathcal{G}(P_{hT}) \tag{6.1a}$$

$$F_{LT}^{\cos(\phi_h-\phi_S)}(x,z,\langle P_{hT}\rangle) = x\sum_q e_q^2\, g_{1T}^{\perp(1)q}(x)\, D_1^q(z)\, c_{\rm B}^{(1)}\left(\frac{z}{\lambda^{1/2}}\right) \tag{6.1b}$$

where $\lambda = z^2\langle k_\perp^2\rangle_{g_{1T}^\perp} + \langle P_\perp^2\rangle_{D_1}$, $b_{\rm B}^{(1)} = 2M_N$, $c_{\rm B}^{(1)} = \sqrt{\pi}\,M_N$, see App. B.5 for details.

This asymmetry was measured at JLab and COMPASS [113, 114]. Left panel of Fig. 11 shows 2010 COMPASS data [113] measured with 160 GeV longitudinally polarized muons impinging on a transversely polarized proton (NH_3) target [115]. We approximate the charged hadrons (90 % of which are $\pi^\pm$ at COMPASS) by charged pions, see App. A.1. Our results are shown as a shaded area which indicates a rough estimate of the uncertainty of the WW-type approximation. We observe that the WW-type approximation describes the data within their experimemental uncertainties. For comparison results from the theoretical works [23, 116, 117] are shown. Our results are also compatible with the JLab data which

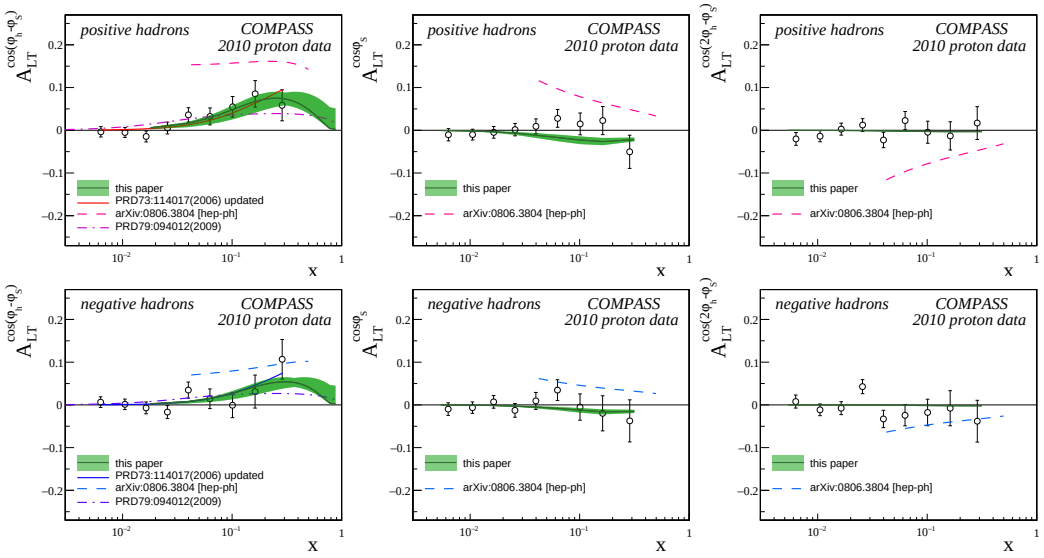

Figure 11. Asymmetries as functions of x from scattering of 160 GeV longitudinally polarized muons off a transversely polarized proton target [113]. Left panel: leading-twist asymmetry $A_{LT}^{\cos(\phi_h-\phi_S)}$ described in Sec. 6.1. Middle panel: subleading-twist $A_{LT}^{\cos\phi_S}$ discussed in Sec. 7.2. Right panel: subleading-twist $A_{LT}^{\cos(2\phi_h-\phi_S)}$ on which we comment in Sec. 7.3.

was taken with a neutron (^{3}He) target [114] and has larger statistical uncertainty than COMPASS data. The middle and right panels of Fig. 11 will be discussed in Secs. 7.2, 7.3.

6.2 Leading twist $A_{UL}^{\sin 2\phi_h}$ Kotzinian-Mulders asymmetry

We use the Gaussian form for the Kotzinian-Mulders function $h_{1L}^{\perp a}$, Eq. (B.9b) in App. B.3, with $\langle k_\perp^2 \rangle_{h_{1L}^\perp} = \langle k_\perp^2 \rangle_{h_1}$ as supported by lattice data [41]. From (3.6b) we obtain the WW-type estimate for $h_{1L}^{\perp(1)a}(x)$ shown in Fig. 10. The structure function $F_{UL}^{\sin(2\phi_h)}$ reads

$$F_{UL}^{\sin(2\phi_h)}(x,z,P_{hT}) = x\sum_q e_q^2\, h_{1L}^{\perp(1)q}(x)\, H_1^{\perp(1)q/h}(z)\left(\frac{zP_{hT}}{\lambda}\right)^2 b_{\rm AB}^{(2)}\,\mathcal{G}(P_{hT})\,, \quad (6.2a)$$

$$F_{UL}^{\sin(2\phi_h)}(x,z,\langle P_{hT}\rangle) = x\sum_q e_q^2\, h_{1L}^{\perp(1)q}(x)\, H_1^{\perp(1)q/h}(z)\left(\frac{z}{\lambda^{1/2}}\right)^2 c_{\rm AB}^{(2)}\,, \quad (6.2b)$$

where $\lambda = z^2\langle k_\perp^2\rangle_{h_{1L}^\perp} + \langle P_\perp^2\rangle_{H_1^\perp}$ and $b_{\rm AB}^{(2)} = c_{\rm AB}^{(2)} = 4M_N m_h$, see App. B.5 for details.

The asymmetry $A_{UL}^{\sin(2\phi_h)} = F_{UL}^{\sin(2\phi_h)}/F_{UU}$ was studied at HERMES [118, 120], COMPASS [113], and JLab [90, 119]. In Fig. 12 proton data are shown. At HERMES $\pi^\pm$ were produced in scattering of 27.6 GeV positrons from the HERA polarized positron storage ring at DESY off nuclear-polarized hydrogen internal gas target [121] for $1\,\mathrm{GeV}^2 < Q^2 < 15\,\mathrm{GeV}^2$, $W > 2\,$Gev, $0.023 < x < 0.4$ and $y < 0.85$. The COMPASS data show the asymmetry for charged hadrons (in practice mainly pions). Since y–dependent prefactors were included in the analyses (see Sec. 2.1), the HERMES data is adequately ("$D(y)$–")rescaled. The CLAS π^0 data in the right panel were measured using 6 GeV longitudinally polarized electrons scattering off longitudinally polarized protons in a cryogenic $^{14}NH_3$ target in the kinematics $1.0\,\mathrm{GeV}^2 < Q^2 < 3.2\,\mathrm{GeV}^2$, $0.12 < x < 0.48$ and $0.4 < z < 0.7$ [119].

$A_{UL}^{\sin(2\phi_h)}$ can be expected to be smaller than $A_{LT}^{\cos(\phi_h-\phi_S)}$ discussed in previous section, even though both are leading twist. This is because $F_{UL}^{\sin(2\phi_h)}$ is quadratic in the hadron transverse momenta $P_{hT} \ll Q$, while $F_{LT}^{\cos(\phi_h-\phi_S)}$ is linear. In addition, the former is proportional to the Collins function which is smaller than $D_1^q(z)$, and the WW-type approximation predicts the magnitude of $h_{1L}^{\perp(1)q}(x)$ to be about half of the size of $g_{1T}^{\perp(1)q}(x)$. The data support these expectations. HERMES and JLab data are compatible with zero for this asymmetry. So are COMPASS data except for the region $x > 0.1$ for negative hadrons, where the trend of the data provides a first encouraging confirmation for our results. The current data are compatible with the WW-type approximation for $h_{1L}^{\perp(1)q}(x)$.

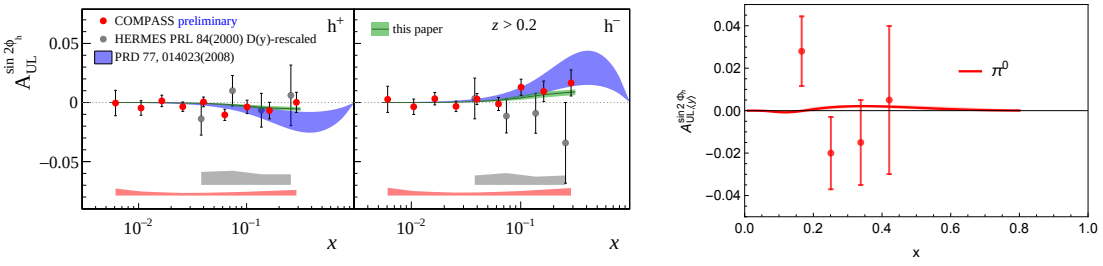

Figure 12. $A_{UL}^{\sin(2\phi_h)}$ as function of x from HERMES [118] and COMPASS [113] experiments (left panel) and at JLab [119] in comparison to predictions from WW-type approximation. Predictions from [24] are shown for comparison.

6.3 Inequalities and a cross check

We discussed WW-type approximations for the twist-2 TMDs $g_{1T}^{\perp q}$ and $h_{1L}^{\perp q}$ in Secs. 6.1, 6.2. Before proceeding with twist-3 let us pause and revisit positivity bounds [10].

The Kotzinian-Mulders function $h_{1L}^{\perp q}$ in conjuction with the Boer-Mulders function, and the TMD $g_{1T}^{\perp q}$ in conjuction with the Sivers function obey the positivity bounds [10]

$$\frac{k_\perp^2}{4M_N^2}\,\left((f_1^q(x,k_\perp^2))^2-(g_1^q(x,k_\perp^2))^2\right)-(h_{1L}^{\perp(1)q}(x,k_\perp^2))^2-(h_1^{\perp(1)q}(x,k_\perp^2))^2\geq 0\,, \tag{6.3a}$$

$$\frac{k_\perp^2}{4M_N^2}\,\left((f_1^q(x,k_\perp^2))^2-(g_1^q(x,k_\perp^2))^2\right)-(f_{1T}^{\perp(1)q}(x,k_\perp^2))^2-(g_{1T}^{\perp(1)q}(x,k_\perp^2))^2\geq 0\,, \tag{6.3b}$$

where $f^{(1)}(x,k_\perp^2)\equiv\frac{k_\perp^2}{2M_N^2}f(x,k_\perp^2)$. The inequalities provide a non-trivial test of our approach. The inequalities (6.3a, 6.3b) must be strictly satisfied by the *exact* leading–order QCD expressions for the TMDs. (For PDFs it is known that positivity can be preserved in some schemes but violated in other schemes. For TMDs not much is known about positivity conditions beyond leading order.) However, here we do not deal with exact TMDs but (i) we invoked strong model assumptions (WW-type approximations for $g_{1T}^{\perp q}$ and $h_{1L}^{\perp q}$ and Gauss Ansatz for all TMDs), and (ii) we deal with first extractions which have sizable uncertainties including poorly controlled systematic uncertainties. Therefore, considering that we deal with approximations (WW-type, Gauss) and considering the current state of TMD-extractions, the inequalities (6.3a, 6.3b) constitute a challenging test for the approach.

To conduct a test we use the Gaussian Ansätze (4.5a, 4.5d, 4.5f, 4.5g, B.9a, B.9b) for the TMDs and integrate over $k_\perp$. The results are shown in Fig. 13 where we plot the "normalized inequalities" defined as follows: given an inequality $a-b-\cdots\geq 0$, the normalized inequality is defined as: $0\leq(a-b-\dots)/(|a|+|b|+\dots)\leq 1$.

Fig. 13 shows that the results of our approach for the "normalized inequalities" for both TMDs lie between between zero and one, as it is dictated by positivity constraints. This is an important consistency cross-check for our approach.

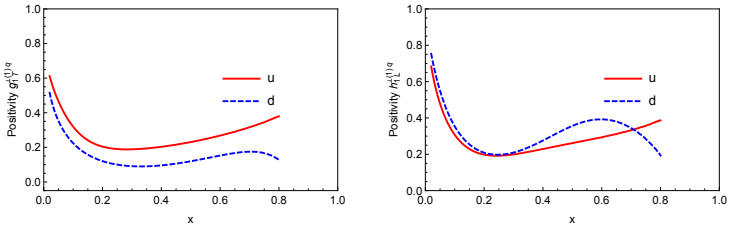

Figure 13. The normalized inequalities for $g_{1T}^{\perp(1)q}(x)$ and $h_{1L}^{\perp(1)q}(x)$ vs x. The normalized inequalities are defined such that they must be positive (and smaller than one), see text for details. Clearly, our approach respects both positivity conditions.

7 Subleading twist asymmetries in WW-type approximation

WW-type approximations can be applied to all 8 subleading–twist observables, as shown in Sec. 4.2. In view of the complex structure of SIDIS at subleading–twist, WW-type approximations are potentially very useful for the interpretation of twist-3 observables.

7.1 Subleading twist $A_{LU}^{\sin\phi_h}$

We start our discussion with the structure function $F_{LU}^{\sin\phi_h}$, Eq. (2.19b), containing 4 terms: 2 term are proportional to pure twist-3 fragmentation functions $\tilde{G}^{\perp a}$ and $\tilde{E}^a$ and neglected; the other 2 terms are proportional to the twist-3 TMDs e^a and $g^{\perp a}$ which also turn out to be given in terms of pure twist-3 terms upon the inspection of Eqs. (3.3a, 3.4d). Hence, after consequently applying the WW-type approximation we are left with no term. Our approximation predicts this structure function to be zero.

Data from JLab, HERMES and COMPASS show a small but clearly non-zero effect of the order of (2-3) % [122–127]. At first glance this may seem a failure of our approach. However, the numerator of the asymmetry is proportional to $\bar{q}gq$–correlators, while the denominator $(f_1^a D_1^a)$ is a qq–correlator. Therefore we may express this observation as

$$|A_{LU}^{\sin\phi_h}| \;\propto\; \frac{\langle\bar{q}gq\rangle}{\langle\bar{q}q\rangle} \;\overset{\text{exp}}{\lesssim}\; \mathcal{O}(3\,\%)\,. \tag{7.1}$$

We should keep in mind several reservations. First, the experimental result quoted in (7.1) contains also kinematic prefactors which help to reduce the value. Second, the denominator contains f_1^a and D_1^a which are the largest TMD and FF because of positivity constraints. Third, the numerator is a sum of 4 terms, so its overall smallness could also result from cancellation of different terms, rather than indicating that all 4 terms are small. Keeping these reservations cautiously in mind, we may nevertheless consider the experimental observation of a (2-3) % asymmetry $A_{LU}^{\sin\phi_h}$ [122–127] as an encouraging indication that $\bar{q}gq$–terms are smaller than $\bar{q}q$ terms, in line with the generic expectation (3.1).

To conclude, the WW-type approximation predicts $A_{LU}^{\sin\phi} \approx 0$ which is "compatible" with experiment in the sense that the data show a small asymmetry. Notice however that some asymmetries appear in experiment even smaller (compatible with zero) despite being non-zero in WW-type approximation. Further work is needed before we can draw definite conclusions. In any case, $F_{LU}^{\sin\phi}$ is the only twist-3 SIDIS structure not "contaminated" by leading twist which provides a unique window into higher twist physics.

7.2 Subleading twist $A_{LT}^{\cos\phi_S}$

In WW-type approximation the structure function $F_{LT}^{\cos\phi_S}$ is due to $g_T^a(x,k_\perp)$ and $D_1^a(z,P_\perp)$ whose collinear counterparts are more or less known, see Secs. 3.4 and 5.1. We assume the Gaussian Ansatz for $g_T^a(x,k_\perp)$ shown in Eq. (B.9c) of App. B.3 with $\langle k_\perp^2\rangle_{g_T} = \langle k_\perp^2\rangle_{g_1}$. We then determine $g_T^q(x)$ according to Eq. (3.2a) which is a well-tested approximation in DIS, see Sec. 3.4. In this way we obtain for $F_{LT}^{\cos\phi_S}$ the result

$$F_{LT}^{\cos\phi_S}(x,z,P_{hT}) = -\frac{2M}{Q}\, x^2 \sum_q e_q^2\, g_T^q(x)\, D_1^q(z)\, \mathcal{G}(P_{hT})\,, \tag{7.2a}$$

$$F_{LT}^{\cos\phi_S}(x,z) = -\frac{2M}{Q}\, x^2 \sum_q e_q^2\, g_T^q(x)\, D_1^q(z)\,, \tag{7.2b}$$

with the width $\lambda = z^2\langle k_\perp^2\rangle_{g_T} + \langle P_\perp^2\rangle_{D_1}$ in the Gaussian $\mathcal{G}(P_{hT})$.

Notice that we followed here the scheme explained in Sec. 4.4: first assume Gaussian Ansatz, then apply WW-type type approximation. For some structure functions the order of these steps is not relevant, but here it is. It is instructive to discuss what the opposite order of these steps yields. One may first plug in the WW-type approximation (3.3e) in the convolution integral (3.2a) and then solve the convolution integral with Gaussian Ansatz. The result is an analytical expression which is bulkier than (7.2a) though it yields a numerically similar result. But there are 2 critical issues with that. First, the WW-type approximation (3.3e) relates $g_T^q(x,k_\perp^2)$ to $g_{1T}^{\perp(1)q}(x,k_\perp^2)$ which (due to the weight $k_\perp^2/(2M_N^2)$ in the (1)-moment) implies a kinematical zero in $k_\perp$ as $g_T^q(x,0)=0$ which is not supported by model calculations [54]. Second, the more economic (because less bulky) expression in (7.2a) automatically yields (7.2b) which is the correct colinear result for this SIDIS function in Eq. (2.21c) in WW-type approximation. This technical remark confirms that consistency of the scheme suggested in Sec. 4.4.

In the middle panel of Fig. 11 our predictions for $A_{LT}^{\cos\phi_S}$ are shown in comparison to preliminary COMPASS data from Ref. [113]. The predicted asymmetry is small and compatible with the COMPASS data within error bars. More precise data is necessary to judge the how well the WW-type approximation works in this case. Such data could come from JLab 12 experiments, see Fig. 14.

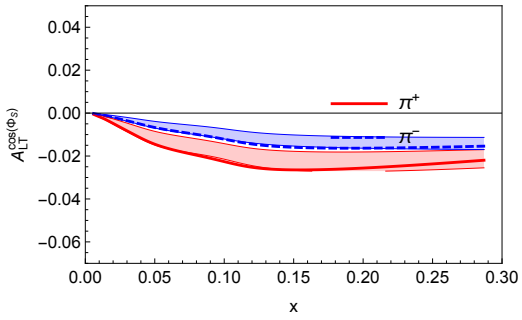

Figure 14. Predictions for the double–spin asymmetry $A_{LT}^{\cos\phi_S}$ as a function of x from a proton target at JLab 12.

7.3 Subleading twist $A_{LT}^{\cos(2\phi_h-\phi_S)}$

In the WW-type approximation this asymmetry is expressed in terms of $g_T^{\perp a}(x,k_\perp)$ for which we assume a Gaussian Ansatz according to Eq. (B.9d) in App. B.3, and use the WW-type approximation (3.3d) as

$$x g_T^{\perp(2)q}(x) = \frac{\langle k_\perp^2\rangle_{g_{1T}^\perp}}{M_N^2}\, g_{1T}^{\perp(1)q}(x)\,, \tag{7.3}$$

where we finally express $g_{1T}^{\perp(1)q}(x)$ in terms of $g_1^q(x)$ according to Eq. (3.6a). For the Gaussian widths we assume $\langle k_\perp^2\rangle_{g_T^\perp} = \langle k_\perp^2\rangle_{g_{1T}^\perp} = \langle k_\perp^2\rangle_{g_1}$. This yields for the structure function

$$F_{LT}^{\cos(2\phi_h-\phi_S)}(x,z,P_{hT}) = -\frac{2M}{Q} x \sum_q e_q^2\, x\, g_T^{\perp(2)q}(x)\, D_1^q(z)\, b_C^{(2)} \left(\frac{zP_{hT}}{\lambda}\right)^2 \mathcal{G}(P_{hT}) \tag{7.4a}$$

$$F_{LT}^{\cos(2\phi_h-\phi_S)}(x,z,\langle P_{hT}\rangle) = -\frac{2M}{Q} x \sum_q e_q^2\, x\, g_T^{\perp(2)q}(x)\, D_1^q(z)\, c_C^{(2)} \left(\frac{z}{\lambda^{1/2}}\right)^2 \tag{7.4b}$$

where $\lambda = z^2\langle k_\perp^2\rangle_{g_T^\perp} + \langle P_\perp^2\rangle_{D_1}$ and $b_{\rm C}^{(2)} = c_{\rm C}^{(2)} = M_N^2$, see App. B.5 for details.

Our predictions for the asymmetry $A_{LT}^{\cos(2\phi_h-\phi_S)} = F_{LT}^{\cos(2\phi_h-\phi_S)}/F_{UU}$ as function of x are displayed in the right panel of Fig. 11 in comparison to preliminary COMPASS data from Ref. [113]. The asymmetry is very small, so we show our predictions on a larger scale in Fig. 15. At the current stage one may conclude that the WW-type approximation for the asymmetry $A_{LT}^{\cos(2\phi_h-\phi_S)}$ is compatible with available data. In view of the smallness of the effect, cf. Fig. 15, it might be difficult to obtain more quantitative insights in near future.

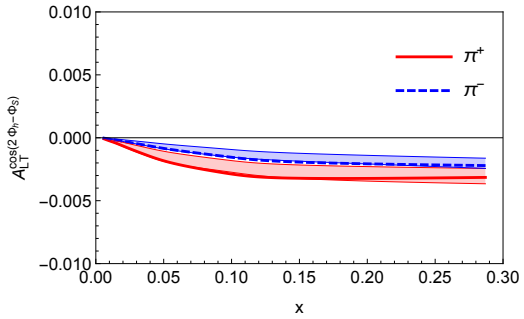

Figure 15. $A_{LT}^{\cos(2\phi_h-\phi_S)}$ as a function of x from a proton target for the COMPASS kinematics (enlarged detail of right panel Fig. 11 where also the preliminary COMPASS data [113] are shown). The smallness of this asymmetry has two natural reasons. First, being twist-3 it is M_N/Q suppressed. Second, it is proportional to P_{hT}^2 with $P_{hT} \ll Q$ in TMD approach.

7.4 Subleading twist $A_{LL}^{\cos\phi_h}$

In WW-type approximation the only contribution to $F_{LL}^{\cos\phi_h}$ is due to $g_L^{\perp q}(x,k_\perp)$ which we assume to be have a Gaussian $k_\perp$–behavior according to Eq. (B.9e) in App. B.3, where assume for the Gaussian width $\langle k_\perp^2\rangle_{g_L^\perp} = \langle k_\perp^2\rangle_{g_1}$. The structure function $F_{UL}^{\cos\phi_h}$ reads

$$F_{LL}^{\cos\phi_h}(x,z,P_{hT}) = -\frac{2M}{Q}\, x \sum_q e_q^2\, x\, g_L^{\perp(1)q}(x)\, D_1^q(z)\, b_{\rm B}^{(1)}\left(\frac{zP_{hT}}{\lambda}\right)\mathcal{G}(P_{hT})\,, \quad (7.5a)$$

$$F_{LL}^{\cos\phi_h}(x,z,\langle P_{hT}\rangle) = -\frac{2M}{Q}\, x \sum_q e_q^2\, x\, g_L^{\perp(1)q}(x)\, D_1^q(z)\, c_{\rm B}^{(1)}\left(\frac{z}{\lambda^{1/2}}\right), \quad (7.5b)$$

where $\lambda = z^2\langle k_\perp^2\rangle_{g_L^\perp} + \langle P_\perp^2\rangle_{D_1}$, $b_{\rm B}^{(1)} = 2M_N$, $c_{\rm B}^{(1)} = \sqrt{\pi}\, M_N$, see App. B.5. Finally we explore the WW-type approximation (3.3c) to relate $x\, g_L^{\perp(1)a}(x) = \frac{\langle k_\perp^2\rangle_{g_1}}{2\,M_N^2}\, g_1^a(x)$.

The asymmetry $A_{LL}^{\cos\phi_h} = F_{LL}^{\cos\phi_h}/F_{UU}$ predicted by the WW-type approximation in this case is small and compatible with presently available data, see Fig. 16.

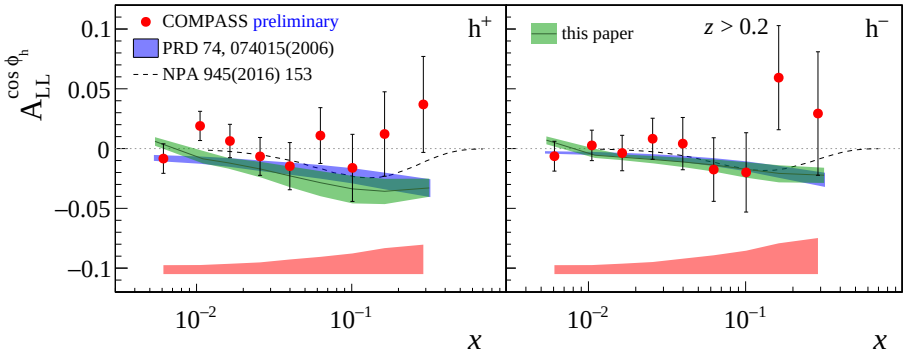

Figure 16. $A_{LL}^{\cos(\phi_h)}$ as a function of x from a proton target for the COMPASS kinematics. The theoretical curves obtained from the WW-type approximation are compared to the preliminary COMPASS data [113].

7.5 Subleading twist $A_{UL}^{\sin\phi_h}$

In the WW-type approximation the asymmetry is described by $h_L^q(x,k_\perp)$ for which we assume the Gaussian Ansatz (B.9f) in App. B.3 with $\langle k_\perp^2\rangle_{h_L} = \langle k_\perp^2\rangle_{h_1}$. We explore (3.3f) to estimate $x h_L^q(x) = -2h_{1L}^{\perp(1)q}(x)$ and express $h_{1L}^{\perp(1)q}(x)$ through $h_1^a(x)$ according to (3.6b). This yield for the structure function the result

$$F_{UL}^{\sin\phi_h}(x,z,P_{hT}) = \frac{2M}{Q}\, x \sum_q e_q^2\, x\, h_L^q(x)\, H_1^{\perp(1)q}(z)\, b_{\rm A}^{(1)}\left(\frac{zP_{hT}}{\lambda}\right) \mathcal{G}(P_{hT})\,, \tag{7.6a}$$

$$F_{UL}^{\sin\phi_h}(x,z,\langle P_{hT}\rangle) = \frac{2M}{Q}\, x \sum_q e_q^2\, x\, h_L^q(x)\, H_1^{\perp(1)q}(z)\, c_{\rm A}^{(1)}\left(\frac{z}{\lambda^{1/2}}\right) \tag{7.6b}$$

where $\lambda = z^2\langle k_\perp^2\rangle_{h_L} + \langle P_\perp^2\rangle_{H_1^\perp}$ and $b_{\rm A}^{(1)} = 2m_h$ and $c_{\rm A}^{(1)} = \sqrt{\pi}\, m_h$, see App. B.5 for details.

The asymmetries $A_{UL}^{\sin\phi_h} = F_{UL}^{\sin\phi_h}/F_{UU}$ are compared to HERMES, JLab, and preliminary COMPASS data in Fig. 17. The WW-type approximation reproduces the positive sign of the asymmetry seen consistently at HERMES and COMPASS for π^+ and positive hadrons but underestimates its magnitude. The results for negative pions and hadrons at HERMES and COMPASS are compatible. An important test for this asymmetry is provided by neutral pions where in WW-type approximation the contributions for Collins fragmentation function largely cancel. The WW-type approximation is not able to explain the large effect observed at JLab for π^0 in the large–x region $0.2 < x < 0.4$ in Fig. 17.

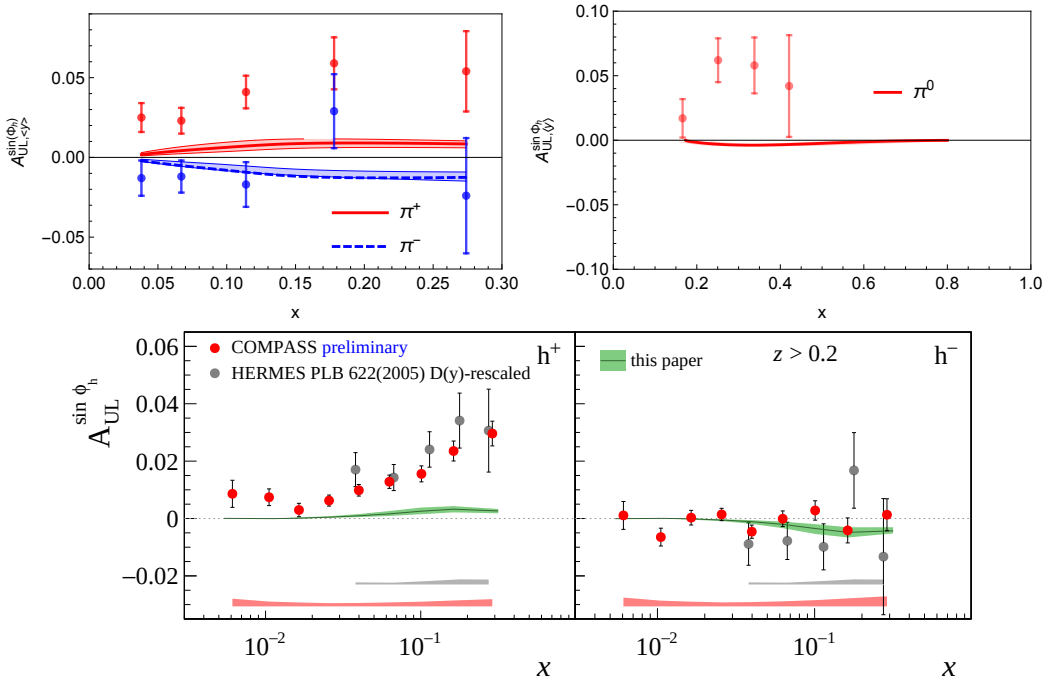

Figure 17. The asymmetry $A_{UL}^{\sin\phi_h}$ as function of x from WW-type approximation in comparison to: (upper panel left) HERMES [128], (upper panel right) JLab [119], and (lower panel) preliminary COMPASS [113] data.

7.6 Subleading twist $A_{UT}^{\sin\phi_S}$

In the structure function $F_{UT}^{\sin\phi_S}$ several interesting features occur not encontered before. Let us summarize the result and follow up with some comments. Assuming Gaussian Ansätze (B.9g, B.9h) for the TMDs $h_T^{\perp q}(x,k_\perp)$, $h_T^q(x,k_\perp)$ in App. B.3, we obtain

$$F_{UT}^{\sin\phi_S}(x,z,P_{hT}) = \frac{2M}{Q}\, x \sum_q e_q^2\, h_1^{(1)q}(x)\, H_1^{\perp(1)q}(z)\, \frac{4z^2 m_h\, M_N}{\lambda}\left(1-\frac{P_{hT}^2}{\lambda}\right)\mathcal{G}(P_{hT}) \tag{7.7a}$$

$$F_{UT}^{\sin\phi_S}(x,z) = 0\,. \tag{7.7b}$$

with $\lambda = z^2\langle k_\perp^2\rangle_{h_T^\perp} + \langle P_\perp^2\rangle_{H_1^\perp}$ and $\langle k_\perp^2\rangle_{h_T^\perp} = \langle k_\perp^2\rangle_{h_T} = \langle k_\perp^2\rangle_{h_1}$. We can then use (3.3g, 3.3h) to relate in the WW-type approximation $-\frac{1}{2}\,x(h_T^{(1)q}(x) - h_T^{\perp(1)q}(x)) = h_1^{(1)q}(x) = \frac{\langle k_\perp^2\rangle_{h_1}}{2M_N^2}\, h_1^q(x)$.

Some comments are in order. The first interesting feature is that after applying the WW-type approximation more than a single term is left. Out of the 6 terms contributing to this structure function in (2.19e) after WW-type approximation initially the 3 terms shown in Eq. (4.2g) remain one of which is proportional to the TMD $f_T^q(x,k_\perp)$.

The second interesting feature not encountered before is associated with $f_T^q(x,k_\perp)$. This T-odd TMD must satisfy the sum rule (2.14), see the discussion in Sec. 3.8. This could be implemented in two ways: one could describe it with a superposition of Gaussians, see App. B.4. At this point, however, we have no guidance from phenomenology or theory to fix additional parameters. Alternatively one could choose a pragmatic and simple solution, namely to neglect the contribution of the TMD $f_T^q(x,k_\perp)$.[3] The result shown in Eq. (7.7a) is obtained using this second "pragmatic" solution.

Interestingly, for the x– and z–dependence of the structure function $F_{UT}^{\sin\phi_S}(x,z)$ it plays no role (footnote 3 vs App. B.4) how we model $f_T^q(x,k_\perp)$: the result is Eq. (7.7b) in either case due to the requirement of the sum rule (2.14). Notice that most of the time we focus on the x–dependence of asymmetries since this allows us to more directly test the WW-type approximations for TMDs, as opposed to e.g. the P_{hT}–dependence where in addition we would test at the same time also the Gaussian Ansatz.

The third interesting feature not seen in previous sections is the occurence of a term which drops out upon integrating the structure function over P_{hT}, cf. Eq. (7.7a) vs. (7.7b). This is a property of the weight $\omega_{\rm B}^{\{2\}}$ in Eq. (2.19e), see Eq. (2.20) and App. B, which appears also in $F_{LT}^{\cos\phi_S}$, Eq. (2.19f), where it however drops out in WW-type approximation. In principle, this property could help to discriminate experimentally the terms associated with this weight.

The final result in Eq. (7.7b) is the consistent result for the structure function $F_{UT}^{\sin\phi_S}(x,z)$ in WW-type approximation, see Eq. (2.21d). Our prediction is therefore $A_{UT}^{\sin\phi_S}(x) = F_{UT}^{\sin\phi_S}(x)/F_{UU}(x) = 0$. This is compatible with preliminary data from HERMES [129] and COMPASS [113] over a wide range of x, see Fig. 18 below. Merely for negative hadrons at large-x there might be a disagreement with our prediction.

[3] Notice that this would correspond to using a "single Gaussian" as $f_T^q(x,k_\perp) = f_T^q(x)\,\frac{\exp(-k_\perp^2/\langle k_\perp^2\rangle_{f_T})}{\pi\langle k_\perp^2\rangle_{f_T}}$ with the "coeffiecient" $f_T^q(x) = 0$ as dictated by the sum rule (2.14).

7.7 Subleading twist $A_{UT}^{\sin(2\phi_h-\phi_S)}$

Also in this asymmetry we end up more than one surviving contribution in our treatment. We assume Gaussian Ansätze for $f_T^{\perp q}(x,k_\perp)$, $h_T^{\perp q}(x,k_\perp)$, $h_T^q(x,k_\perp)$ according to Eqs. (B.9g, B.9h, B.9i) in App. B.3 with $\langle k_\perp^2\rangle_{h_T^\perp} = \langle k_\perp^2\rangle_{h_T} = \langle k_\perp^2\rangle_{h_{1T}^\perp}$ and $\langle k_\perp^2\rangle_{f_T^\perp} = \langle k_\perp^2\rangle_{f_{1T}^\perp}$ and obtain

$$F_{UT}^{\sin(2\phi_h-\phi_S)}(x,z,P_{hT}) = \frac{2M}{Q}\, x \sum_q e_q^2 \left[x\, f_T^{\perp(2)q}(x)\, D_1(z)\, b_{\rm C}^{(2)} \left(\frac{zP_{hT}}{\lambda}\right)^2 \mathcal{G}(P_{hT}) \right.$$
$$\left. + \frac{x}{2}\left(h_T^{(1)q}(x) + h_T^{\perp(1)q}(x)\right) H_1^{\perp(1)q}(z)\, b_{\rm AB}^{(2)} \left(\frac{zP_{hT}}{\lambda}\right)^2 \mathcal{G}(P_{hT}) \right] \quad (7.8a)$$

$$F_{UT}^{\sin(2\phi_h-\phi_S)}(x,z,\langle P_{hT}\rangle) = \frac{2M}{Q}\, x \sum_q e_q^2 \left[x\, f_T^{\perp(2)q}(x)\, D_1(z)\, c_{\rm C}^{(2)} \left(\frac{z}{\lambda^{1/2}}\right)^2 \right.$$
$$\left. + \frac{x}{2}\left(h_T^{(1)q}(x) + h_T^{\perp(1)q}(x)\right) H_1^{\perp(1)q}(z)\, c_{\rm AB}^{(2)} \left(\frac{z}{\lambda^{1/2}}\right)^2 \right] \quad (7.8b)$$

with respectively $\lambda = z^2\langle k_\perp^2\rangle_{f_T^\perp} + \langle P_\perp^2\rangle_{D_1}$ in the first, and $\lambda = z^2\langle k_\perp^2\rangle_{h_T^\perp} + \langle P_\perp^2\rangle_{H_1^\perp}$ in the second terms in Eqs. (7.8a, 7.8b). The coefficients $b_i^{(2)}$ and $c_i^{(2)}$ are defined in App. B.5. In the next step we explore the WW-type approximations (3.3g, 3.3h, 3.4f) to relate $x\, f_T^{\perp(2)q}(x) = \frac{\langle k_\perp^2\rangle_{f_{1T}^\perp}}{M_N^2}\, f_{1T}^{\perp(1)q}(x)$ and $-\frac{1}{2}\, x \left(h_T^{(1)q}(x) + h_T^{\perp(1)q}(x)\right) = h_{1T}^{\perp(2)q}(x)$.

The asymmetries $A_{UT}^{\sin(2\phi_h-\phi_S)} = F_{UT}^{\sin(2\phi_h-\phi_S)}/F_{UU}$ are plotted in the right panel of Fig. 18 in comparison to preliminary COMPASS data [113]. The predicted asymmetry is small and compatible with data which are consistent with a zero effect within error bars.

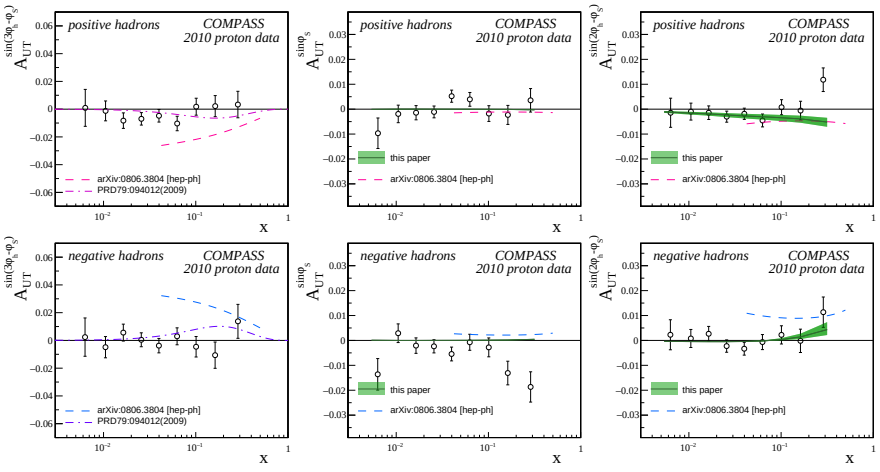

Figure 18. Preliminary data for azimuthal transverse target single–spin asymmetries as functions of x from the COMPASS experiment [113]. Left panel: leading–twist $A_{UT}^{\sin(3\phi_h-\phi_S)}(x)$ which determines the pretzelosity TMD, one of our basis functions. This asymmetry was discussed in Sec. 5.6 and is included here for completeness. Middle panel: subleading–twist $A_{UT}^{\sin\phi_S}(x)$ which is predicted to vanish in the WW-type approximation, see Sec. 7.6. Right panel: leading–twist $A_{UT}^{\sin(2\phi_h-\phi_S)}(x)$.

7.8 Subleading twist $A_{UU}^{\cos\phi_h}$

Historically this was the earliest azimuthal SIDIS asymmetry to be discussed in literature: the first prediction for this asymmetry from intrinsic $k_\perp$ was made in [108, 130], a first measurement was reported in [131].[4] This structure function contains after the WW-type approximation initially two contributions, proportional to $f^\perp(x,P_\perp)$ and $h^q(x,k_\perp)$. The latter is T-odd and obeys the sum rule (2.14). We treat $h^q(x,k_\perp)$ exactly as $f_T^q(x,k_\perp)$ in Sec. 7.6. Using the Gaussian Ansatz for $f^\perp(x,k_\perp)$ in Eq. (B.9j) of App. B.3 we obtain

$$F_{UU}^{\cos\phi_h}(x,z,P_{hT}) = \frac{2M}{Q}\, x \sum_q e_q^2 \left[-x\, f^{\perp(1)q}(x)\, D_1^q(z)\, b_{\rm B}^{(1)}\left(\frac{zP_{hT}}{\lambda}\right) \mathcal{G}(P_{hT}) \right] \tag{7.9a}$$

$$F_{UU}^{\cos\phi_h}(x,z,\langle P_{hT}\rangle) = \frac{2M}{Q}\, x \sum_q e_q^2 \left[-x\, f^{\perp(1)q}(x)\, D_1^q(z)\, c_{\rm B}^{(1)}\left(\frac{z}{\lambda^{1/2}}\right) \right] \tag{7.9b}$$

with $\lambda = z^2\langle k_\perp^2\rangle_{f^\perp} + \langle P_\perp^2\rangle_{D_1}$. The coefficients $b_i^{(1)}$ and $c_i^{(1)}$ are defined in App. B.5. Note that Eq. (7.9a) is valid in the "scheme" of footnote 3, but Eq. (7.9a) holds independently how one implements the sum rule (2.14) (as in footnote 3 or App. B.4).

For $f^{\perp(1)}(x)$ we explore Eq. (3.3b) as $xf^{\perp(1)q}(x) = \frac{\langle k_\perp^2\rangle_{f_1}}{2M_N^2}\, f_1^q(x)$ and estimate its Gaussian width as $\langle k_\perp^2\rangle_{f^\perp} = \langle k_\perp^2\rangle_{f_1}$. The latter means the Gaussian factors of $F_{UU}^{\cos\phi_h}$ and F_{UU} cancel out, i.e. at some point for $P_{hT} \gtrsim 1\,\text{GeV}$ we would obtain from (7.9a) an asymmetry $A_{UU}^{\cos\phi_h} = F_{UU}^{\cos\phi_h}/F_{UU}$ exceeding 100 % and violating unitarity. This is of course an artifact of our approximations, and reminds us that Gaussian and WW-type approximations as well as the entire TMD formalism must be applied to small $P_{hT} \ll Q$.

The asymmetries $A_{UU}^{\cos\phi_h}$ were measured in experiments at EMC [131], JLab [86, 133], HERMES [107], and COMPASS [126]. In Fig. 19 we compare our predictions to the HERMES and COMPASS data. Clearly, the WW-type approximation strongly overestimates the data.

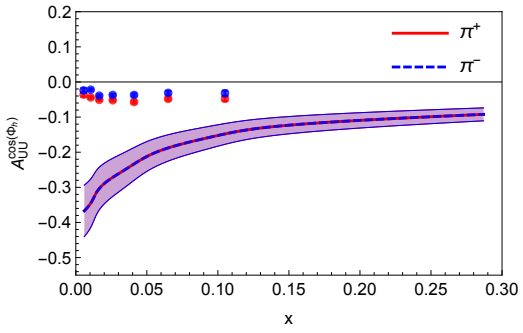

Figure 19. Left panel: asymmetry $A_{UU}^{\cos\phi_h}$ for positive and negative hadrons at COMPASS for a proton target [126]. Right panel: the same for $\pi^\pm$ from HERMES [107] (Figure missing! Could not find data. Please, somebody help to find data.)

[4] First hints [132] of azimuthal modulations in SIDIS date back to the early 1970s, i.e., 10 years before the CERN measurements, but (unfortunately) were discarded by the authors.

8 Conclusions

In this work a comprehensive and complete treatment of SIDIS spin and azimuthal asymmetries was presented. The leading–twist SIDIS structure functions for the production of unpolarized hadrons, which were proven to factorize, are unambiguously expressed in terms of one of 8 twist-2 TMDs convoluted with one of 2 twist-2 FFs. For the subleading–twist SIDIS structure functions the situation is far more complex for two reasons. First, factorization is not proven and must be assumed. Second, each of the subleading–twist structure functions receives 4 or 6 contributions from various TMDs and FFs one of which is twist-2 and the other twist-3. Clearly, to make predictions for new experiment or interpret early data, an organizing theoretical guideline is needed.

In this work we have explored the so–called WW–type approximation as a candidate guideline for the description of SIDIS structure functions. This approximation consists of a systematic neglect of $\bar{q}gq$-terms in the correlators defining the TMDs and FFs. We have shown that in such an approach all twist-2 and twist-3 structure functions can be described in terms of 8 basis functions: 6 TMDs and 2 FFs which are each twist-2. All other TMDs and FFs, assuming this approximation, are either related to the basis functions or vanish. To make this work self-contained we reviewed the phenomenological information available on the basis functions which is given in terms of 6 SIDIS structure functions. (Of course, one cannot extract 8 basis functions from 6 observables: in particular 2 basis functions, the unpolarized TMD and FF $f_1^q(x, k_\perp)$ and $D_1^q(x, P_\perp)$, are determined from other experiments, most notably Drell-Yan and hadron production in e^+e^- annihilations.)

The WW-type approximation for TMDs and FFs is inspired by the observation that the classical WW-approximation for the twist-3 SIDIS structure function $g_2(x)$ (or PDF $g_T^q(x)$) works well. This was predicted in theoretical studies in the instanton model of the QCD vacuum, and confirmed by data and lattice QCD studies. The classic WW-approximation for $g_2(x)$ works with a relative accuracy of $\pm\,40\,\%$ or better. This is remarkable. The instanton vacuum model predicts an analog WW-approximation for the chirally odd twist-3 PDF $h_L^q(x)$ to work similarly well. This predictions remains to be tested in experiment.

In each case, $g_T^q(x)$ and $h_L^q(x)$, we deal with nucleon matrix elements of different $\bar{q}gq$ correlators, which are assumed to be small. Can one generalize these approximations to TMDs? This is a key question, which has been addressed in the past in literature in selected cases. This work is the first systematic investigation of this question. As in the unintegrated correlators one deals with different classes of operators, we prefer to speak of the WW-type approximation to distinguish from the colinear case.

We have studied in detail all SIDIS structure function in this approximation. This includes a review of results from lattice QCD calculations, effective theories and models. We found that from theoretical point of view the WW-type approximations receive certain support, though the evidence is less than in the colinear case. Most importantly, we have conducted systematic test of WW-approximations with available published or preliminary (and soon to be published) SIDIS data from HERMES, COMPASS, and JLab.

We found the following results. The two leading–twist structure functions amenable to WW-type approximation $F_{LT}^{\cos(\phi_h-\phi_S)}$ and $F_{UL}^{\sin(2\phi_h)}$ are well–described (the former) or

at least compatible (the latter) with the data in this approximation. For $F_{UT}^{\sin(2\phi_h)}$ more precise data are needed, but also in this case the trend is encouraging especially thanks to the recent COMPASS data. We have also shown that our approach satisfies positivity inequalities which is a non–trivial consistency check considering the crude approximations (WW-type, Gaussian Ansatz for TMDs) in our approach.

At subleading twist the WW-type approximation for the structure functions $F_{LT}^{\cos\phi_S}$, $F_{LT}^{\cos(2\phi_h-\phi_S)}$, $F_{LL}^{\cos\phi_h}$, $F_{UT}^{\sin\phi_S}$, $F_{UT}^{\sin(2\phi_h-\phi_S)}$ is compatible with data, too. Some of these asymmetries are predicted to be very small in the WW-type approximation, sometimes smaller than a fraction or a percent. This is compatible with the available data in the sense that the data are consistent with zero within their statistical accuracies. This cannot be considered a thorough evidence for the applicability of the WW-type approximations, but on the positive site we also observe no alarming hints that the WW-type approximations fail in these cases. Merely for $F_{UT}^{\sin\phi_S}$ in the region of large-x there is an indication that the asymmetry could be non-zero while the WW-type approximation proposes a much smaller effect. But more higher-statistic data are needed before we can draw definitive conclusions.

In the case of the three subleading–twist structure functions $F_{UU}^{\cos(2\phi_h)}$, $F_{UL}^{\sin\phi_h}$, $F_{LU}^{\sin\phi_h}$ the situation is clearer and indicates that here the WW-type approximations do not work. Incidently, these asymmetries include: $F_{UU}^{\cos(2\phi_h)}$ which is the very first non–zero azimuthal asymmetry measured in unpolarized SIDIS, $F_{UL}^{\sin\phi_h}$ which is the very first non–zero azimuthal target spin asymmetry measured in SIDIS, and $F_{LU}^{\sin\phi_h}$ which is the very first non–zero azimuthal beam spin asymmetry measured in SIDIS. The WW-type prediction for $F_{UU}^{\cos(2\phi_h)}$ suggest a large asymmetry which overshoots data by a factor of three. In the case of $F_{UL}^{\sin\phi_h}$ the WW-type approximation undershoots data by a factor of 2 or so. Most interestingly, in the case of $F_{LU}^{\sin\phi_h}$ the WW-type approximation predicts exactly a zero asymmetry, but in experiment a small but clearly non-zero effect is seen.

The non–aplicability of the WW–type approximation in these three cases should not be too surprizing. After all it is a crude method to model TMDs and FFs and an uncontrollable "expansion" (in nuclear physics the concept of 2–body, 3–body, etc operators is well-justified and an effective expansion can be conducted; in the case of TMDs however it is less appropriate to speak about a systematic expansion in terms of $\bar{q}q$, $\bar{q}gq$, etc correlators). It will be very interesting to learn whether e.g. in $F_{UL}^{\sin\phi_h}$ or $F_{LU}^{\sin\phi_h}$ a single $\bar{q}gq$–term is anomalously large, or whether it is a accumulative effect of several small terms $\bar{q}gq$–terms adding up to the observed asymmetry.

Among all SIDIS structure functions $F_{LU}^{\sin\phi_h}$ emerges as a particularly interesing case: this asymmetry is due to $\bar{q}gq$ only with no contamination from $\bar{q}q$ terms. So $F_{LU}^{\sin\phi_h}$ offers a unique view on the physics of $\bar{q}gq$ correlators which is worth–exploring for its own sake.

The results presented in this work are of importance for several reasons. First, to the best of our knowledge it is the first complete study of all SIDIS structure functions up to twist-3 in a unique approach. Second, the results are of use for experiments prepared in the near-term (JLab 12) or proposed in the long-term (Electron Ion Collider), and provide helpful input for Monte Carlo event generators [28]. Third, our predictions will help to interpret data.

It is important to remark that the generalized parton model approach of Ref. [134] provides a description, which is largely equivalent to ours. As the quality of the approximations can only be determined experimentally, future high–precision data will shed new light and allow us to access new insights abour the quark-gluon structure of the nucleon.

9 Acknowledgments

First and foremost, the authors would like to thank their families for patience and constant support throughout writing this paper. This work was partially supported by the U.S. Department of Energy under Contract No. DE-AC05-06OR23177 (A.P.) and by the National Science Foundation under Contract No. PHY-1623454 (A.P.) and Contract No. PHY-1406298 (P.S.).

A The "minimal basis" of TMDs and FFs

This Appendix describes the technical details of the parametrizations used in this work.

A.1 Unpolarised functions $f_1^a(x, k_\perp^2)$ and $D_1(z, P_\perp^2)$

In this work we use the leading-order parametrizations from [82] for the unpolarized PDF $f_1^a(x)$ and from [84] for the unpolarized FF $D_1^a(z)$. If not otherwise stated the parametrizations are taken at the scale $Q^2 = 2.4\,\mathrm{GeV}^2$ typical for many currently available SIDIS data. These parametrizations were used in [73] and other works whose extractions we adopt.

To describe the transverse momentum dependence of $f_1^a(x, k_\perp^2)$ and $D_1(z, P_\perp^2)$ we use the Gaussian Ansatz in Eqs. (4.5a, 4.5b). All early [73–76] and some recent [77] analyses employed flavor and x– or z–independent widths $\langle k_\perp^2 \rangle$ and $\langle P_\perp^2 \rangle$. In the analysis [78] of HERMES multiplicities flavor-independence of the widths was assumed. On long run one may anticipate that new precision data will require to relax these assumptions. However, one may also expect that the Gaussian Ansatz will remain a useful *approximation* as long as one is interested in describing data on transverse hadron momenta $P_{hT} \ll Q$.

The parameters resulting from calculations or extractions are presented in Table 1. As most extractions of TMDs that we will use are done with the choice of $\langle k_\perp^2 \rangle_{f_1} = 0.25$ GeV^2, $\langle P_\perp^2 \rangle_{D_1} = 0.2$ GeV^2, for our numerical estimates in this work we will use these fixed widths.

Some comments are in order. In [73] no attempt was made to assign an uncertainty of the best fit result. The uncertainty of the numbers from [76] includes only the statistical uncertainty, but no systematic uncertainty. For comparison lattice results from [41] are included whose range indicates flavor-dependence (first number u–flavor, second number d–flavor). Notice that this is the contribution of the flavor averaged over contributions from the respective quarks and antiquarks. Chiral theories predict significant differences in the $k_\perp$–behavior of sea and valence quarks [85]. We will comment more on the lattice results in the next section. In view of the large (and partly underestimated) uncertainties and the fact that those parameters are anti-correlated the numbers from the different approaches quoted in Table 1 can be considered to be in good agreement.

A.2 Helicity distribution $g_1^a(x, k_\perp^2)$

For the helicity PDF $g_1^a(x) = \int d^2k_\perp\, g_1^a(x, k_\perp^2) \equiv \int d^2k_\perp\, g_{1L}^a(x, k_\perp^2)$ we use in this work the leading-order parametrizations from [83]. If not otherwise stated the parametrizations are taken at the scale $Q^2 = 2.5\,\mathrm{GeV}^2$.

In lack of phenomenological information on the $k_\perp$–dependence of $g_1^a(x, k_\perp^2)$ we explore lattice QCD results from [41] to constrain the Gaussian width in Eq. (4.5c). On a lattice with pion and nucleon masses $m_\pi \approx 500\,\mathrm{MeV}$ and $M_N = 1.291(23)\,\mathrm{GeV}$ and with an axial coupling constant $g_A^{(3)} = 1.209(36)$ reasonably close to its physical value 1.2695(29) the following results were obtained for the mean square transverse parton momenta [41]. For the unpolarized TMDs it was found $\langle k_\perp^2 \rangle_{f_1^u} = (0.3741\,\mathrm{GeV})^2$ and $\langle k_\perp^2 \rangle_{f_1^d} = (0.3839\,\mathrm{GeV})^2$. For the helicity TMDs it was found $\langle k_\perp^2 \rangle_{g_1^u} = (0.327\,\mathrm{GeV})^2$ and $\langle k_\perp^2 \rangle_{g_1^d} = (0.385\,\mathrm{GeV})^2$. These values are quoted in Table 1.

study	$\langle Q^2\rangle$, $\langle x\rangle$, $\langle z\rangle$ [GeV^2]	$\langle k_\perp^2\rangle_{f_1}$ [GeV^2]	$\langle P_\perp^2\rangle_{D_1}$ [GeV^2]	$\langle k_\perp^2\rangle_{g_1}$ [GeV^2]
fit of [73]	5, 0.1, 0.3	~ 0.25	~ 0.2	–
fit of [76]	2.5, 0.1, 0.4	0.38 ± 0.06	0.16 ± 0.01	–
fit of [78]	2.4, 0.1, 0.3	0.57 ± 0.08	0.12 ± 0.01	–
fit of [77]	2.4, 0.1, 0.5	~ 0.3	~ 0.18	–
lattice [41]	4, – , –	0.14–0.15	–	0.11-0.15

Table 1. Gaussian model parameters for $f_1^a(x,k_\perp)$, $D_1^a(z,P_\perp)$, $g_1^a(x,k_\perp)$ from phenomenological and lattice QCD studies. The kinematics to which the phenomenological results and the renormalization scale of the lattice results are indicated. The range of lattice values indicates flavor dependence (first number refers to u–flavor, second number to d–flavor).

The lattice values for $\langle k_\perp^2\rangle_{f_1}$ consistently underestimate the phenomenological numbers, see Table 1. The exact reasons for that are unknown, but it is natural to think it might be related to the fact that the lattice predictions [41] do not refer to TMDs entering in SIDIS (or Drell-Yan or other process) because a different gauge link was chosen, see Sec. 3.5. Still one may expect these results to bear considerable information on QCD dynamics.[5] To make use of this information we shall assume that the lattice results [41] provide robust predictions for the *ratios* $\langle k_\perp^2\rangle_{g_1^u}/\langle k_\perp^2\rangle_{f_1^u} \approx 0.76$. With the phenomenological value $\langle k_\perp^2\rangle_{f_1} = 0.25$ GeV^2 we then obtain the estimate for the width of the helicity TMD $\langle k_\perp^2\rangle_{g_1} = 0.19$ GeV^2. In our phenomenological study we use this value for u–quarks and for simplicity also for d–quarks. Even though the lattice values indicate an interesting flavor dependence, see Table 1, for a proton target this is a very good approximation due to u–quark dominance. When precision data for deuterium and especially for ^{3}He from JLab become available, it will be interesting to re-investigate this point in detail.

A.3 Sivers function $f_{1T}^{\perp q}(x,k_\perp)$

Sivers distribution function was studied in Refs. [96–98, 100, 134–139]. We will use parametrizations from Refs. [96, 100, 134]:

$$\langle k_\perp^2\rangle_{f_{1T}^\perp} \equiv \frac{\langle k_\perp^2\rangle M_1^2}{\langle k_\perp^2\rangle + M_1^2} \tag{A.1}$$

$$f_{1T}^\perp(x,k_\perp^2) = -\frac{M}{M_1}\sqrt{2e}\,\mathcal{N}_q(x)\,f_{q/p}(x,Q)\,\frac{e^{-k_\perp^2/\langle k_\perp^2\rangle_{f_{1T}^\perp}}}{\pi\langle k_\perp^2\rangle}, \tag{A.2}$$

[5] The results [41] refer also to pion masses above the physical value. This caveat is presumably less critical and will be overcome as lattice QCD simulations are becoming feasible at physical pion masses.

$N_u = 0.40$	$\alpha_u = 0.35$	$\beta_u = 2.6$
$N_d = -0.97$	$\alpha_d = 0.44$	$\beta_d = 0.90$
	$M_1^2 = 0.19$ (GeV^2)	

Table 2. Best values of the fit of the Sivers functions. Table from Ref. [100]

where M_1 is a mass parameter, M the proton mass and

$$\mathcal{N}_q(x) = N_q\, x^\alpha (1-x)^\beta\, \frac{(\alpha+\beta)^{(\alpha+\beta)}}{\alpha^\alpha \beta^\beta} \tag{A.3}$$

The first moment of Sivers function is:

$$f_{1T}^{\perp(1)q}(x) = -\frac{\sqrt{\frac{e}{2}}\,\langle k_\perp^2\rangle M_1^3}{M(\langle k_\perp^2\rangle + M_1^2)^2}\,\mathcal{N}_q(x) f_q(x,Q) = -\sqrt{\frac{e}{2}}\frac{1}{MM_1}\frac{\langle k_\perp^2\rangle^2_{f_{1T}^\perp}}{\langle k_\perp^2\rangle}\,\mathcal{N}_q(x) f_q(x,Q) \tag{A.4}$$

We can rewrite parametrizations of Sivers functions as

$$f_{1T}^{\perp q}(x,k_\perp^2) = f_{1T}^{\perp(1)q}(x)\frac{2M^2}{\pi\langle k_\perp^2\rangle^2_{f_{1T}^\perp}} e^{-k_\perp^2/\langle k_\perp^2\rangle_{f_{1T}^\perp}}\ . \tag{A.5}$$

The fit the HERMES proton and COMPASS deuteron data from including only Sivers functions for u and d quarks was done in Ref. [100], corresponding to seven free parameters, and parameters are shown in Table 2.

A.4 Transversity $h_1^q(x,k_\perp)$ and Collins function $H_1^{\perp q}(x,P_\perp)$

These functions were studied in Refs. [38, 39, 102–104, 140]. The following shape was assumed for parametrizations in Refs. [38, 39, 102]:

$$h_1^q(x,k_\perp^2) = h_1^q(x)\frac{e^{-k_\perp^2/\langle k_\perp^2\rangle_{h_1}}}{\pi\langle k_\perp^2\rangle_{h_1}}\,, \tag{A.6}$$

$$h_1^q(x) = \frac{1}{2}\mathcal{N}_q^T(x)\left[f_1(x)+g_1(x)\right], \tag{A.7}$$

$$H_{1h/q}^\perp(z,P_\perp^2) = \frac{zm_h}{2P_\perp}\Delta^N D_{h/q^\uparrow}(z,P_\perp^2) = \frac{zm_h}{M_C}e^{-p_\perp^2/M_C^2}\sqrt{2e}H_{1h/q}^\perp(z)\,\frac{e^{-P_\perp^2/\langle P_\perp^2\rangle}}{\pi\langle P_\perp^2\rangle}\,, \tag{A.8}$$

with m_h the mass of the produced hadron and

$$\mathcal{N}_q^T(x) = N_q^T\, x^\alpha(1-x)^\beta\,\frac{(\alpha+\beta)^{(\alpha+\beta)}}{\alpha^\alpha\beta^\beta}\,, \tag{A.9}$$

$$H_{1h/q}^\perp(z) = \mathcal{N}_q^C(z) D_{h/q}(z)\,, \tag{A.10}$$

$$\mathcal{N}_q^C(z) = N_q^C\, z^\gamma(1-z)^\delta\,\frac{(\gamma+\delta)^{(\gamma+\delta)}}{\gamma^\gamma\delta^\delta}\,, \tag{A.11}$$

and $-1 \le N_q^T \le 1$, $-1 \le N_q^C \le 1$. The helicity distributions $g_1(x)$ are taken from Ref. [141], parton distribution and fragmentation functions are the GRV98LO PDF set [83] and the

DSS fragmentation function set [84]. Notice that with these choices both the transversity and the Collins function automatically obey their proper positivity bounds. Note that as in Ref. [102] we use two Collins fragmentation functions, *favored* and *disfavored* ones, see Ref. [102] for details on implementation, and corresponding parameters N_a^C are then N_{fav}^C and N_{dis}^C. For numerical estimates we use parameters extracted in Ref. [102], see Table 3.

$N_u^T = 0.46^{+0.20}_{-0.14}$	$N_d^T = -1.00^{+1.17}_{-0.00}$
$\alpha = 1.11^{+0.89}_{-0.66}$	$\beta = 3.64^{+5.80}_{-3.37}$
$\langle k_\perp^2\rangle_{h_1} = 0.25$ (GeV^2)	
$N^C_{\rm fav} = 0.49^{+0.20}_{-0.18}$	$N^C_{\rm dis} = -1.00^{+0.38}_{-0.00}$
$\gamma = 1.06^{+0.45}_{-0.32}$	$\delta = 0.07^{+0.42}_{-0.07}$
$M_C^2 = 1.50^{+2.00}_{-1.12}$ (GeV^2)	

Table 3. Best values of the 9 free parameters fixing the u and d quark transversity distribution functions and the favored and disfavored Collins fragmentation functions. The table is from Ref. [102].

According to Eq. (B.8) we obtain the following expression for the first moment of Collins fragmentation function:

$$H_{1h/q}^{\perp(1)}(z) = \frac{H_{1h/q}^{\perp}(z)\sqrt{e/2}\langle P_\perp^2\rangle M_C^3}{z m_h (M_C^2 + \langle P_\perp^2\rangle)^2} \,. \tag{A.12}$$

We also define the following variable:

$$\langle P_\perp^2\rangle_{H_1^\perp} = \frac{\langle P_\perp^2\rangle M_C^2}{\langle P_\perp^2\rangle + M_C^2}. \tag{A.13}$$

We can rewrite the parametrizations of Collins FF as

$$H_1^\perp(z, P_\perp^2) = H_1^{\perp(1)}(z)\frac{2z^2 m_h^2}{\pi\langle P_\perp^2\rangle^2_{H_1^\perp}} e^{-P_\perp^2/\langle P_\perp^2\rangle_{H_1^\perp}} \,. \tag{A.14}$$

A.5 Boer-Mulders function $h_1^\perp(x, k_\perp)$

The Boer-Mulders function $h_1^\perp$ [2] measures the transverse polarization asymmetry of quarks inside an unpolarized nucleon. The Boer-Mulders functions were studied phenomenologically in Refs. [106, 109, 110]

Ref. [110] used the parametrization in which Boer-Mulders function is proportional to the Sivers functions, such that:

$$\langle k_\perp^2\rangle_{h_1^\perp} = \frac{\langle k_\perp^2\rangle\, M_{BM}^2}{\langle k_\perp^2\rangle + M_{BM}^2} \,, \tag{A.15}$$

$$h_1^\perp(x, k_\perp^2) = -\frac{M}{M_{BM}}\sqrt{2e}\; N_{BM}^q N_q(x)\, f_{q/p}(x, Q)\frac{e^{-k_\perp^2/\langle k_\perp^2\rangle_{h_1^\perp}}}{\pi\langle k_\perp^2\rangle}, \tag{A.16}$$

$N^u_{BM} = 2.1 \pm 0.1$	$N^d_{BM} =$	-1.111 ± 0.001
Fixed	parameters:	
$N_u = 0.35$	$\alpha_u = 0.73$	$\beta_u = 3.46$
$N_d = -0.9$	$\alpha_d = 1.08$	$\beta_d = 3.46$
	$M^2_{BM} =$	0.34 (GeV^2)

Table 4. Fitted parameters of Boer-Mulders quark distributions. Values are from Ref. [109].

where

$$\mathcal{N}_q(x) = N_q\, x^\alpha (1-x)^\beta\, \frac{(\alpha+\beta)^{(\alpha+\beta)}}{\alpha^\alpha \beta^\beta}\,. \tag{A.17}$$

The first moment of Boer-Mulders function is:

$$h_1^{\perp(1)q}(x) = -\frac{\sqrt{\frac{e}{2}}\,\langle k_\perp^2\rangle M_{BM}^3}{M(\langle k_\perp^2\rangle + M_{BM}^2)^2}\; N_q f_q(x,Q) = -\sqrt{\frac{e}{2}}\frac{1}{M M_{BM}}\frac{\langle k_\perp^2\rangle^2_{h_1^\perp}}{\langle k_\perp^2\rangle}\; N_q f_q(x,Q) \tag{A.18}$$

We can rewrite parametrizations of Boer-Mulders functions as

$$h_1^{\perp q}(x,k_\perp^2) = h_1^{\perp(1)q}(x)\frac{2M^2}{\pi\langle k_\perp^2\rangle^2_{h_1^\perp}} e^{-k_\perp^2/\langle k_\perp^2\rangle_{h_1^\perp}}\,. \tag{A.19}$$

A.6 Pretzelosity distribution $h_{1T}^\perp(x, k_\perp)$

Pretzelosity distribution function $h_{1T}^\perp$ [112] describes transversely polarized quarks inside a transversely polarized nucleon. We use the following form of $h_{1T}^{\perp a}$ [112]:

$$h_{1T}^{\perp a}(x,k_\perp^2) = \frac{M^2}{M_{TT}^2} e^{-k_\perp^2/M_{TT}^2} h_{1T}^{\perp a}(x)\frac{e^{-k_\perp^2/\langle k_\perp^2\rangle}}{\pi\langle k_\perp^2\rangle} = \frac{M^2}{M_T^2} h_{1T}^{\perp a}(x)\frac{e^{-k_\perp^2/\langle k_\perp^2\rangle_{h_{1T}^\perp}}}{\pi\langle k_\perp^2\rangle}\,, \tag{A.20}$$

where

$$h_{1T}^{\perp a}(x) = e\,\mathcal{N}^a(x)(f_1^a(x,Q) - g_1^a(x,Q)), \tag{A.21}$$

$$\mathcal{N}^a(x) = N^a x^\alpha (1-x)^\beta \frac{(\alpha+\beta)^{\alpha+\beta}}{\alpha^\alpha\beta^\beta}\,, \tag{A.22}$$

$$\langle k_\perp^2\rangle_{h_{1T}^\perp} = \frac{\langle k_\perp^2\rangle M_{TT}^2}{\langle k_\perp^2\rangle + M_{TT}^2}\,, \tag{A.23}$$

where N^a, α, β, and M_T are parameters fitted to data that can be found in Table 5.

We use Eq. (B.8) to calculate the second moment of $h_{1T}^{\perp a}(x,k_\perp^2)$ of Eq. (A.20) and obtain:

$$h_{1T}^{\perp(2)a}(x) = \frac{h_{1T}^{\perp a}(x)\langle k_\perp^2\rangle^3_{h_{1T}^\perp}}{2M^2 M_{TT}^2\langle k_\perp^2\rangle}\,. \tag{A.24}$$

We can rewrite parametrization of pretzelosity functions as

$$h_{1T}^{\perp q}(x,k_\perp^2) = h_{1T}^{\perp(2)q}(x)\frac{2M^4}{\pi\langle k_\perp^2\rangle^3_{h_{1T}^\perp}} e^{-k_\perp^2/\langle k_\perp^2\rangle_{h_{1T}^\perp}}\,. \tag{A.25}$$

α	=	2.5 ± 1.5	β	=	2 fixed
N_u	=	1 ± 1.4	N_d	=	-1 ± 1.3
M_{TT}^2	=	0.18 ± 0.7	(GeV^2)		

Table 5. Fitted parameters of the pretzelosity quark distributions. Table from Ref. [112]

B Convolution integrals and expressions in Gaussian Ansatz

In this Appendix we explain the notation for convolution integrals of TMDs and FFs and give the explicit results obtained assuming the Gaussian Ansatz.

B.1 Notation for convolution integrals

Structure functions are expressed as convolutions of TMDs and FFs in the Bjorken limit at tree level. For reference we quote the convolution integrals in "Amsterdam notation" [4]

$$\mathcal{C}\big[w\,f\,D\big] = x\sum_a e_a^2 \int d^2\boldsymbol{p}_T\, d^2\boldsymbol{k}_T\, \delta^{(2)}\big(\boldsymbol{p}_T - \boldsymbol{k}_T - \boldsymbol{P}_{h\perp}/z\big)\, w(\boldsymbol{p}_T,\boldsymbol{k}_T)\, f^a(x,p_T^2)\, D^a(z,z^2k_T^2), \tag{B.1}$$

where all transverse momenta refer to the virtual photon-proton center-of-mass frame and $\hat{\boldsymbol{h}} = \boldsymbol{P}_{h\perp}/P_{h\perp}$. Hereby $\boldsymbol{p}_T$ is the transverse momentum of quark with respect to nucleon, $\boldsymbol{k}_T$ is the transverse momentum of the fragmenting quark with respect to produced hadron. The notation is not unique. The one chosen in this work, in comparison to other works, is

$$\text{transverse momentum in TMD:}\quad [\boldsymbol{k}_\perp]_{\text{our}} = [\boldsymbol{k}_\perp]_{\text{Ref.[134]}} = [\boldsymbol{p}_T]_{\text{Ref.[4]}}\,, \tag{B.2}$$

$$\text{transverse momentum in FF:}\quad [\boldsymbol{P}_\perp]_{\text{our}} = [\boldsymbol{p}_\perp]_{\text{Ref.[134]}} = -z\,[\boldsymbol{k}_T]_{\text{Ref.[4]}}\,, \tag{B.3}$$

$$\text{transverse hadron momenta:}\quad [\boldsymbol{P}_{hT}]_{\text{our}} = [\boldsymbol{P}_T]_{\text{Ref.[134]}} = [\boldsymbol{P}_{h\perp}]_{\text{Ref.[4]}}\,. \tag{B.4}$$

Notice that $[\boldsymbol{P}_\perp]_{\text{our}} = -z\,[\boldsymbol{k}_T]_{\text{Ref.[4]}}$ is the transverse momentum the hadron acquires in the fragmentation process. The normalization for unpolarized fragmentation functions is

$$D_1^a(z) = \left[\int d^2\boldsymbol{P}_\perp D_1^a(z,P_\perp^2)\right]_{\text{our}} = \left[z^2\int d^2\boldsymbol{k}_T D_1^a(z,z^2k_T^2)\right]_{\text{Ref. [4]}}\,. \tag{B.5}$$

The "Amsterdam" convolution integral (B.1) reads in our notation

$$\mathcal{C}\big[w\,f\,D\big] = x\sum_a e_a^2 \int d^2\boldsymbol{k}_\perp\, d^2\boldsymbol{P}_\perp\, \delta^{(2)}\big(z\boldsymbol{k}_\perp + \boldsymbol{P}_\perp - \boldsymbol{P}_{hT}\big)\, w\left(\boldsymbol{k}_\perp, -\frac{\boldsymbol{P}_\perp}{z}\right) f^a(x,k_\perp^2)\, D^a(z,P_\perp^2). \tag{B.6}$$

B.2 Gaussian Ansatz

For a generic TMD and FF the Gaussian Ansatz is given by

$$f^a(x,k_\perp^2) = f^a(x)\,\frac{\exp(-k_\perp^2/\langle k_\perp^2\rangle)}{\pi\langle k_\perp^2\rangle}\,,\quad D^a(z,P_\perp^2) = D^a(z)\,\frac{\exp(-P_\perp^2/\langle P_\perp^2\rangle)}{\pi\langle P_\perp^2\rangle} \tag{B.7}$$

where $\langle k_\perp^2\rangle$ could be x–dependent, and $\langle P_\perp^2\rangle$ z–dependent. Both could be flavor-dependent. The variable $P_\perp$ is convenient because phenomenological experience shows that $P_\perp$ in

$D_1^{q/h}(z, P_\perp^2)$ exhibits a Gaussian distribution with weakly z–dependent Gaussian width. The distribution of transverse momenta in $\left[D^a(z, z^2 k_T^2)\right]_{\text{Ref.[4]}}$ would require a strongly z–dependent Gaussian width. It is a matter of taste which one prefers to use.

It is convenient to work with transverse moments of TMDs and FFs which are defined, and in the Gaussian model given by

$$\begin{aligned} f^{(n)}(x) = & \int d^2\boldsymbol{k}_\perp \left(\frac{k_\perp^2}{2M^2}\right)^n f(x, k_\perp^2) \overset{\text{Gauss}}{=} \frac{n!\,\langle k_\perp^2\rangle^n}{2^n\, M_N^{2n}}\, f(x), \\ D^{(n)}(z) = & \int d^2\boldsymbol{P}_\perp \left(\frac{P_\perp^2}{2z^2 m_h^2}\right)^n D(z, P_\perp^2) \overset{\text{Gauss}}{=} \frac{n!\,\langle P_\perp^2\rangle^n}{2^n z^{2n}\, m_h^{2n}} D(z)\,. \end{aligned} \tag{B.8}$$

It is important to keep in mind that these objects are well-defined in the Gaussian model. However, in QCD and even in simple models [54, 85] one faces issues with UV divergences and has to carefully define how to deal with them.

In Eqs. (B.8) the Gaussian dependence is factorized from x or z dependence and parametrizations are made with respect to either $f(x)$ or $D(z)$. As we saw in Appendix A some TMD functions are parametrized with higher moments directly as operator product expansion of TMDs may start from higher twist matrix element instead of the usual twist-2 one. In those cases equivalent formulas to Eqs. (B.8) can be easily derived.

B.3 Gaussian Ansätze for the derived TMDs used in this work

The Gaussian Ansätze for the 8 basis functions were shown in Eqs. (4.5a–4.5h) in Sec. 4.4, and the pertinent parameters and parametrizations were reviewed in App. A. Besides the basis function we also need Ansätze for the following TMDs as listed below:

$$g_{1T}^{\perp q}(x,k_\perp^2) = g_{1T}^{\perp(1)q}(x)\,\frac{2M_N^2}{\pi\langle k_\perp^2\rangle_{g_{1T}^\perp}^2}\,e^{-k_\perp^2/\langle k_\perp^2\rangle_{g_{1T}^\perp}}\,, \qquad \text{cf. Sec. 6.1,} \tag{B.9a}$$

$$h_{1L}^{\perp a}(x,k_\perp^2) = h_{1L}^{\perp(1)a}(x)\,\frac{2M_N^2}{\pi\langle k_\perp^2\rangle_{h_{1L}^\perp}^2}\,e^{-k_\perp^2/\langle k_\perp^2\rangle_{h_{1L}^\perp}^2} \qquad \text{cf. Sec. 6.2,} \tag{B.9b}$$

$$g_T^q(x,k_\perp^2) = g_T^q(x)\,\frac{1}{\pi\langle k_\perp^2\rangle_{g_T}}\,e^{-k_\perp^2/\langle k_\perp^2\rangle_{g_T}}\,, \qquad \text{cf. Sec. 7.2,} \tag{B.9c}$$

$$g_T^{\perp q}(x,k_\perp^2) = g_T^{\perp(2)q}(x)\,\frac{2M^4}{\pi\langle k_\perp^2\rangle_{g_T^\perp}^3}\,e^{-k_\perp^2/\langle k_\perp^2\rangle_{g_T^\perp}}\,, \qquad \text{cf. Sec. 7.3,} \tag{B.9d}$$

$$g_L^{\perp q}(x,k_\perp^2) = g_L^{\perp(1)q}(x)\,\frac{2M_N^2}{\pi\langle k_\perp^2\rangle_{g_L^\perp}^2}\,e^{-k_\perp^2/\langle k_\perp^2\rangle_{g_L^\perp}}\,, \qquad \text{cf. Sec. 7.4,} \tag{B.9e}$$

$$h_L^q(x,k_\perp^2) = h_L^q(x)\,\frac{1}{\pi\langle k_\perp^2\rangle_{h_L}}\,e^{-k_\perp^2/\langle k_\perp^2\rangle_{h_L}}\,, \qquad \text{cf. Sec. 7.5,} \tag{B.9f}$$

$$h_T^{\perp q}(x,k_\perp^2) = h_T^{\perp(1)q}(x)\,\frac{2M^2}{\pi\langle k_\perp^2\rangle_{h_T^\perp}^2}\,e^{-k_\perp^2/\langle k_\perp^2\rangle_{h_T^\perp}}\,, \qquad \text{cf. Sec. 7.6,} \tag{B.9g}$$

$$h_T^q(x,k_\perp^2) = h_T^{(1)q}(x)\,\frac{2M^2}{\pi\langle k_\perp^2\rangle_{h_T}^2}\,e^{-k_\perp^2/\langle k_\perp^2\rangle_{h_T}}\,, \qquad \text{cf. Sec. 7.6,} \tag{B.9h}$$

$$f_T^{\perp q}(x,k_\perp^2) = f_T^{\perp(2)q}(x)\,\frac{2M^4}{\pi\langle k_\perp^2\rangle_{f_T^\perp}^3}\,e^{-k_\perp^2/\langle k_\perp^2\rangle_{f_T^\perp}}\,, \qquad \text{cf. Sec. 7.7,} \tag{B.9i}$$

$$f^{\perp q}(x,k_\perp^2) = f^{\perp(1)q}(x)\,\frac{2M^2}{\pi\langle k_\perp^2\rangle_{f^\perp}^2}\,e^{-k_\perp^2/\langle k_\perp^2\rangle_{f^\perp}}\,, \qquad \text{cf. Sec. 7.8,} \tag{B.9j}$$

B.4 Comment on TMDs subject to the sum rules (2.14)

In this section we comment on the twist-3 TMDs $f_T^q(x,k_\perp)$, $h^q(x,k_\perp)$, $e_L^q(x,k_\perp)$, which are T-odd, appear in the decompositions of the correlator with no explicit $k_\perp^j$–prefactors, and would have colinear PDF counterparts. But T-odd PDFs are forbidden by time-reversal and parity invariance of strong interactions, which dictate the sum rules (2.14), see Sec. 3.8. Such TMDs could be described by functions with a node in $k_\perp$[6] such that they can integrate to zero in Eq. (2.14). A single Gaussian has no node and is not adequate for that. However,

[6]The possibility of TMDs with nodes is not unrealistic. For instance in the covariant parton model the helicity TMDs exhibit nodes for the u– and d–flavor [65]. We will have to revise our description of $g_1^q(x,k_\perp)$ in Eq. (4.5c) and App. A.2 to something of the type (B.10), if that prediction is confirmed experimentally.

one could work with a superposition of Gaussians with different widths,

$$x\, f_T^q(x,k_\perp) = -\, f_{1T}^{\perp(1)q}(x) \sum_{i=1}^{n} a_i \, \frac{\exp(-k_\perp^2/\langle k_\perp^2\rangle_i)}{\pi\langle k_\perp^2\rangle_i}\,, \qquad \text{(B.10)}$$

$$\sum_{i=1}^{n} a_i = 0\,, \quad \langle k_\perp^2\rangle_i \neq \langle k_\perp^2\rangle_j \;\; \forall\, i\neq j,\; 1\leq i,\, j\leq n,\; n\geq 2.$$

Notice that in (B.10) we cannot write "$f_T^q(x)$" which would be zero according to (2.14) and we explore here the WW-type approximation (3.4g). The minimal choice would be $n=2$ with $a_1=-a_2=1$ and $\langle k_\perp^2\rangle_1 = \langle k_\perp^2\rangle_{f_{1T}^\perp}$ to make use of the theoretical guidance provided by the WW-type approximation (3.4g). The second Gaussian width $\langle k_\perp^2\rangle_2$ could be chosen very large $\langle k_\perp^2\rangle_2 \gg \langle k_\perp^2\rangle_{f_1^\perp}$ to model the Gaussian description of $f_T^q(x,k_\perp)$ similar to that of $f_{1T}^{\perp(1)q}(x,k_\perp^2)$ at intermediate $k_\perp$. A very large parameter $\langle k_\perp^2\rangle_2$ could be thought of as a relict which enters in the sum rule (2.14) where the $k_\perp$–integration formally extends up to infinity where the TMD description does not apply. The theoretical understanding of higher–twist TMDs is too limited at the present stage, but in principle this could be a pragmatic way of modelling the TMD $f_T^q(x,k_\perp)$ and analogously $h^q(x,k_\perp)$, $e_L^q(x,k_\perp)$.

B.5 Convolution integrals in Gaussian Ansatz

Solving the convolution integrals relevant for SIDIS in the Gaussian Ansatz yields

$$\mathcal{C}\big[\,\omega^{\{0\}}\,f\,D\big] = \quad u\,\mathcal{G}(P_{hT}) \tag{B.11a}$$

$$\mathcal{C}\big[\omega_{\mathrm{A}}^{\{1\}}\,f\,D\big] = \quad u\,\mathcal{G}(P_{hT})\left(\frac{zP_{hT}}{m_h}\right)\frac{\langle P_\perp^2\rangle}{z^2\lambda} \tag{B.11b}$$

$$\mathcal{C}\big[\omega_{\mathrm{B}}^{\{1\}}\,f\,D\big] = -\,u\,\mathcal{G}(P_{hT})\left(\frac{zP_{hT}}{M_N}\right)\frac{\langle k_\perp^2\rangle}{\lambda} \tag{B.11c}$$

$$\mathcal{C}\big[\omega_{\mathrm{A}}^{\{2\}}\,f\,D\big] = \quad u\,\mathcal{G}(P_{hT})\,\frac{\langle k_\perp^2\rangle\langle P_\perp^2\rangle}{\lambda M_N m_h}\left(-1+\frac{2P_{hT}^2}{\lambda}\right) \tag{B.11d}$$

$$\mathcal{C}\big[\omega_{\mathrm{B}}^{\{2\}}\,f\,D\big] = \quad u\,\mathcal{G}(P_{hT})\,\frac{\langle k_\perp^2\rangle\langle P_\perp^2\rangle}{\lambda M_N m_h}\left(1-\frac{P_{hT}^2}{\lambda}\right) \tag{B.11e}$$

$$\mathcal{C}\big[\,\omega_{\mathrm{AB}}^{\{2\}}\,f\,D\big] = \quad u\,\mathcal{G}(P_{hT})\left(\frac{zP_{hT}}{M_N}\right)\left(\frac{zP_{hT}}{M_h}\right)\frac{\langle k_\perp^2\rangle}{\lambda}\,\frac{\langle P_\perp^2\rangle}{z^2\lambda} \tag{B.11f}$$

$$\mathcal{C}\big[\,\omega_{\mathrm{C}}^{\{2\}}\,f\,D\big] = \quad \frac{u}{2}\,\mathcal{G}(P_{hT})\left(\frac{zP_{hT}}{M_N}\right)\left(\frac{zP_{hT}}{M_N}\right)\frac{\langle k_\perp^2\rangle}{\lambda}\,\frac{\langle k_\perp^2\rangle}{\lambda} \tag{B.11g}$$

$$\mathcal{C}\big[\,\omega^{\{3\}}\,f\,D\big] = \quad \frac{u}{2}\,\mathcal{G}(P_{hT})\left(\frac{zP_{hT}}{M_N}\right)\left(\frac{zP_{hT}}{M_N}\right)\left(\frac{zP_{hT}}{m_h}\right)\frac{\langle k_\perp^2\rangle}{\lambda}\,\frac{\langle k_\perp^2\rangle}{\lambda}\,\frac{\langle P_\perp^2\rangle}{z^2\lambda} \tag{B.11h}$$

with the $\omega_i^{\{n\}}$ as defined in Eq. (2.20), and we introduced the abbreviations

$$u = x\sum_a e_a^2 f^a(x)D^a(z)\,,\quad \mathcal{G}(P_{hT}) = \frac{\exp(-P_{hT}^2/\lambda)}{\pi\lambda}\,,\quad \lambda = z^2\langle k_\perp^2\rangle + \langle P_\perp^2\rangle\,, \tag{B.12}$$

with the normalization $\int d^2P_{hT}\,\mathcal{G}(P_{hT}) = 1$. It is important to keep in mind that strictly speaking $\mathcal{G}(P_{hT}) = \mathcal{G}(P_{hT}, x, z)$ *also* depends on x and z. The "non-compact" notation in Eqs. (B.11) was chosen to display the pattern. The masses M_N or m_h in the denominators of the P_{hT} indicate the "origins" of the contributions: due to intrinsic $k_\perp$ from target, due to transverse momenta $P_\perp$ acquired during fragmentation, or both. The weight $\omega_{\mathrm{B}}^{\{2\}}$ is the only which enters cross sections and does not have a homogeneous scaling in P_{hT}.

For practical application it is convenient to absorb as many (Gaussian model) parameters as possible into expressions that can be more easily fitted to data. One way to achieve this is to make use of the transverse moments (B.8). We introduce the following abbreviations

$$u_{\mathrm{A}}^{\{1\}} = \quad x\sum_a e_a^2 f^a(x)D^{(1)a}(z)\,,\qquad u_{\mathrm{B}}^{\{1\}} = x\sum_a e_a^2 f^{(1)a}(x)D^a(z)\,, \tag{B.13}$$

$$u_{\mathrm{AB}}^{\{2\}} = x\sum_a e_a^2 f^{(1)a}(x)D^{(1)a}(z)\,,\qquad u_{\mathrm{C}}^{\{2\}} = x\sum_a e_a^2 f^{(2)a}(x)D^a(z)\,, \tag{B.14}$$

$$u_{\mathrm{C}}^{\{3\}} = x\sum_a e_a^2 f^{(2)a}(x)D^{(1)a}(z)\,. \tag{B.15}$$

In this notation the results in Eqs. (B.11) read

$$\mathcal{C}\big[\omega_{\rm A}^{\{1\}}\, f\, D\big] = \quad u_{\rm A}^{(1)}\, \mathcal{G}(P_{hT})\, \left(\frac{zP_{hT}}{m_h}\right) \frac{2m_h^2}{\lambda} \tag{B.16a}$$

$$\mathcal{C}\big[\omega_{\rm B}^{\{1\}}\, f\, D\big] = -\, u_{\rm B}^{(1)}\, \mathcal{G}(P_{hT})\, \left(\frac{zP_{hT}}{M_N}\right) \frac{2M_N^2}{\lambda} \tag{B.16b}$$

$$\mathcal{C}\big[\omega_{\rm B}^{\{2\}}\, f\, D\big] = \quad u_{\rm B}^{(2)}\, \mathcal{G}(P_{hT})\, \frac{4z^2 m_h\, M_N}{\lambda} \left(1 - \frac{P_{hT}^2}{\lambda}\right) \tag{B.16c}$$

$$\mathcal{C}\big[\,\omega_{\rm AB}^{\{2\}}\, f\, D\big] = \quad u_{\rm AB}^{(2)}\, \mathcal{G}(P_{hT})\, \left(\frac{zP_{hT}}{M_N}\right)\left(\frac{zP_{hT}}{M_h}\right) \frac{2M_N^2}{\lambda}\, \frac{2m_h^2}{\lambda} \tag{B.16d}$$

$$\mathcal{C}\big[\,\omega_{\rm C}^{\{2\}}\, f\, D\big] = \quad \frac{u_{\rm C}^{(2)}}{2}\, \mathcal{G}(P_{hT})\, \left(\frac{zP_{hT}}{M_N}\right)\left(\frac{zP_{hT}}{M_N}\right) \frac{2M_N^2}{\lambda}\, \frac{2M_N^2}{\lambda} \tag{B.16e}$$

$$\mathcal{C}\big[\,\omega^{\{3\}}\, f\, D\big] = \quad \frac{u^{(3)}}{2}\, \mathcal{G}(P_{hT})\, \left(\frac{zP_{hT}}{M_N}\right)\left(\frac{zP_{hT}}{M_N}\right)\left(\frac{zP_{hT}}{m_h}\right) \frac{2M_N^2}{\lambda}\, \frac{2M_N^2}{\lambda}\, \frac{2m_h^2}{\lambda} \tag{B.16f}$$

In this notation the results in Eqs. (B.11) read

$$\mathcal{C}\big[\omega_i^{\{n\}}\, f\, D\big] = u_i^{(n)}\, \mathcal{G}(P_{hT}) \;\times \left[\delta_{n2}\, \delta_{i\rm B}\, a_B^{(2)} + b_i^{(n)} \left(\frac{zP_{hT}}{\lambda}\right)^n\right] \tag{B.17}$$

with

$$b^{(0)} = 1\,, \tag{B.18}$$

$$b_{\rm A}^{(1)} = 2m_h\,, \qquad b_{\rm B}^{(1)} = 2M_N\,, \tag{B.19}$$

$$a_{\rm B}^{(2)} = 4M_N m_h \lambda^{-1}\, z^2\,, \qquad b_{\rm AB}^{(2)} = -\, b_{\rm B}^{(2)} = 4M_N m_h\,, \qquad b_{\rm C}^{(2)} = M_N^2\,, \tag{B.20}$$

$$b^{(3)} = 2M_N^2 m_h\,. \tag{B.21}$$

Finally, integrating out transverse hadron momenta yields

$$\int d^2P_{hT}\, \mathcal{C}\big[\,\omega_i^{\{n\}}\, f\, D\big] = u_i^{(n)}\, c_i^{(n)}\, \left(\frac{z}{\lambda^{1/2}}\right)^n \tag{B.22}$$

with

$$c^{(0)} = 1\,, \tag{B.23}$$

$$c_{\rm A}^{(1)} = \sqrt{\pi}\, m_h\,, \qquad c_{\rm B}^{(1)} = \sqrt{\pi}\, M_N\,, \tag{B.24}$$

$$c_{\rm AB}^{(2)} = 4M_N m_h\,, \qquad c_{\rm C}^{(2)} = M_N^2\,, \qquad c_{\rm B}^{(2)} = 0\,, \tag{B.25}$$

$$c^{(3)} = \tfrac{3}{2}\sqrt{\pi}\, M_N^2 m_h\,. \tag{B.26}$$

References

[1] P. J. Mulders and R. D. Tangerman, *The complete tree-level result up to order 1/Q for polarized deep-inelastic leptoproduction*, *Nucl. Phys.* **B461** (1996) 197–237, [hep-ph/9510301].

[2] D. Boer and P. J. Mulders, *Time-reversal odd distribution functions in leptoproduction*, *Phys. Rev.* **D57** (1998) 5780–5786, [hep-ph/9711485].

[3] K. Goeke, A. Metz and M. Schlegel, *Parameterization of the quark-quark correlator of a spin- 1/2 hadron*, *Phys. Lett.* **B618** (2005) 90–96, [hep-ph/0504130].

[4] A. Bacchetta et al., *Semi-inclusive deep inelastic scattering at small transverse momentum*, *JHEP* **02** (2007) 093, [hep-ph/0611265].

[5] S. Arnold, A. Metz and M. Schlegel, *Dilepton production from polarized hadron hadron collisions*, 0809.2262.

[6] A. Metz and A. Vossen, *Parton Fragmentation Functions*, *Prog. Part. Nucl. Phys.* **91** (2016) 136–202, [1607.02521].

[7] G. A. Miller, *Densities, Parton Distributions, and Measuring the Non-Spherical Shape of the Nucleon*, *Phys.Rev.* **C76** (2007) 065209, [0708.2297].

[8] M. Burkardt, *Spin-orbit correlations and single-spin asymmetries*, 0709.2966.

[9] M. Burkardt, *The g(2) Structure Function*, *AIP Conf.Proc.* **1155** (2009) 26–34, [0905.4079].

[10] A. Bacchetta, M. Boglione, A. Henneman and P. J. Mulders, *Bounds on transverse momentum dependent distribution and fragmentation functions*, *Phys. Rev. Lett.* **85** (2000) 712–715, [hep-ph/9912490].

[11] S. Wandzura and F. Wilczek, *Sum Rules for Spin Dependent Electroproduction: Test of Relativistic Constituent Quarks*, *Phys. Lett.* **B72** (1977) 195.

[12] R. Jaffe and X.-D. Ji, *Chiral odd parton distributions and Drell-Yan processes*, *Nucl.Phys.* **B375** (1992) 527–560.

[13] R. Jaffe, *G(2): The Nucleon's Other Spin Dependent Structure Function*, *Comments Nucl.Part.Phys.* **19** (1990) 239.

[14] J. Balla, M. V. Polyakov and C. Weiss, *Nucleon matrix elements of higher twist operators from the instanton vacuum*, *Nucl.Phys.* **B510** (1998) 327–364, [hep-ph/9707515].

[15] B. Dressler and M. V. Polyakov, *On the twist - three contribution to h(L) in the instanton vacuum*, *Phys.Rev.* **D61** (2000) 097501, [hep-ph/9912376].

[16] M. Gockeler, R. Horsley, W. Kurzinger, H. Oelrich, D. Pleiter et al., *A Lattice calculation of the nucleon's spin dependent structure function g(2) revisited*, *Phys.Rev.* **D63** (2001) 074506, [hep-lat/0011091].

[17] M. Gockeler, R. Horsley, D. Pleiter, P. E. Rakow, A. Schafer et al., *Investigation of the second moment of the nucleon's g(1) and g(2) structure functions in two-flavor lattice QCD*, *Phys.Rev.* **D72** (2005) 054507, [hep-lat/0506017].

[18] E143 collaboration, K. Abe et al., *Measurements of the proton and deuteron spin structure functions g1 and g2*, *Phys. Rev.* **D58** (1998) 112003, [hep-ph/9802357].

[19] E155 collaboration, P. L. Anthony et al., *Precision measurement of the proton and deuteron spin structure functions g2 and asymmetries A(2)*, *Phys. Lett.* **B553** (2003) 18–24, [hep-ex/0204028].

[20] HERMES collaboration, A. Airapetian et al., *Measurement of the virtual-photon asymmetry A_2 and the spin-structure function g_2 of the proton*, *Eur. Phys. J.* **C72** (2012) 1921, [1112.5584].

[21] A. M. Kotzinian and P. J. Mulders, *Longitudinal quark polarization in transversely polarized nucleons*, *Phys. Rev.* **D54** (1996) 1229–1232, [hep-ph/9511420].

[22] A. M. Kotzinian and P. J. Mulders, *Probing transverse quark polarization via azimuthal asymmetries in leptoproduction*, *Phys. Lett.* **B406** (1997) 373–380, [hep-ph/9701330].

[23] A. Kotzinian, B. Parsamyan and A. Prokudin, *Predictions for double spin asymmetry A(LT) in semi inclusive DIS*, *Phys. Rev.* **D73** (2006) 114017, [hep-ph/0603194].

[24] H. Avakian et al., *Are there approximate relations among transverse momentum dependent distribution functions?*, *Phys. Rev.* **D77** (2008) 014023, [0709.3253].

[25] A. Metz, P. Schweitzer and T. Teckentrup, *Lorentz invariance relations between parton distributions and the Wandzura-Wilczek approximation*, *Phys. Lett.* **B680** (2009) 141–147, [0810.5212].

[26] T. Teckentrup, A. Metz and P. Schweitzer, *Lorentz invariance relations and Wandzura-Wilczek approximation*, *Mod.Phys.Lett.* **A24** (2009) 2950–2959, [0910.2567].

[27] R. Tangerman and P. Mulders, *Polarized twist - three distributions g(T) and h(L) and the role of intrinsic transverse momentum*, hep-ph/9408305.

[28] H. Avakian, H. Matevosyan, B. Pasquini and P. Schweitzer, *Studying the information content of TMDs using Monte Carlo generators*, *J. Phys.* **G42** (2015) 034015.

[29] J. C. Collins, *Leading-twist single-transverse-spin asymmetries: Drell- Yan and deep-inelastic scattering*, *Phys. Lett.* **B536** (2002) 43–48, [hep-ph/0204004].

[30] J. P. Ralston and D. E. Soper, *Production of Dimuons from High-Energy Polarized Proton Proton Collisions*, *Nucl. Phys.* **B152** (1979) 109.

[31] A. Efremov and P. Schweitzer, *The Chirally odd twist 3 distribution e(a)(x)*, *JHEP* **0308** (2003) 006, [hep-ph/0212044].

[32] R. L. Jaffe, *Spin, twist and hadron structure in deep inelastic processes*, hep-ph/9602236.

[33] E. V. Shuryak, *The Role of Instantons in Quantum Chromodynamics. 1. Physical Vacuum*, *Nucl.Phys.* **B203** (1982) 93.

[34] D. Diakonov and V. Y. Petrov, *Instanton Based Vacuum from Feynman Variational Principle*, *Nucl.Phys.* **B245** (1984) 259.

[35] D. Diakonov, M. V. Polyakov and C. Weiss, *Hadronic matrix elements of gluon operators in the instanton vacuum*, *Nucl.Phys.* **B461** (1996) 539–580, [hep-ph/9510232].

[36] A. Accardi, A. Bacchetta, W. Melnitchouk and M. Schlegel, *What can break the Wandzura–Wilczek relation?*, *JHEP* **11** (2009) 093, [0907.2942].

[37] A. V. Efremov, K. Goeke and P. Schweitzer, *Collins effect in semi-inclusive deeply inelastic scattering and in e+ e- annihilation*, *Phys. Rev.* **D73** (2006) 094025.

[38] M. Anselmino et al., *Transversity and Collins functions from SIDIS and e+ e- data*, *Phys. Rev.* **D75** (2007) 054032, [hep-ph/0701006].

[39] M. Anselmino et al., *Update on transversity and Collins functions from SIDIS and e+ e- data*, *Nucl. Phys. Proc. Suppl.* **191** (2009) 98–107, [0812.4366].

[40] Y. Koike, K. Tanaka and S. Yoshida, *Drell-Yan double-spin asymmetry A(LT) in polarized p anti-p collisions: Wandzura-Wilczek contribution*, *Phys.Lett.* **B668** (2008) 286–292, [0805.2289].

[41] P. Hagler, B. U. Musch, J. W. Negele and A. Schafer, *Intrinsic quark transverse momentum in the nucleon from lattice QCD*, *Europhys. Lett.* **88** (2009) 61001, [0908.1283].

[42] B. U. Musch, P. Hagler, J. W. Negele and A. Schafer, *Exploring quark transverse momentum distributions with lattice QCD*, *Phys. Rev.* **D83** (2011) 094507, [1011.1213].

[43] B. Yoon, M. Engelhardt, R. Gupta, T. Bhattacharya, J. R. Green, B. U. Musch et al., *Nucleon Transverse Momentum-dependent Parton Distributions in Lattice QCD: Renormalization Patterns and Discretization Effects*, *Phys. Rev.* **D96** (2017) 094508, [1706.03406].

[44] M. Engelhardt, P. Hägler, B. Musch, J. Negele and A. Schäfer, *Lattice QCD study of the Boer-Mulders effect in a pion*, *Phys. Rev.* **D93** (2016) 054501, [1506.07826].

[45] X. Ji, P. Sun, X. Xiong and F. Yuan, *Soft factor subtraction and transverse momentum dependent parton distributions on the lattice*, *Phys. Rev.* **D91** (2015) 074009, [1405.7640].

[46] B. U. Musch, P. Hagler, M. Engelhardt, J. W. Negele and A. Schafer, *Sivers and Boer-Mulders observables from lattice QCD*, *Phys. Rev.* **D85** (2012) 094510, [1111.4249].

[47] LHPC collaboration, LHPC et al., *Transverse structure of nucleon parton distributions from lattice QCD*, *Phys. Rev. Lett.* **93** (2004) 112001, [hep-lat/0312014].

[48] LHPC Collaborations collaboration, P. Hagler et al., *Nucleon Generalized Parton Distributions from Full Lattice QCD*, *Phys.Rev.* **D77** (2008) 094502, [0705.4295].

[49] QCDSF collaboration, M. Gockeler et al., *Quark helicity flip generalized parton distributions from two-flavor lattice QCD*, *Phys. Lett.* **B627** (2005) 113–123, [hep-lat/0507001].

[50] M. Burkardt and Y. Koike, *Violation of sum rules for twist three parton distributions in QCD*, *Nucl.Phys.* **B632** (2002) 311–329, [hep-ph/0111343].

[51] S. D. Bass, *Fixed poles, polarized glue and nucleon spin structure*, *Acta Phys.Polon.* **B34** (2003) 5893–5926, [hep-ph/0311174].

[52] M. Stratmann, *Bag model predictions for polarized structure functions and their Q**2 evolutions*, *Z.Phys.* **C60** (1993) 763–772.

[53] A. Signal, *Calculations of higher twist distribution functions in the MIT bag model*, *Nucl.Phys.* **B497** (1997) 415–434, [hep-ph/9610480].

[54] H. Avakian, A. Efremov, P. Schweitzer and F. Yuan, *The transverse momentum dependent distribution functions in the bag model*, *Phys.Rev.* **D81** (2010) 074035, [1001.5467].

[55] R. Jakob, P. Mulders and J. Rodrigues, *Modeling quark distribution and fragmentation functions*, *Nucl.Phys.* **A626** (1997) 937–965, [hep-ph/9704335].

[56] M. Wakamatsu, *Polarized structure functions g(2)(x) in the chiral quark soliton model*, *Phys.Lett.* **B487** (2000) 118–124, [hep-ph/0006212].

[57] B. Pasquini, S. Cazzaniga and S. Boffi, *Transverse momentum dependent parton distributions in a light-cone quark model*, *Phys.Rev.* **D78** (2008) 034025, [0806.2298].

[58] C. Lorce, B. Pasquini and M. Vanderhaeghen, *Unified framework for generalized and transverse-momentum dependent parton distributions within a 3Q light-cone picture of the nucleon*, *JHEP* **1105** (2011) 041, [1102.4704].

[59] R. Kundu and A. Metz, *Higher twist and transverse momentum dependent parton distributions: A Light front Hamiltonian approach*, *Phys.Rev.* **D65** (2002) 014009, [hep-ph/0107073].

[60] M. Schlegel and A. Metz, *On the validity of Lorentz invariance relations between parton distributions*, hep-ph/0406289.

[61] K. Goeke, A. Metz, P. Pobylitsa and M. Polyakov, *Lorentz invariance relations among parton distributions revisited*, *Phys.Lett.* **B567** (2003) 27–30, [hep-ph/0302028].

[62] C. Lorcé, B. Pasquini and P. Schweitzer, *Unpolarized transverse momentum dependent parton distribution functions beyond leading twist in quark models*, *JHEP* **01** (2015) 103, [1411.2550].

[63] C. Lorcé, B. Pasquini and P. Schweitzer, *Transverse pion structure beyond leading twist in constituent models*, *Eur. Phys. J.* **C76** (2016) 415, [1605.00815].

[64] P. Zavada, *The Structure functions and parton momenta distribution in the hadron rest system*, *Phys.Rev.* **D55** (1997) 4290–4299, [hep-ph/9609372].

[65] A. V. Efremov, P. Schweitzer, O. V. Teryaev and P. Zavada, *The relation between TMDs and PDFs in the covariant parton model approach*, *Phys. Rev.* **D83** (2011) 054025, [1012.5296].

[66] A. V. Efremov, P. Schweitzer, O. V. Teryaev and P. Zavada, *Transverse momentum dependent distribution functions in a covariant parton model approach with quark orbital motion*, *Phys. Rev.* **D80** (2009) 014021, [0903.3490].

[67] P. Schweitzer, *The Chirally odd twist three distribution function e**alpha(x) in the chiral quark soliton model*, *Phys. Rev.* **D67** (2003) 114010, [hep-ph/0303011].

[68] Y. Ohnishi and M. Wakamatsu, *pi N sigma term and chiral odd twist three distribution function e(x) of the nucleon in the chiral quark soliton model*, *Phys. Rev.* **D69** (2004) 114002, [hep-ph/0312044].

[69] C. Cebulla, J. Ossmann, P. Schweitzer and D. Urbano, *The Twist-3 parton distribution function e**a(x) in large-N(c) chiral theory*, *Acta Phys. Polon.* **B39** (2008) 609–640, [0710.3103].

[70] S. Meissner, A. Metz and K. Goeke, *Relations between generalized and transverse momentum dependent parton distributions*, *Phys.Rev.* **D76** (2007) 034002, [hep-ph/0703176].

[71] A. Mukherjee, *Twist Three Distribution e(x): Sum Rules and Equation of Motion Relations*, *Phys.Lett.* **B687** (2010) 180–183, [0912.1446].

[72] A. Harindranath and W.-M. Zhang, *Examination of Wandzura-Wilczek relation for g2 (x, q**2) in pQCD*, *Phys.Lett.* **B408** (1997) 347–356, [hep-ph/9706419].

[73] M. Anselmino et al., *The role of Cahn and Sivers effects in deep inelastic scattering*, *Phys. Rev.* **D71** (2005) 074006, [hep-ph/0501196].

[74] J. C. Collins et al., *Sivers effect in semi-inclusive deeply inelastic scattering*, *Phys. Rev.* **D73** (2006) 014021, [hep-ph/0509076].

[75] U. D'Alesio and F. Murgia, *Azimuthal and Single Spin Asymmetries in Hard Scattering Processes*, *Prog. Part. Nucl. Phys. 61* **2008** (2008) 394–454, [0712.4328].

[76] P. Schweitzer, T. Teckentrup and A. Metz, *Intrinsic transverse parton momenta in deeply inelastic reactions*, *Phys.Rev.* **D81** (2010) 094019, [1003.2190].

[77] A. Signori, A. Bacchetta, M. Radici and G. Schnell, *Investigations into the flavor dependence of partonic transverse momentum*, *JHEP* **11** (2013) 194, [1309.3507].

[78] M. Anselmino, M. Boglione, J. O. Gonzalez Hernandez, S. Melis and A. Prokudin, *Unpolarised Transverse Momentum Dependent Distribution and Fragmentation Functions from SIDIS Multiplicities*, *JHEP* **04** (2014) 005, [1312.6261].

[79] A. Bacchetta, D. Boer, M. Diehl and P. J. Mulders, *Matches and mismatches in the descriptions of semi- inclusive processes at low and high transverse momentum*, *JHEP* **08** (2008) 023, [0803.0227].

[80] S. M. Aybat and T. C. Rogers, *TMD Parton Distribution and Fragmentation Functions with QCD Evolution*, *Phys.Rev.* **D83** (2011) 114042, [1101.5057].

[81] F. Landry, R. Brock, P. M. Nadolsky and C. Yuan, *Tevatron Run-1 Z boson data and Collins-Soper-Sterman resummation formalism*, *Phys.Rev.* **D67** (2003) 073016, [hep-ph/0212159].

[82] A. D. Martin, W. J. Stirling, R. S. Thorne and G. Watt, *Parton distributions for the LHC*, *Eur. Phys. J.* **C63** (2009) 189–285, [0901.0002].

[83] M. Gluck, E. Reya and A. Vogt, *Dynamical parton distributions revisited*, *Eur. Phys. J.* **C5** (1998) 461–470, [hep-ph/9806404].

[84] D. de Florian, R. Sassot and M. Stratmann, *Global analysis of fragmentation functions for pions and kaons and their uncertainties*, *Phys. Rev.* **D75** (2007) 114010, [hep-ph/0703242].

[85] P. Schweitzer, M. Strikman and C. Weiss, *Intrinsic transverse momentum and parton correlations from dynamical chiral symmetry breaking*, *JHEP* **01** (2013) 163, [1210.1267].

[86] CLAS Collaboration collaboration, M. Osipenko et al., *Measurement of unpolarized semi-inclusive pi+ electroproduction off the proton*, *Phys.Rev.* **D80** (2009) 032004, [0809.1153].

[87] HERMES collaboration, A. Airapetian et al., *Multiplicities of charged pions and kaons from semi-inclusive deep-inelastic scattering by the proton and the deuteron*, *Phys. Rev.* **D87** (2013) 074029, [1212.5407].

[88] COMPASS collaboration, M. Aghasyan et al., *Transverse-momentum-dependent Multiplicities of Charged Hadrons in Muon-Deuteron Deep Inelastic Scattering*, 1709.07374.

[89] J. Collins, L. Gamberg, A. Prokudin, T. C. Rogers, N. Sato and B. Wang, *Relating Transverse Momentum Dependent and Collinear Factorization Theorems in a Generalized Formalism*, *Phys. Rev.* **D94** (2016) 034014, [1605.00671].

[90] CLAS collaboration, H. Avakian et al., *Measurement of Single and Double Spin Asymmetries in Deep Inelastic Pion Electroproduction with a Longitudinally Polarized Target*, *Phys. Rev. Lett.* **105** (2010) 262002, [1003.4549].

[91] D. W. Sivers, *Single spin production asymmetries from the hard scattering of point - like constituents*, *Phys. Rev.* **D41** (1990) 83.

[92] M. Anselmino, M. Boglione, U. D'Alesio, S. Melis, F. Murgia and A. Prokudin, *New insight on the Sivers transverse momentum dependent distribution function*, *J. Phys. Conf. Ser.* **295** (2011) 012062, [1012.3565].

[93] M. Anselmino et al., *Extracting the sivers function from polarized sidis data and making predictions*, *Phys. Rev.* **D72** (2005) 094007, [hep-ph/0507181].

[94] M. Anselmino et al., *Comparing extractions of Sivers functions*, hep-ph/0511017.

[95] W. Vogelsang and F. Yuan, *Single-transverse spin asymmetries: From dis to hadronic collisions*, *Phys. Rev.* **D72** (2005) 054028.

[96] M. Anselmino et al., *Sivers Effect for Pion and Kaon Production in Semi- Inclusive Deep Inelastic Scattering*, *Eur. Phys. J.* **A39** (2009) 89–100, [0805.2677].

[97] A. Bacchetta and M. Radici, *Constraining quark angular momentum through semi-inclusive measurements*, *Phys. Rev. Lett.* **107** (2011) 212001, [1107.5755].

[98] M. G. Echevarria, A. Idilbi, Z.-B. Kang and I. Vitev, *QCD Evolution of the Sivers Asymmetry*, *Phys. Rev.* **D89** (2014) 074013, [1401.5078].

[99] HERMES collaboration, A. Airapetian et al., *Observation of the Naive-T-odd Sivers Effect in Deep-Inelastic Scattering*, *Phys. Rev. Lett.* **103** (2009) 152002, [0906.3918].

[100] M. Anselmino, M. Boglione, U. D'Alesio, S. Melis, F. Murgia and A. Prokudin, *Sivers Distribution Functions and the Latest SIDIS Data*, in *19th International Workshop on Deep-Inelastic Scattering and Related Subjects (DIS 2011) Newport News, Virginia, April 11-15, 2011*, 2011. 1107.4446.

[101] J. C. Collins, *Fragmentation of transversely polarized quarks probed in transverse momentum distributions*, *Nucl. Phys.* **B396** (1993) 161–182.

[102] M. Anselmino, M. Boglione, U. D'Alesio, S. Melis, F. Murgia and A. Prokudin, *Simultaneous extraction of transversity and Collins functions from new SIDIS and e+e- data*, *Phys. Rev.* **D87** (2013) 094019, [1303.3822].

[103] Z.-B. Kang, A. Prokudin, P. Sun and F. Yuan, *Nucleon tensor charge from Collins azimuthal asymmetry measurements*, *Phys. Rev.* **D91** (2015) 071501, [1410.4877].

[104] M. Anselmino, M. Boglione, U. D'Alesio, J. O. Gonzalez Hernandez, S. Melis, F. Murgia et al., *Collins functions for pions from SIDIS and new e^+e^- data: a first glance at their transverse momentum dependence*, *Phys. Rev.* **D92** (2015) 114023, [1510.05389].

[105] HERMES collaboration, A. Airapetian et al., *Effects of transversity in deep-inelastic scattering by polarized protons*, *Phys. Lett.* **B693** (2010) 11–16, [1006.4221].

[106] V. Barone, M. Boglione, J. O. Gonzalez Hernandez and S. Melis, *Phenomenological analysis of azimuthal asymmetries in unpolarized semi-inclusive deep inelastic scattering*, *Phys. Rev.* **D91** (2015) 074019, [1502.04214].

[107] HERMES collaboration, A. Airapetian et al., *Azimuthal distributions of charged hadrons, pions, and kaons produced in deep-inelastic scattering off unpolarized protons and deuterons*, *Phys. Rev.* **D87** (2013) 012010, [1204.4161].

[108] R. N. Cahn, *Azimuthal Dependence in Leptoproduction: A Simple Parton Model Calculation*, *Phys.Lett.* **B78** (1978) 269.

[109] V. Barone, S. Melis and A. Prokudin, *The Boer-Mulders effect in unpolarized SIDIS: An Analysis of the COMPASS and HERMES data on the cos 2 phi asymmetry*, *Phys. Rev.* **D81** (2010) 114026, [0912.5194].

[110] V. Barone, S. Melis and A. Prokudin, *Azimuthal asymmetries in unpolarized Drell-Yan*

processes and the Boer-Mulders distributions of antiquarks, *Phys. Rev.* **D82** (2010) 114025, [1009.3423].

[111] B. Parsamyan, *Transverse spin dependent azimuthal asymmetries at COMPASS*, *J.Phys.Conf.Ser.* **295** (2011) 012046, [1012.0155].

[112] C. Lefky and A. Prokudin, *Extraction of the distribution function $h_{1T}^{\perp}$ from experimental data*, *Phys. Rev.* **D91** (2015) 034010, [1411.0580].

[113] B. Parsamyan, *Transverse spin azimuthal asymmetries in SIDIS at COMPASS: Multidimensional analysis*, *Int. J. Mod. Phys. Conf. Ser.* **40** (2016) 1660029, [1504.01599].

[114] Jefferson Lab Hall A collaboration, J. Huang et al., *Beam-Target Double Spin Asymmetry A_{LT} in Charged Pion Production from Deep Inelastic Scattering on a Transversely Polarized He-3 Target at $1.4 < Q^2 < 2.7GeV^2$*, *Phys. Rev. Lett.* **108** (2012) 052001, [1108.0489].

[115] S. Goertz, W. Meyer and G. Reicherz, *Polarized H, D and He-3 targets for particle physics experiments*, *Prog. Part. Nucl. Phys.* **49** (2002) 403–489.

[116] A. Kotzinian, *SIDIS Asymmetries in Quark-Diquark Model*, in *Transversity 2008: 2nd International Workshop on Transverse Polarization Phenomena in Hard Processes Ferrara, Italy, May 28-31, 2008*, 2008. 0806.3804. DOI.

[117] S. Boffi, A. V. Efremov, B. Pasquini and P. Schweitzer, *Azimuthal spin asymmetries in light-cone constituent quark models*, *Phys. Rev.* **D79** (2009) 094012, [0903.1271].

[118] HERMES Collaboration collaboration, A. Airapetian et al., *Observation of a single spin azimuthal asymmetry in semiinclusive pion electro production*, *Phys.Rev.Lett.* **84** (2000) 4047–4051, [hep-ex/9910062].

[119] S. Jawalkar et al., *Semi-Inclusive π_0 target and beam-target asymmetries from 6 GeV electron scattering with CLAS*, 1709.10054.

[120] HERMES Collaboration collaboration, A. Airapetian et al., *Measurement of single spin azimuthal asymmetries in semiinclusive electroproduction of pions and kaons on a longitudinally polarized deuterium target*, *Phys.Lett.* **B562** (2003) 182–192, [hep-ex/0212039].

[121] F. Stock et al., *The FILTEX / HERMES polarized hydrogen atomic beam source*, *Nucl. Instrum. Meth.* **A343** (1994) 334–342.

[122] CLAS Collaboration collaboration, H. Avakian et al., *Measurement of beam-spin asymmetries for pi + electroproduction above the baryon resonance region*, *Phys.Rev.* **D69** (2004) 112004, [hep-ex/0301005].

[123] HERMES Collaboration collaboration, A. Airapetian et al., *Beam-Spin Asymmetries in the Azimuthal Distribution of Pion Electroproduction*, *Phys.Lett.* **B648** (2007) 164–170, [hep-ex/0612059].

[124] W. Gohn, H. Avakian, K. Joo and M. Ungaro, *Beam spin asymmetries from semi-inclusive pion electroproduction in deep inelastic scattering*, *AIP Conf.Proc.* **1149** (2009) 461–464.

[125] M. Aghasyan, H. Avakian, P. Rossi, E. De Sanctis, D. Hasch et al., *Precise Measurements of Beam Spin Asymmetries in Semi-Inclusive π^0 production*, *Phys.Lett.* **B704** (2011) 397–402, [1106.2293].

[126] COMPASS collaboration, C. Adolph et al., *Measurement of azimuthal hadron asymmetries in semi-inclusive deep inelastic scattering off unpolarised nucleons*, *Nucl. Phys.* **B886** (2014) 1046–1077, [1401.6284].

[127] CLAS collaboration, W. Gohn et al., *Beam-spin asymmetries from semi-inclusive pion electroproduction*, *Phys. Rev.* **D89** (2014) 072011, [1402.4097].

[128] HERMES Collaboration collaboration, A. Airapetian et al., *Subleading-twist effects in single-spin asymmetries in semi-inclusive deep-inelastic scattering on a longitudinally polarized hydrogen target*, *Phys.Lett.* **B622** (2005) 14–22, [hep-ex/0505042].

[129] HERMES Collaboration collaboration, G. Schnell, *The Sivers and other semi-inclusive single-spin asymmetries at HERMES*, *PoS* **DIS2010** (2010) 247.

[130] T. P. Cheng and A. Zee, *Coincidence electroproduction and scaling in the regge region*, *Phys. Rev.* **D6** (1972) 885–893.

[131] European Muon collaboration, J. J. Aubert et al., *Measurement of Hadronic Azimuthal Distributions in Deep Inelastic Muon Proton Scattering*, *Phys. Lett.* **130B** (1983) 118–122.

[132] J. T. Dakin, G. J. Feldman, W. L. Lakin, F. Martin, M. L. Perl, E. W. Petraske et al., *PRELIMINARY RESULTS ON THE INCLUSIVE ELECTROPRODUCTION OF HADRONS*, 1972.

[133] H. Mkrtchyan, P. Bosted, G. Adams, A. Ahmidouch, T. Angelescu et al., *Transverse momentum dependence of semi-inclusive pion production*, *Phys.Lett.* **B665** (2008) 20–25, [0709.3020].

[134] M. Anselmino, M. Boglione, U. D'Alesio, S. Melis, F. Murgia et al., *General Helicity Formalism for Polarized Semi-Inclusive Deep Inelastic Scattering*, *Phys.Rev.* **D83** (2011) 114019, [1101.1011].

[135] A. V. Efremov, K. Goeke, S. Menzel, A. Metz and P. Schweitzer, *Sivers effect in semi-inclusive DIS and in the Drell-Yan process*, *Phys. Lett.* **B612** (2005) 233–244, [hep-ph/0412353].

[136] S. M. Aybat, J. C. Collins, J.-W. Qiu and T. C. Rogers, *The QCD Evolution of the Sivers Function*, *Phys. Rev.* **D85** (2012) 034043, [1110.6428].

[137] L. Gamberg, Z.-B. Kang and A. Prokudin, *Indication on the process-dependence of the Sivers effect*, *Phys. Rev. Lett.* **110** (2013) 232301, [1302.3218].

[138] M. Anselmino, M. Boglione and S. Melis, *A Strategy towards the extraction of the Sivers function with TMD evolution*, *Phys. Rev.* **D86** (2012) 014028, [1204.1239].

[139] P. Sun and F. Yuan, *Energy Evolution for the Sivers Asymmetries in Hard Processes*, *Phys. Rev.* **D88** (2013) 034016, [1304.5037].

[140] Z.-B. Kang, A. Prokudin, P. Sun and F. Yuan, *Extraction of Quark Transversity Distribution and Collins Fragmentation Functions with QCD Evolution*, *Phys. Rev.* **D93** (2016) 014009, [1505.05589].

[141] M. Gluck, E. Reya, M. Stratmann and W. Vogelsang, *Models for the polarized parton distributions of the nucleon*, *Phys. Rev.* **D63** (2001) 094005, [hep-ph/0011215].